SCUOLA INTERNAZIONALE SUPERIORE STUDI AVANZATI (SISSA)
INTERNATIONAL SCHOOL FOR ADVANCED STUDIES (ISAS)
PHD COURSE IN FUNCTIONAL AND STRUCTURAL GENOMICS
Trieste, Italy

Modelling etiopathogenesis of the FOXG1-duplication-linked variant of West syndrome

Thesis submitted for the degree of “Doctor Philosophiae”

Academic year 2014-2015

Candidate:
Moira Pinzan

Supervisor:
Prof. Antonello Mallamaci

ABSTRACT

Here we describe the characterization of a novel *Foxg1*-GOF model we created to dissect the role of *Foxg1* in postmitotic neuronal differentiation and reconstruct pathogenetic mechanisms which underlie the *FOXG1* duplication-linked West syndrome. This is a devastating neurological disorder, triggered by a complex variety of pathogenic conditions. It is characterized by infantile spasms, abnormal EEG with hypsarrhytmia and seizures and dramatic cognitive impairment. For it only symptomatic treatments are presently available.

As expected, these *Foxg1*-GOF mice showed increased neuronal activity in baseline conditions and were more prone to limbic motor seizures upon kainic acid administration.

A preliminary developmental profiling of their cerebral cortex unveiled four major histogenetic anomalies, likely contributing to their hyperexcitability. These anomalies were: (1) an altered neocortical laminar blueprint with impaired layer VI/layer V segregation and defective activation of layer IV-II programs; (2) a substantial reduction of PV^+ interneurons; (3) a patterned, area- and lamina-specific astrocyte deprivation; (4) a defective expression of the Gabra1 receptor subunit. Similar phenomena might concur to neurological anomalies of West syndrome patients harboring *FOXG1* duplications.

A parallel in vitro study, run on dissociated cortico-cerebral cultures, revealed that a substantial *Foxg1* upregulation occurred upon delivery of depolarizing stimuli. Neuronal, activity-linked *Foxg1* elevation required the presence of astrocytes. Activity-linked *Foxg1* fluctuations were inter-twinned with immediate-early genes fluctuations and depended on them, according to distinct, neuron- and astrocyte-specific patterns. In West syndrome patients with augmented *FOXG1* dosage, a *FOXG1*-mRNA increase evoked by depolarizing stimuli might ignite a vicious circle, exacerbating neuronal hyperactivity and contributing to interictal EEG anomalies and seizures.

INDEX

1. INTRODUCTION

1.1 Neocortex development

The neocortex is a telencephalic structure unique to mammals. It is the largest region of the cerebral cortex, positioned between two other regions, the archicortex (midline cortex and hippocampus) and paleocortex (olfactory piriform cortex); the neocortex has undergone the most considerable phylogenetic expansion and specialization (Doetsch et al., 1999);(Krubitzer and Kaas, 2005). It is also the most highly differentiated region of the cerebral cortex, having a laminar patterning characterized by six layers in its radial dimension (morphologically and connectionally distinct) while, in its tangential dimension, it is subdivided in "areas" (i.e. functional subdivisions distinguished by differences in cytoarchitecture, connections and gene pattern expression) (O'Leary and Nakagawa, 2002; O'Leary et al., 2007; Rash and Grove, 2006; Sur and Rubenstein, 2005).

The increase in the neocortical size and complexity is due to a rapid expanding diversity of neuronal and glial subtypes (Edlund and Jessell, 1999);(Ramon y Cajal, 1995).
Initially, the neocortex is composed of a thin neuroepithelium lining the dorsal wall of the lateral ventricles, called the ventricular zone (VZ). As neurogenesis proceeds, an additional proliferative layer superficial to the VZ will form the subventricular zone (SVZ).
The first postmitotic neurons will accumulate on the top of the VZ, forming the preplate (PP) that is positioned just beneath the pial surface. Subsequently generated neurons will migrate along radial glia, aggregating within the PP, and forming the cortical plate (CP) which will split the PP into a superficial marginal zone (MZ) and a deep subplate (SP). The CP will develop between these two layers and will become the multilayered neocortex in an "inside-out fashion", so that early-born neurons populate deeper neocortical layers (layer VI, then layer V), and late-born neurons migrate past them to progressively populate more superficial layers (layer IV, then layer II/III) (Angevine and Sidman, 1961; Rakic, 1974)(Fig.1.1).

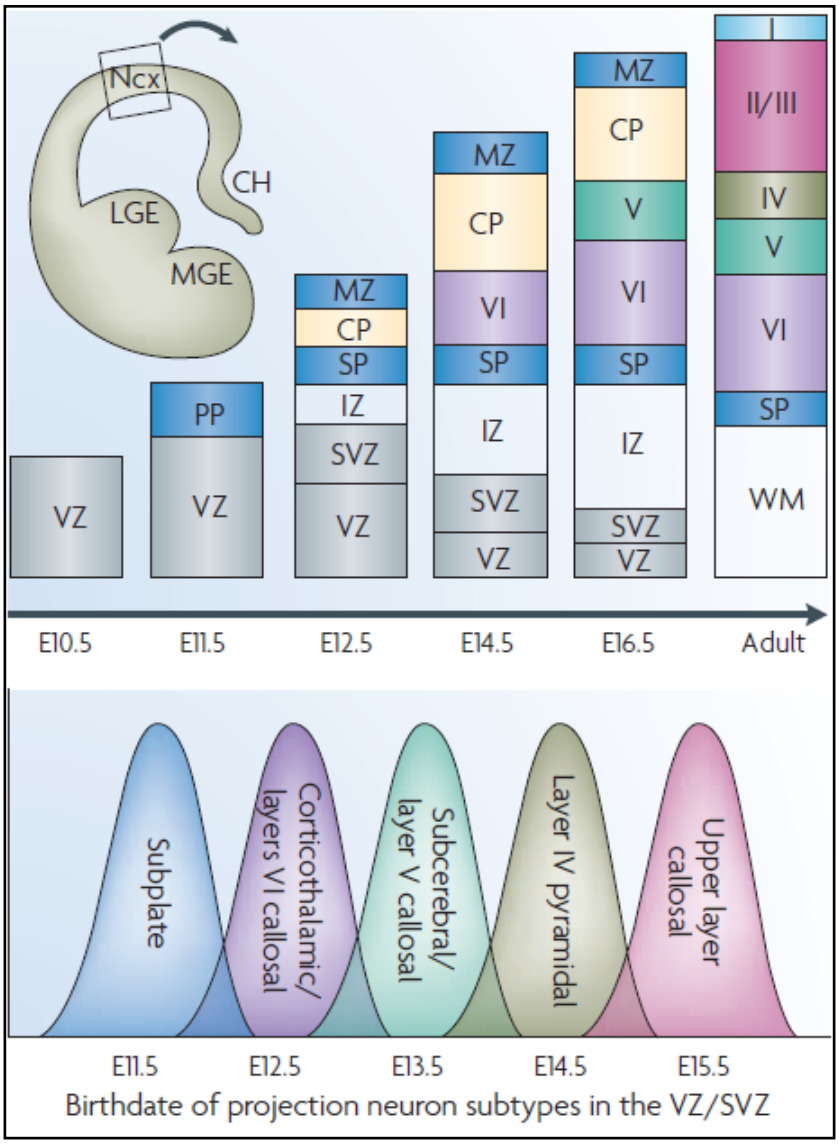

Fig.1.1 Timing of cortical neurogenesis

Adapted from (Molyneaux et al., 2007)

In mice, this process starts at embryonic day 9.5 (E9.5) with the proliferation of neuroepithelial cells that undergo symmetric cell divisions to expand the pool of multipotent progenitors as well as a smaller percentage of asymmetric cell divisions to generate the earliest born neurons. (Chenn and McConnell, 1995; Götz and Huttner, 2005; Smart, 1973). As the developing cortical epithelium thickens, neuroepithelial cells elongate and differentiate into radial glial progenitors. A particular feature of these cells is a long process

that extends from the ventricular wall to the pial surface, having thus a crucial role in guiding neurons to their final locations in the cortical plate, by serving as a migratory scaffolding (Rakic, 1972, 2003). Moreover, radial glia function also as progenitors that make more contributions to cortical neurogenesis by generating neurons directly in the VZ, or indirectly through the production of proliferating intermediate progenitors (Anthony et al., 2004; Malatesta et al., 2000; Miyata et al., 2004; Noctor et al., 2001).

Intermediate progenitors (also known as basal progenitors because they divide without touching the apical surface) are the other major type of neuron-producing progenitor. They act primarily as transit-amplifying cells, undergoing limited proliferative divisions and more often dividing symmetrically to produce two neurons (Haubensak et al., 2004; Kowalczyk et al., 2009; Noctor et al., 2004). They are located in the SVZ and in the basal VZ early in neurogenesis before SVZ forms. The SVZ begins to form at E13.5 in mice and increases significantly during late corticogenesis (Smart, 1982). The SVZ has further expanded in primates giving rise to an inner and an outer SVZ, whose progenitors are distinct. Inner SVZ progenitors resemble rodent SVZ intermediate progenitors, while primate outer SVZ progenitors are more similar to radial glial cells, both in morphology and molecular identity. Moreover, the radial glial-like progenitors of the OSVZ are able to undergo symmetric (self-renewing), as well as asymmetric (neurogenic and self-renewing) divisions, thus generating progenitors that can further proliferate. This latter capacity of OSVZ progenitors enhances neuronal output and represents an important evolutionary step in the expansion of the neocortex (Fietz and Huttner, 2011; Hansen et al., 2010; Smart et al., 2002)(Fig.1.2).

Another class of progenitors are the short neural precursors. They appear to be similar to intermediate progenitors, suggesting that they might be radial glia that is in the process of becoming intermediate progenitors (Smart et al., 2002).

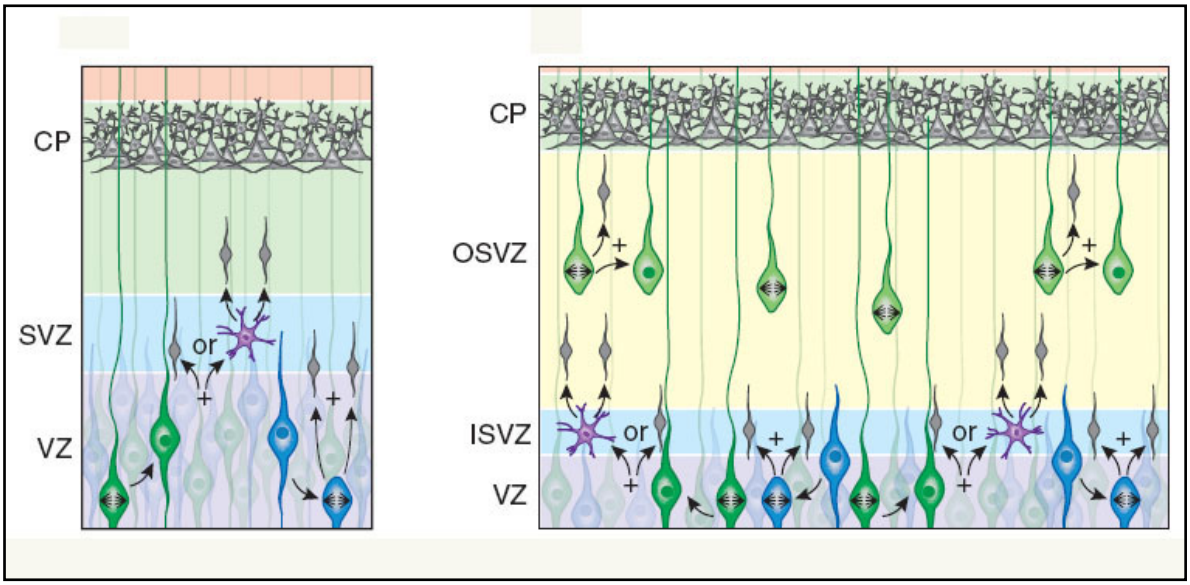

Fig.1.2 Comparison of germinal zones in rodent and primates embryonic neocortex during midneurogenesis (mouse E13.5; Human 8.5GW)

Adapted from (Tyler and Haydar, 2010)

Given the heterogeneity of progenitor types and their different locations it is not clear how the balance of extrinsic and intrinsic signals combines to determine neuronal fate. The common view about layer-specific production is that progenitor cells, after successive rounds of asymmetric cell division, progressively restrict their competence producing at first deep layer neurons (DL neurons) and then upper layer neurons (UL neurons) (Desai and McConnell, 2000; Frantz and McConnell, 1996).

More recently, new studies have discovered UL fate-committed early progenitors, which raise an alternative view regarding the lineage relation between DL and UL neurons (Franco et al., 2012) Besides, genetic studies have shown that a closed transcriptional network is responsible to establish segregation among the principal layer subtypes of the cerebral cortex. In particular, the cross-repression among four transcription factors (TFs) - Fezf2, Ctip2, Satb2, and Tbr1- is sufficient to establish the subcerebral, intracortical, and cortico-thalamic projection identities within the postmitotic neurons (Alcamo et al., 2008; Britanova et al., 2008; Chen et al., 2008; Han et al., 2011; McKenna et al., 2011; Srinivasan et

al., 2012). UL competence is tightly linked to DL neurogenesis and this sequence of layer neurogenesis is determined through Tbr1 repression (Fig.1.3).

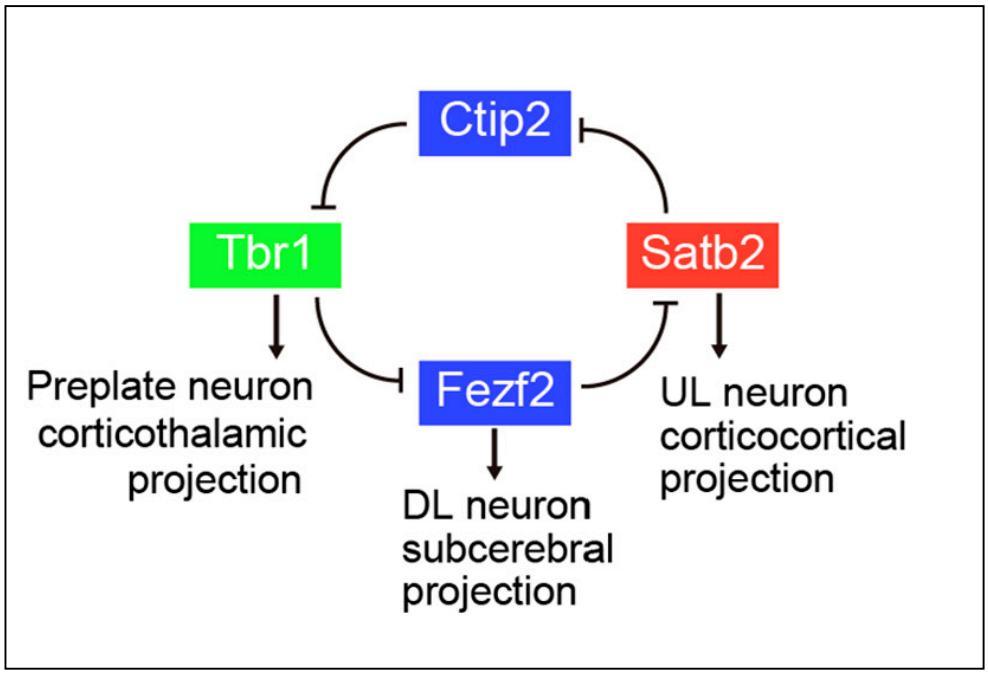

Fig.1.3 Schematic model of identified genetic interactions between the layer-subtype TFs. Adapted from (Toma et al., 2014)

A continued repression of *Tbr1*, expressed in the majority of early-born neurons including preplate Cajal Retzius cells and subplate (SP) neurons (Hevner et al., 2001), favors the acquisition of Fezf2 DL neuron identity. Moreover, the subsequent transition from DL to UL competence requires the repression of DL determinants to terminate DL competence. The onset of UL competence is achieved thanks to negative feedback propagated from postmitotic DL neurons (Toma et al., 2014).

Cortical neurogenesis is essentially completed during the embryonic period, followed by gliogenesis, which largely occurs in the first month of postnatal life (Bystron et al., 2008)

1.2 Origin of glutamatergic and gabaergic neurons

Two broad classes of neurons populate the neocortex: interneurons and projection neurons. Projection neurons are excitatory glutamatergic neurons characterized by a typical pyramidal morphology and extend their axons to distant intracortical, subcortical and subcerebral targets in order to transmit information from the neocortex to other cortical areas. By contrast, GABA (ϒ-aminobutyric acid)-containing interneurons are nonpyramidal neurons, which connect locally within the neocortex and are largely inhibitory (Molyneaux et al., 2007). During development, they are generated by different progenitor zones. Interneurons are generated by progenitors in the ventral (subpallial) telencephalon and migrate tangentially over long distances to reach their final position within the neocortex (Wonders and Anderson, 2006); projection neurons are generated from progenitors of the neocortical germinal zone located in the dorsolateral (pallial) wall of the telencephalon and migrate radially to their final neocortical position (Anderson et al., 2002; Gorski et al., 2002; Leone et al., 2008; Molyneaux et al., 2007; Rakic, 1972).

Upon induction by gradients of different signalling molecules such as sonic hedgehog (Shh), fibroblast growth factor (Fgf) and bone morphogenetic proteins (BMP), the interplay between different transcription factor genes will lead to the progressive specification of projection neurons. These include LIM homeobox 2 (*Lhx2*), *Foxg1*, empty spiracles homologue 2 (*Emx2*) and paired box 6 (*Pax6*). These TFs have crucial roles in in establish the neocortical progenitor domain by repressing dorsal midline (*Lhx2* and *Foxg1*) and ventral (*Emx2* and *Pax6*) fates.

Within the mature neocortex, there are distinct populations of projection neurons located in different cortical layers and areas, with unique morphological features and gene expression and ultimately serving different functions. Projection neurons can be divided into three broad types according to whether they extend axons within a single cortical hemisphere (associative projection neurons), across the midline to the contralateral hemisphere (commissural projection neurons), or away from the cortex (corticofugal projection neurons) (Fig.1.4).

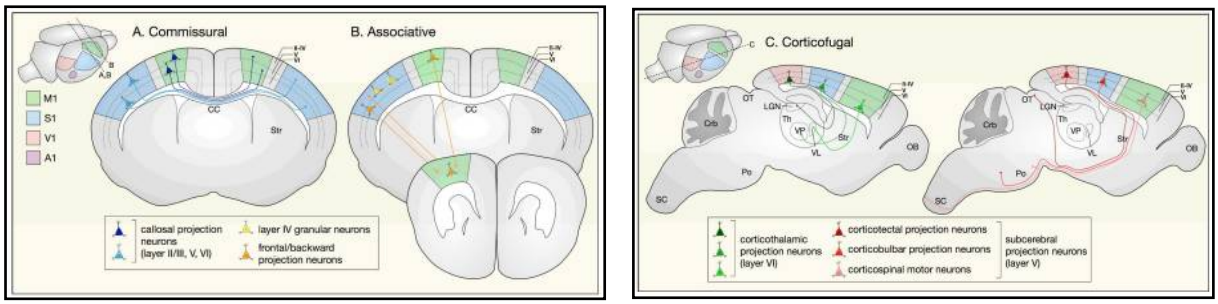

Fig.1.4 Projection neuron diversity in the cerebral cortex

Modified from (Greig et al., 2013)

Axons from commissural projection neurons cross the midline through the corpus callosum (CC). These neurons are called callosal projection neurons (CPNs). Axons from a smaller population of these neurons cross through the anterior commissure. CPNs reside mainly in layer II/III, with fewer residing in layers V and VI, all of them enabling bilateral integration of information by extending axons to mirror-image locations in the same functional area of the contralateral hemisphere.

Associative projection neurons are present in all cortical layers. They include:

- Short-distance intrahemispheric projection neurons, which extend axons within a single cortical column or to the nearby cortical columns.
- Long-distance intrahemispheric projection neurons, which extend axons to adjacent or distant cortical areas.

Corticofugal projection neurons include corticothalamic projection neurons (CThPN), which reside in layer VI and extend axons to specific thalamic nuclei, and subcerebral projection neurons (SCPN), which reside in layer V and extend axons to different primary targets in the brainstem and spinal cord.

As for interneurons, they account for about 20% of all cortical neurons. They were described firstly by Ramon y Cajal as ”cells with short axons” (locally projecting axon), aspiny or sparsely spiny dendrites and with a cell soma smaller than most cortical pyramidal neurons. They are across all cortical layers and establish unique connections with excitatory and inhibitory cells in their vicinity. Some of them extend horizontal or vertical axon collaterals within the cortex and have their cell bodies mostly dispersed into layers II-VI.

Many efforts have been made to classify them and are still underway, but are complicated because of their variability in morphology, connectivity, neurochemistry and expression of ion/physiology channel (Markram et al., 2004).

Cortical interneurons originate within different regions of the ventral telencephalon over a period of time that spans from embryonic day E9.0 until birth. In particular, most if not all cortical interneurons arise from the ventral ganglionic eminences, namely, the medial ganglionic eminence (MGE) and the caudal ganglionic eminence (CGE) (Ang et al., 2003; Marín and Rubenstein, 2003; Nery et al., 2002). These ganglionic eminences arise in a discrete temporal order with the 'earlier-generated ventral eminence' named MGE appearing at the telencephalic-diencephalic junction, followed by a 'later appearing dorsal eminence', later named the lateral ganglionic eminence (LGE) (Smart, 1976). The CGE was proposed more recently as a discrete entity, being defined as the eminence that is posterior to the fusion of the MGE and LGE (Anderson et al., 2001). Even in this case, regional identity is regulated by a combination of TFs with overlapping expression patterns, some of them showing cell fate restriction functions (Anderson et al., 1997; Flames and Marín, 2005; Sussel et al., 1999). From E9, Shh act on MGE cells inducing the expression of *Nkx2.1* and *Lhx6* TFs. As for the CGE specification, TFs involved are *CoupTF1/2*, *Gsh1/2* (Sousa et al., 2009);(Lee et al., 2010). *Gsh1/2* controls in turn the expression of *Mash1*, *ASCL1*, *Dlx2* required for CGE patterning(Fig.1.5).

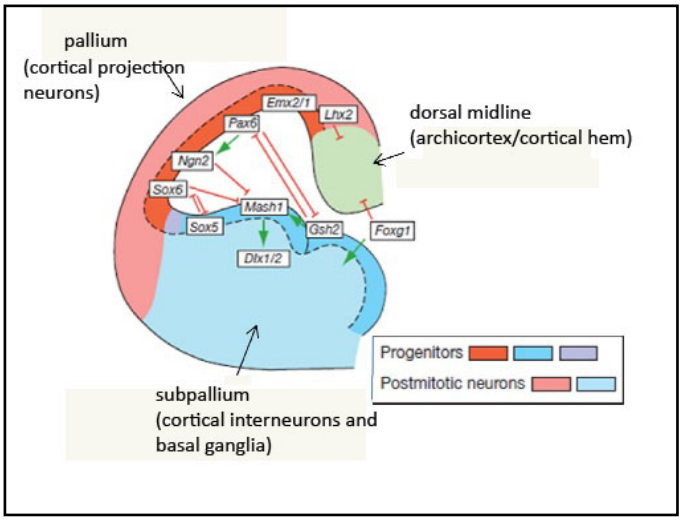

Fig. 1.5 Transcriptional facors involved in pallial and subpallial patterning

Adapted from John Rubenstein and Pasko Rakic, 2013

GABAergic interneurons that populate the neocortex typically express distinct neuropeptide that helps to define their multiple subclasses like somatostatin (SST), neuropeptide-Y (NPY), vasoactive intestinal peptide (VIP) and calcium-binding proteins like parvalbumin (PV), calretinin (CR) and calbindin (CB)(Cherubini and Conti, 2001; DeFelipe, 1993; Gonchar et al., 2007; Houser et al., 1983; Kawaguchi and Kondo, 2002; Krimer and Goldman-Rakic, 2001). Thanks to several fate mapping experiments and transgenic mice became available, it has been possible to establish a correlation between the place and time of origin of interneuron precursors and determine their ultimate fate. Most MGE- derived interneurons contain either parvalbumin (PV) or somatostatin (SST). PV and SST interneurons are the two most abundant classes of cortical interneurons with non-overlapping molecular identities (DeFelipe, 1993, 1997). GABAergic interneurons expressing PV make up ~40% of all cortical interneurons of which basket and chandelier cells are typical members. SST-expressing interneurons, on the other hands, comprise ~30% of the cortical inhibitory cells, distributed across deep cortical layers V-VI and axons branching into layer I where they exert inhibitory control over distal dendritic processes of pyramidal neurons.

The other major contributing region for the generation of cortical GABAergic interneurons is the CGE. It is the source of VIP- and Reelin-expressing (SST-negative) interneurons (Miyoshi et al., 2007; Vucurovic et al., 2010) (Fig.1.6). Temporal fate mapping has shown that MGE progenitors give rise to different cortical interneurons subtypes at discrete ages or developmental times (Miyoshi et al., 2007). Furthermore, MGE-derived cortical interneurons show the same inside-out pattern of generation that is observed for pyramidal cells (Anderson et al., 2002; Cavanagh and Parnavelas, 1989). Early born MGE-derived interneurons end up in deep layers, while late- born IN occupy superficial layers of the mature neocortex (Miyoshi et al., 2007).

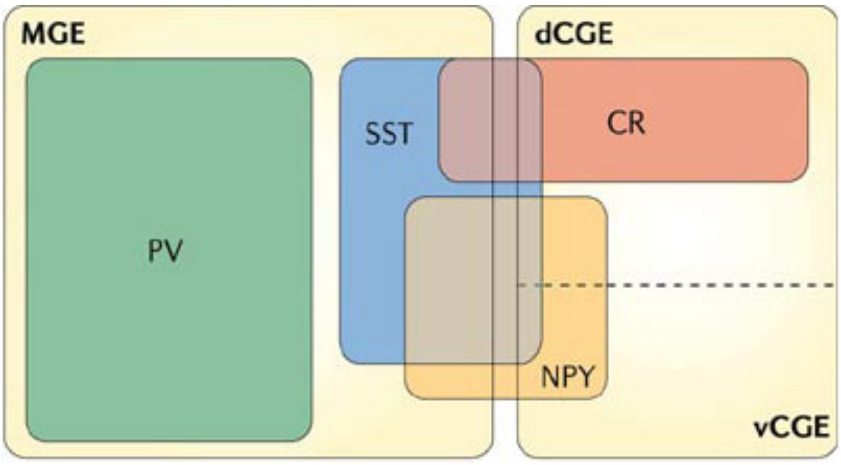

Fig. 1.6 Relative contribution of MGE and CGE to cortical interneuron subgroups

Adapted from (Wonders and Anderson, 2006)

CGE- derived interneurons are late-born cells with peak production around E16.5; they migrate tangentially toward the pallium through the SVZ and MZ (Cavanagh and Parnavelas, 1989). They do not follow a temporal-positioning code, but instead are distributed homogeneously across superficial cortical layers (layer I-III). An exception to this rule is the outside-in neurogenic gradient observed in CR-positive interneurons (Lee et al., 2010) follow different temporal rules than MGE-derived internuerons (Miyoshi and Fishell, 2011).

Interneurons then enter the cortex through two different migratory routes, both of which avoid the cortical plate: a superficial path within the marginal zone (MZ); and a deep route positioned at the subplate-SVZ interface (Lavdas et al., 1999). After a period of tangential migration, interneurons shift to a radial mode of migration when they enter the cortical plate (Ang et al., 2003; Polleux et al., 2002). The timing of this shift seems to be regulated by chemokines (Stumm et al., 2003; Tiveron et al., 2006). (Fig.1.7)

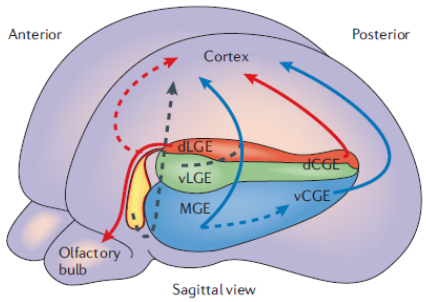

Fig. 1.7 Migration pathways of cortical interneuron from the ventral telencephalon

Adapted from (Wonders and Anderson, 2006)

Cajal-Retzius neurons, a third general category of cortical neurons, populate the MZ (layer I) and express Reelin, a secreted protein required for a proper cortical layering by influencing the radial migration and settling patterns of cortical neurons (Tissir and Goffinet, 2003). Cajal-Retzius neurons are generated mainly within the cortical hem, subpallium and septum (Bielle et al., 2005; Yoshida et al., 2006).

1.3 Astrogenesis

Astrocytes are specialized star-shaped glial cells and the most numerous non-neuronal cells type in the central nervous system. These cells perform several essential functions for normal neuronal activity, from structural support to maintenance of water balance, ion distribution and neurotransmitter metabolism as well as blood flow (Sofroniew and Vinters, 2010).

Astrocytes are classically divided into three major types according to morphology and spatial organization: radial astrocytes surrounding ventricles, protoplasmic astrocytes in grey matter and fibrous astrocytes located in white matter (Privat, 1995). Radial astrocytes are perpendicularly oriented to the ventricular surface and have long and unbranched processes; protoplasmic astrocytes have a bushy morphology with many highly branched short processes, while fibrous astrocytes display a stellate shape with smooth and long processes less branched.

Astrocytes are generated after neurons from the same pool of neural stem cells (NSCs) located in the ventricular and subventricular zone in the gliogenic phase of late gestation (Fig.1.8).

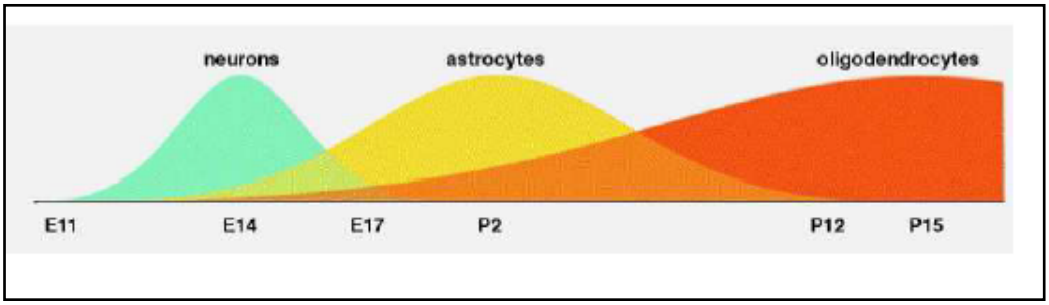

Fig. 1.8 Timing of mice cortico-cerebral histogenesis

During development, when the morphology of NSCs changes, they start to display extended radial processes to the pial surface from their somata and become known as radial glial cells (RGCs). RGCs will generate more neurons, yet having the additional potential to differentiate into astrocytes and oligodendrocytes. At late gestational and early postnatal stages, most RGCs begin to detach from the apical side and migrate to the cortex where they differentiate into astrocytes (Juliandi et al., 2010; Kriegstein and Alvarez-Buylla, 2009).

The onset of astrogenesis is a crucial point in the developing brain. Neuron-to-astrocyte switch must be tightly controlled and cooperation between environmental cues and cell-intrinsic program is necessary in order to get the correct timing, allowing the generation of a sufficient amount of neurons to form all neuronal layers.

JAK/STAT is the key signaling pathway involved in the induction of astrocyte specification. It is induced via cytokines such as ciliary neurotrophic factor (CNTF), leukaemia inhibitory factor (LIF) and interleukin-6 (IL-6)(Heinrich et al., 1998). These astrogenic cytokines bind to their co-receptor and trigger the heterodimerization of the Jak receptor. Following receptor activation, phosphorylation and acetylation activate STAT3, which dimerizes and translocate in the nucleus to activate transcription of key astrocyte genes like GFAP and S100β initiating thus astrocyte differentiation (Fig1.9).

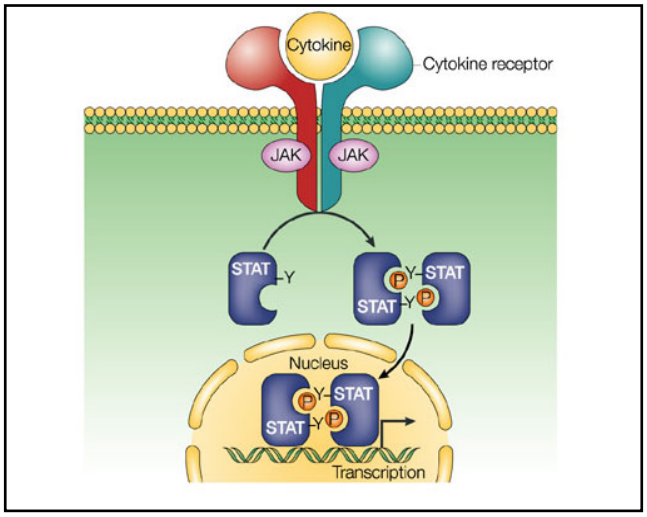

Fig. 1.9 JAK/ST AT signalling pathways

Adapted from (Shuai and Liu, 2003)

During neurogenesis, pro-neural factor like Neurogenin1 (Ngn1), binds the p300/CBP, co-activator complex, preventing its interaction with STAT3 (Sun et al., 2001); this prevents STAT3-dependent transcription and reduced acetylation at the binding sites on the promoters of astrocytic genes. Even the loss of other bHLH transcription factors, essential for neuronal differentiation, such Ngn2, NeuroD1 and Mash1, has been demonstrated to lead astrocyte differentiation induction (Nieto et al., 2001).

Besides, JAK/STAT act synergistically with the Notch signalling to promote astrogenesis. Notch signalling has an important role in the NSC fate during development; it maintains neural stem cell (NSC) renewal by inhibition of their differentiation until the correct differentiation cue is available. Thus, Notch signalling can be considered a major point of convergence between different regulators of the neuron-to astrocyte switch (Fig.1.10).

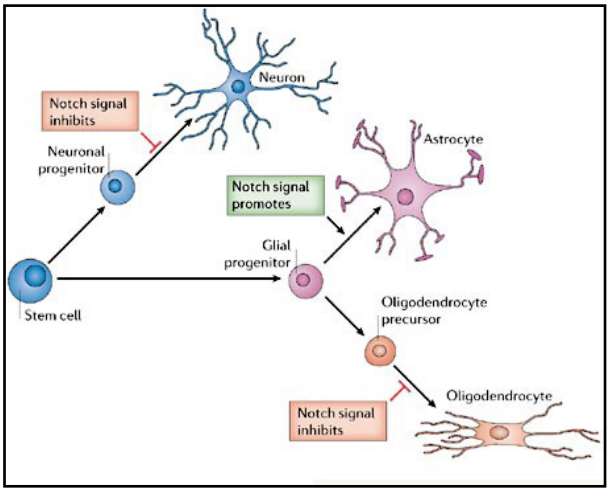

Fig. 1.10 Roles of Notch signalling pathway in differentiation process

Adapted from (Louvi and Artavanis-Tsakonas, 2006)

Notch and JAK/STAT interaction is mainly established by STAT3. STAT3 induces Notch ligand Dll1, which in turn activates Notch signalling in adjacent cells. Notch appears to promote the astrocytic phenotype through its downstream effectors, hairy enhancer of split (Hes), Hes1 and Hes5, which are known to promote astrocytic differentiation via suppressing the function of proneural bHLHs (Kopan and Ilagan, 2009). New born neurons stimulate Notch signalling in NSCs by expressing Notch ligands such as Jagged 1 and Delta-like 1 (Namihira et al., 2009). This activation is necessary and sufficient to induce astrocyte differentiation. Upon ligand binding, Notch is cleaved by the ϒ-secretase complex, releasing the notch intracellular domain (NICD). NICD translocates into the nucleus, where it regulates transcription of Notch target genes via DNA binding proteins (Guruharsha et al., 2012).

In addition, calcium signalling stimulates astrogenesis as well. The cAMP-dependent pituitary adenylate cyclase-activating polypeptide (PACAP) triggers intracellular cAMP production and in turn, entry of calcium in NSCs. Calcium will activate the transcription factor DREAM whose binding to responsive elements in the GFAP promoter will stimulate its expression. Moreover, the PACAP/DREAM pathway can act in synergy with the JAK/STAT pathway via the NF1A transcription factor, downstream factor of Notch. (Fig.1.11)

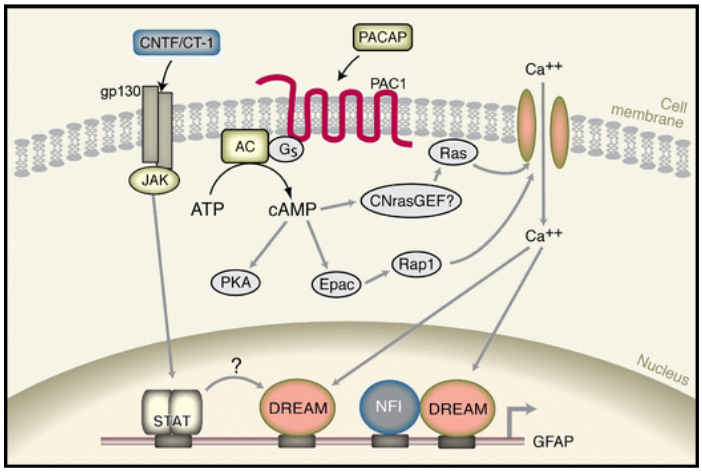

Fig. 1.11 PACAP/Dream and JAK/STAT pathway interactions

Modified from (Vallejo, 2009)

Lastly, another pathway play a special role in astrogenesis, in particular is crucial to prevent premature astrogenesis in vivo. It is the ErbB4-NCoR signalling, activated by neuregulins secreted by neurons (Fox and Kornblum, 2005). ErbB4 is a tyrosine kinase receptor of the EGF receptor family, which forms a repressor complex together with NcoR. Upon activation of the receptor, the intracellular domain of the ErbB4 receptor translocates

together with NcoR into the nucleus to inactivate GFAP expression (Sardi et al., 2006)(Fig.1.12).

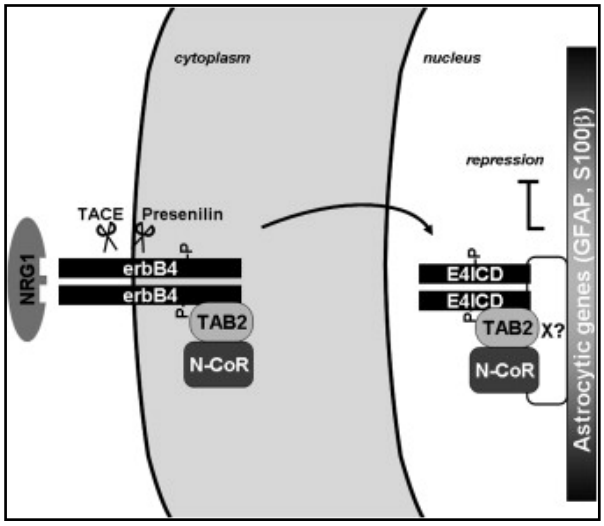

Fig. 1.12 ErbB4-NCoR signalling

Modified from (Sardi et al., 2006)

1.4 Astrocyte modulation of neuronal excitability

For a long time glial cells and astrocytes in particular have been largely viewed as simple gap fillers. More recently, the function of astrocytes has been reconsidered playing a number of active roles in the brain. There is a body of evidence that glia actively signal with neurons and influence synaptic development, neuronal excitability and plasticity through an array of secreted and contact-dependent signals. It is clear that a disruption in neuron-glia signalling contributes to the initiation and progression of many neurological disorders and diseases, in particular epilepsy. Epilepsy is a condition of the brain characterized by periodic manifestation of burst of electrical activity (seizures), in which unusual intense neuronal firing occurs. Development of an epileptic seizure requires physiological changes that lead to an amplified neuronal excitability and synchronization within the affected neuronal network.

Considering all the many functions exerted by astrocytes, it is clear that each of them if disrupted can affect neuronal excitability and thus play prominent roles in pathogenesis of neurological disorders.

Astrocyte buffering of extracellular K^+

Neuronal excitability is tightly coupled to the extracellular space (ECS) volume and its K^+ levels. Astrocytes regulate K^+ flow between neurons and the extracellular space. During normal periods of activity, much of the potassium released into the ESC by spiking neurons is taken up by astrocytes and neurons. Impaired astrocytic K^+ buffering results in a slower K^+ clearance, which in turn lower seizure threshold and thereby contribute to seizure generation. Astrocytes exhibits both passive and active mechanisms for limiting elevations in extracellular K^+. The inward rectifying K^+ channel, Kir4.1, is the main Kir channel subunit in astrocytes and in charge for the spatial buffering of the K^+ (Kofuji and Newman, 2004). Genetic downregulation of Kir4.1, strongly impair the ability of astrocytes to remove glutamate and K^+ from the ECS, both in cell culture (Kucheryavykh et al., 2007) and in vivo (Djukic et al., 2007). Besides, from ultrastructural analyses in rat, it resulted there is a spatial overlap of Kir4.1 and the water channel aquaporin 4 (AQP4) in astroglial endfeet contacting the capillaries (Higashi et al., 2001; Nielsen et al., 1997). The idea is they act in concert in the clearance of the K^+ and water after neural activity: potassium uptake is accompanied by water influx via AQP4 into astrocytes, to dissipate osmotic imbalances due to K^+ redistribution. More marked accumulations in extracellular K^+ trigger active uptake of K^+, via the activation of astrocyte Na^+/K^+ ATPase (Walz and Hertz, 1982) and the Na-K-Cl co-transporter NKCC1, at the cost of cell swelling due to a subsequent osmotic movement of water (Kofuji and Newman, 2004).

Glutamate uptake

Glutamate uptake from the extracellular space helps to terminate the action of this neurotransmitter at synapses. Uptake mechanisms are of particular importance as they prevent spill-out of transmitter from the synaptic cleft, thus regulating crosstalk between

neighbouring synapses and the activation of perisynaptic/extrsynaptic glutamate receptors. Glutamate uptake is mainly mediated by transporters localized at the astrocytes membranes. Five glutamate transporters are present in the brain; GLAST and GLT-1 (human forms: EAAT1 and EAAT2, respectively) are glial-specific transporters expressed in astrocytes, largely responsible for glutamate clearance from the extracellular space (Lehre et al., 1995; Rothstein et al., 1994). Several experiments in knockout mice suggest that impaired glutamate uptake by astrocytes has the potential to contribute to the development of seizures (Tanaka et al., 1997).

Glutamate release

Glutamate released from neurons activates metabotropic glutamate receptors (mGluRs), in particular mGluR3 and mGluR5, predominant subtypes expressed in neighbouring astrocytes. Activation of these receptors affects cAMP accumulation and leads to increase in their cytosolic Ca^{2+} (Araque et al., 1999). Increased intracellular Ca^{2+} induces astrocytes to release glutamate. Glutamate once released will modulate synaptic activity in nearby neurons and thus increasing their excitability. Besides, as single astrocytes are in close proximity to a large number of neurons they can promote synchrony of neuronal action potential firing (Fellin and Carmignoto, 2004; Parri et al., 2001). In addition, astrocyte swelling induced by elevated extracellular K^+ or other factors can induce glutamate efflux via volume sensitive anion channels (Kimelberg and Kettenmann, 1990). Both alterations in this glia-derived excitatory pathway and impaired glutamate uptake might increase excitability of the neuron-astrocyte network, favour neuronal synchronization and ultimately predispose neurons to seizure.

Release of metabolic intermediates

Glutamate released during neurotransmission is taken up primarily by neighbouring astrocytes through excitatory amino acid transporters GLAST and GLT-1. A fraction of astrocyte glutamate is then converted to glutamine by glutamine synthetase. Glutamine is in turn exported and taken up by neurons where it is metabolized back to glutamate or GABA

and then packaged into synaptic vesicles (Pow and Robinson, 1994; Shigeri et al., 2004). Several evidences support the idea that impaired glutamate to glutamine cycling can contribute to neuronal hyperexcitability and lead to seizures. An example is a downregulation of glutamine synthetase. This can results in the accumulation of glutamate in astrocytes and thus its build-up in the extracellular space (glutamate uptake into astrocytes need a rapid metabolism of the intracellular glutamate) (Otis and Jahr, 1998). Moreover, its downregulation can partially deplete inhibitory synaptic terminals of GABA and thus impair GABAergic inhibiton. (Liang et al., 2006).

1.5 *Foxg1* gene, structure and function

FoxG1 (*Forkhead box G1*) is an evolutionary conserved transcription factor gene belonging to the forkhead box family, named after the first member, *forkhead*, discovered in Drosophila (123). Forkhead genes play central roles in patterning, morphogenesis, cell fate determination and proliferation (122). Currently, they are divided into 17 subclasses (A to Q), according to the amino acid sequence of their conserved forkhead domains (Kaestner et al., 1993). The *Foxg1* gene is located on the long (q) arm of chromosome 14 at position 13 (Fig.1.13).

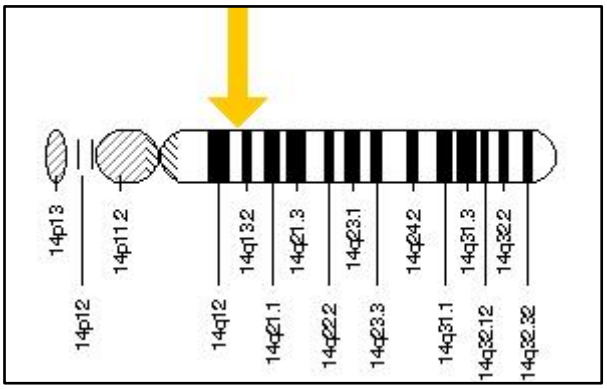

Fig. 1.13 *Foxg1* locus on chromosome 14

The defining feature of FOX proteins is the *forkhead box*, a sequence of 80 to 100 amino acids forming a motif that binds to DNA, highly conserved across all members. It consists in three amino-terminal alpha helices, three beta strands, and two loops. The peculiar folding of the loops around the helices resembles butterfly wings and accounts for the 'winged helix' nickname.

Foxg1, play a central role in the developing telencephalon (Tao and Lai, 1992). Being one of the first TFs expressed in the developing rostral brain it is crucial for many aspects of cerebral cortex development: from cerebral cortex morphogenesis, including early distinction between pallial and subpallial fields, to dorsoventral patterning of the pallium, regulation of the balance between neural progenitor proliferation and differentiation, neocortical layering and tuning of astrogenesis rates. The body of functions exerted by this TF suggest that a proper dosage allele of this gene is extremely crucial, even subtle alterations in its expression can lead to defects on the brain development.

1.6 *Foxg1* in the telencephalic patterning

The telencephalon arises from the most rostral region of the neural tube. The patterning of the telencephalon is regulated by distinct mechanisms operating in different parts of this structure in a concerted action. Regional specification, growth, differentiation and subdivisions of the telencephalon occurs through the action of morphogens. These are signalling molecules secreted from a localized area that direct tissue patterning by forming a concentration gradient thus producing concentration-dependent responses. Thus, by specifying the overall R-C and D-V coordinates, pools of progenitors cells can be given an internal ‘address’ that is then interpreted as regional specification.

Rostro-caudal specification

Starting from E7, the early rostro-caudal patterning of the anterior and posterior neural tissues is mediated from signals coming from the primitive node or organizer and the anterior visceral endoderm (AVE), required for neural induction and maintenance (Thomas and Beddington, 1996) (Fig.1.14a). The AVE, an extra-embryonic tissue underlying the neural plate, secretes molecules like cerberus and dickkopf. These two protein antagonize the effects of posteriorizing molecules expressed by the neural plate, including Wnt and fibroblast growth factor (Fgfs) family members as well as retinoic acid (RA) (Altmann and Brivanlou, 2001; Sasai and De Robertis, 1997)(Fig.1.14b).

a) b)

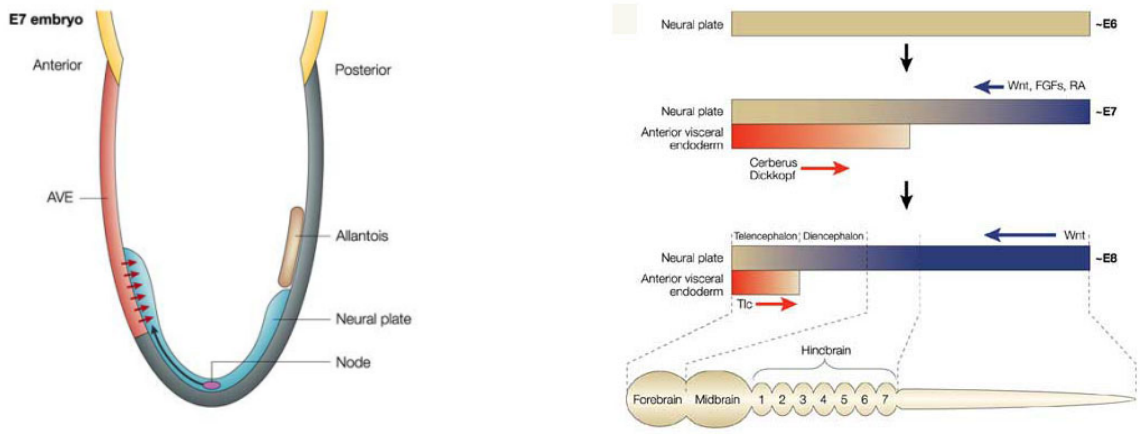

Fig. 1.14 Tissue and signals involved in anterior necural character specification

a) Anterior visceral endoderm (AVE), located beneath the future neural plate

b) Progressive specification of the telencephalon

Modified from (Rallu et al., 2002)

After the anterior neural induction a secondary organizer, the Anterior Neural Ridge (ANR), promotes telencephalic development triggering *Foxg1* expression via Fgf8 secretion (Houart et al., 1998; Shimamura and Rubenstein, 1997). Ablation of the ANR in mice

prevents the expression of the telencephalic markers Foxg1 and Emx1 (Shimamura and Rubenstein, 1997). Besides, also Hedgehog signalling contributes in *Foxg1* induction as demonstrated that its block before telencephalon specification strongly impairs initial levels of Foxg1 expression (Danesin et al., 2009). The concomitant activation of *Foxg1* expression by Fgf8 from the ANR and Shh provided by the prechordal plate, allow a graded *Foxg1* expression: high ventral/anterior to low dorsal/posterior.

Dorso-ventral specification

The initial subdivision defining dorsal and ventral telencephalon is due to the dorsalizing effects of Gli3 (a zinc-finger transcription factor) expression and the ventralizing influence of *Shh* expression. Gli3 knockouts reveals a disrupted dorsal telencephalon development (choroid plexus, cortical hem and hippocampus fail to form and neocortex development is progressively compromised) (Grove et al., 1998; Kuschel et al., 2003; Theil et al., 1999). As for Sonic hedgehog protein (Shh), it is expressed in the ventral midline throughout the development and counteracts the dorsalizing effect of Gli3. *Shh*$^{-}$/$^{-}$ mouse embryos display a telencephalon reduced in size and ventral cell type are lost (Ohkubo et al., 2002). In double mutants mice that lack both *Shh* and *Gli3*, however, ventral patterning is largely rescued suggesting a role for *Shh* in promoting ventral identity by preventing dorsalizaton of the telencephalon rather than a direct promotion of the ventral character. Moreover, it means that other genes acting independently or downstream of *Shh* function to generate ventral cell types (Rallu et al., 2002). This ventralizing signal is mediated by the cooperation of Foxg1 and Fgfs. In *Foxg1* $^{-}$/$^{-}$ mice, the formation of the subpallium is strongly impaired (Xuan et al., 1995) and ventral cells are not rescued by removal of Gli3. Telencephalon is completely lost in *Foxg1/Gli3* double mutant, suggesting that *Gli3* and *Foxg1* are essential for generate and maintain respectively dorsal and ventral subdivisions of the telencephalon (Hanashima et al., 2007). Fgf signalling is essential too for the generation of the ventral cell types (Gutin et al., 2006). It acts in a dose-dependent manner: moderate inhibition of Fgf signalling results in a loss of ventral precursor cells while there is no

telencephalon specification upon deletion of multiple Fgf receptors (Fgfr1,Fgfr2 and Fgfr3)(Paek et al., 2009). *Foxg1* is required for *Fgf8* expression from the ANR (Martynoga et al., 2005) and conversely, *Foxg1* expression is itself regulated by FGF signalling forming a positive feedback loop (Shimamura and Rubenstein, 1997; Storm et al., 2006). Besides, to its key role in determining ventral character in the telencephalon, *Foxg1* is also required to restrict dorsal fates limiting expression of Wnt ligands. Foxg1 binds to *Wnt8b* promoter and represses its transcriptional activity, preventing thus expansion of the Wnt-secreted population (Danesin et al., 2009). Therefore, Foxg1 act as an integrator of a complex network of interactions between several signalling pathways: promotes ventral identity downstream of Shh and concomitantly controls the extension of dorsal territory through direct transcriptional repression of the Wnt ligands (Fig.1.15).

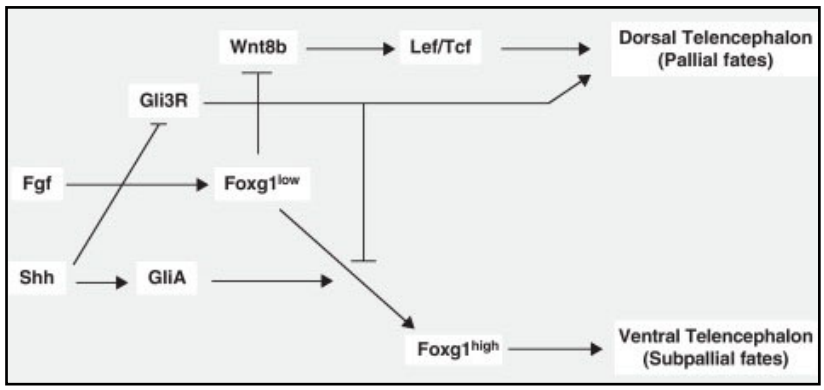

Fig. 1.15 Foxg1, integrator between several signalling pathways

Modified from (Danesin and Houart, 2012)

As a results of R-C and D-V patterning events, the telencephalon will be subdivided in pallial and subpallial territories, characterized by the expression of specific set of TFs. The subpallium will give rise to the medial ganglionic eminence (MGE) and to the lateral ganglionic eminence (LGE) expressing respectively the TFs *Nkx2.1* and *Gsh2*; while in the pallium TFs *Pax6* and empty spiracles homeobox2 (*Emx2*) are expressed along opposite gradients.

1.7 *Foxg1* in cortical arealization

The interplay between intrinsic and extrinsic factors in the telencephalic field will further subdivide the cerebral cortex in distinct anatomical and functional areas. This process is the cortical arealization. Area patterning is a critical development event, even a small change during its steps may lead to severe defect in brain functioning.

In the mouse, cortical arealization starts at early stages (E9.5) with different secreted ligands released from structures lying at the borders of the cortical field. Such molecules, diffusing through the cortical field, will regulate the expression of cortical transcription factor genes in a dose-dependent manner accounting in this way for further generation of concentration gradients of this latter. Transcription factors gradients will finally encode for positional values specifying area identity. Subsequently, from E13.5 onward, cortical arealization will be refined based on information transported by thalamocortical axons (TCA) relaying sensory information from the principal sensory nuclei of dorsal thalamus.

Patterning centres most directly implicated in the cortical arealization are:

1) rostrally, the commissural plate (CoP) secreting Fgfs (Fgf3,8,17,and 18)

2) dorsocaudally, the cortical hem secreting bone morphogenetic proteins (Bmp2,4,5,6,7) and Wnt (Wnt2b, 3a, 5a, tb, 8b)

3) lateroventrally, the cortical antihem secreting epidermal growth factor family members (Tgfα, Nrg1 and Nrg3), Fgf7, as well as the Wnt signaling inhibitor Sfrp2 (Fig.1.16)

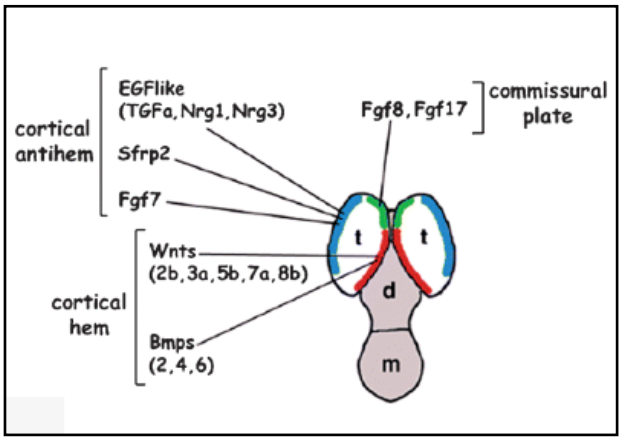

Fig. 1.16 Patterning centers and their secreted ligands implicated in the cortical arealization
Modified from (Mallamaci and Stoykova, 2006)

Several transcription factor genes involved in specification of cortical areas are expressed by neural progenitors of the developing neocortex. They include *Lhx2, Foxg1, Pax6, Emx2, Coup-tf1 and Sp8.* Graded expression of these TFs will impart positional identities to cortical progenitors which is imparted to their neuronal progeny that form the cortical plate.

Foxg1 is expressed in progenitors along a caudo/medial^{low} to rostro/lateral ^{high} gradient. As previously described, *Foxg1* is necessary to establish ventral identity of the telencephalon. Early expression of *Foxg1* is triggered by Fgf8 (Shimamura and Rubenstein, 1997) and Fgf8 is, in turn, down regulated in *Foxg1*$^{-}$/$^{-}$ (Martynoga et al., 2005). Besides, in *Foxg1*$^{-}$/$^{-}$ cortical field is abnormally specified as a hippocampal anlage (Muzio and Mallamaci, 2005) moreover there is an excess of Cajal-Retzius neurons production (Hanashima et al., 2004).

1.8 *Foxg1* in cortical precursors kinetics

During corticogenesis, neural precursors will give rise to all cells populating the cortex. In order to assure a correct final output of neurons and glial cells at the end of the embryonic life, the balance between proliferation and differentiation must be tightly regulated. Control of the cell cycle progression is a major key point in this balance. During the neurogenesis, there is a progressive lengthening of the cell cycle duration that can be largely attributed to a lengthening of the G1 phase. Besides, lengthening of the cycle is accompanied by an increase in the fraction of cells exiting from cell cycle (Q) (Takahashi et al., 1995). The increase in Q is due to a switch from proliferative to differentiative divisions. As the G1 phase length increase, cell division switch from a symmetrical self-renewing to asymmetrical neurogenic differentiating pattern and, lastly to an asymmetrical differentiative one (Calegari and Huttner, 2003; Götz and Huttner, 2005). Therefore, the transition through the G1 to S phase is particularly crucial for proliferative or differentiative fate choice. Major roles in the balance bewtween these two processes are due to Cdk-cyclin

complex inhibitors of the Kip/Cip family (p21^{Cip1}, p27^{Kip1}, p57^{Kip2}) and Ink4 (p16^{Ink4}, p15^{Ink4}, p19^{Ink4} p18^{Ink4}). P21^{Cip1} knockout lead to exhaustion of proliferative pools in embryonic cortical progenitor in vitro culture (Kippin et al., 2005)(Fig.1.17).

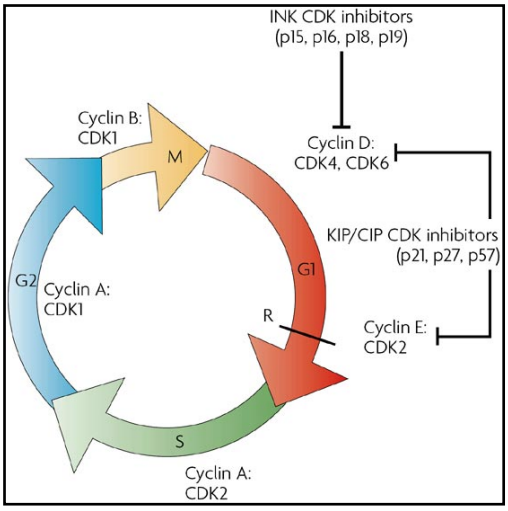

Fig. 1.17 Structure and regulation of the cell cycle

Cyclin-CDK (cyclin-dependent kinase) complexes and their inhibitors (Ink4 family and Kip/Cip family) control the transition from a phase of the cell cycle to the next.

Modified from (Dehay and Kennedy, 2007)

Besides, evidences point to the G1 mode of division relationship as an essential control mechanism of corticogenesis. Cyclin D1 and cyclin E1 overexpression experiments by in utero electroporation in mouse embryo demonstrated there is a causative link between G1 phase and the mode of division. In these experiments, G1 phase reduction promoted apical progenitors self-renewal followed by an increased transition to the basal progenitors compartment and, subsequently an expansion of the basal progenitors compartment at the expense of neurogenesis. Moreover, there is an impact also on laminar fate and cytoarchitecture (Pilaz et al., 2009).

Foxg1 contributes to the development of the telencephalon by maintaining telencephalic progenitor status and ensuring that these progenitors maintain appropriate cell cycle kinetics, particularly in the rostral telencephalon. *Foxg1* is highly expressed in the proliferating cells of the neuroepithelium during the necortical development and its expression decline as the cells become postmitotic. In *Foxg1*$^{-}$/$^{-}$ mice the size of the cerebral hemispheres are reduced; ventral telencephalic development is more severely affected than the dorsal one. Telencephalic neuroepithelial cells are specified but their proliferation is reduced. Besides, there is increased rate of differentiation (leading to early depletion of the

progenitor population), cell cycle lengthening and reduction in apoptosis. (Hanashima et al., 2002; Martynoga et al., 2005; Xuan et al., 1995).

Foxg1 proliferative effects depend on its ability to inhibit the FoxO-Smad transcriptional complex and, therefore, to block $p21^{Cip1}$ induction by TGF-beta signals in neuroepithelial cells. Smad proteins, activated by TGF-beta signaling, form a complex with FoxO proteins to turn on $p21^{Cip1}$ gene. This latter, mediates cell cycle arrest at G1 phase. Dysregulation of p21 has the potential to induce cell cycle exit and thus influence the proliferative fate choices of progenitor cell population. An example are experiments with *Foxg1*$^{+}$/$^{-}$ heterozygous mice where it has been shown that Foxg1 reduces the intermediate progenitor cell population increasing p21 expression. (Siegenthaler et al., 2008). In accordance with this role in progenitors proliferation, *Foxg1* mutant display a remarkable reduction of the telencephalic vesicles due to a compromised growth of the telencephalon. Besides, Foxg1 act with Polycomb factor Bmi-1, repressor of the cell cycle inhibitors p16, p19, and p21. Bmi-1 overexpression rapidly upregulates *Foxg1* that is in turn necessary to mediate promotion of neural progenitor cells (NPCs) self-renewal (Fasano et al., 2009). Furthermore, *Foxg1* overexpression experiments in neural stem cells (NSCs) lead to an expansion of this compartment, possibly by increasing NSCs self-renewal, promotion of progenitor survival and delayed neurogenesis. Moreover, *Foxg1* overexpression under the control of the neuronal lineage-specific promoter Tubulin alpha1 (ptα1) neural progenitors are forced to keep proliferating, thus impairing neuron maturation. (Brancaccio et al., 2010).

1.9 *Foxg1* in the migration of pyramidal neurons

Pyramidal neurons are born within the proliferative layers of the cerebral cortex (Götz and Huttner, 2005). The appropriate laminar position will be achieved not only through vertical migration along radial glial fibers but, like interneurons, they tangentially disperse during their integration in the cortex (O'Rourke et al., 1992). During this phase, pyramidal neuron precursors within the intermediate zone adopt transiently a characteristic

"multipolar" morphology, detach from the radial glia scaffold and initiate axonal outgrowth (Barnes et al., 2007) prior entering the cortical plate (Noctor et al., 2004; Tabata and Nakajima, 2003). As pyramidal neurons transit through these migratory phases *Foxg1* is expressed in a dynamic manner. This dynamic expression is critical; it regulates the assembly and integration of pyramidal neuron precursors into the cortical network (Miyoshi and Fishell, 2012). In a first phase *Foxg1* expression is transiently downregulated in nascent pyramidal neuron precursors. Downregulation occurs precisely at the beginning of the multipolar cell phase, coincident with the starting point of NeuroD1 expression; it is called "early phase". *Foxg1* downregulation is necessary to initiate Unc5d expression, which is critical for the rapid transition to the "late" multipolar phase. Failure in *Foxg1* downregulation at the beginning of the multipolar phase transiently stalls pyramidal neuron precursors within the lower intermediate zone delaying their entry into the cortical plate resulting in a switch in their laminar identity. Subsequently, *Foxg1* upregulation is specifically required for cells to transit out of the multipolar state and enter into the cortical plate. Failure in *Foxg1* upregulation results in a regression to the early multipolar phase by re-expressing genes associated with this phase (*Neurod1 and Uncd5*) and in a permanently loss of pyramidal neuron precursors to enter into the cortical plate. Thus, timing and duration of the multipolar phase during tangential neuronal migration is precisely regulated by *Foxg1* activity and is therefore crucial to the assembly of the laminar organization suggesting once again that the cortex is highly sensitive to *Foxg1* dosage.

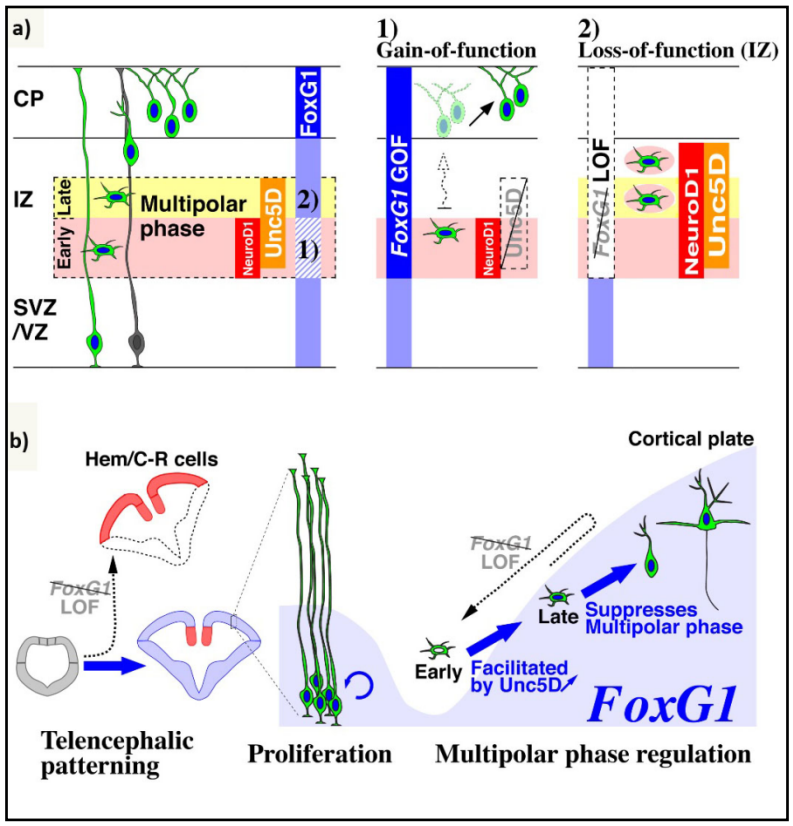

Fig. 1.18 Dynamic *Foxg1* expression in pyramidal neurons

a) Dynamic *Foxg1* expression through the multipolar phase of pyramidal neurons

b) Scheme summarizing *Foxg1* roles in pyramidal neuron development.

Modified from (Miyoshi and Fishell, 2012)

1.10 *Foxg1* and neuronal differentiation

During early phases of cortical development, *Foxg1* is essential for the correct neurogenesis of the telencephalic progenitor cells. However, the protein is still expressed in post-natal tissues, suggesting that its function could be essential also in post-mitotic neurons. In fact, several evidences are starting to cast light on its function in neuronal differentiation.

In particular, *Foxg1* has a role in the timing of layer neurogenesis. It confers the sequence of deep layer (DL) and upper layer (UL) competence through *Tbr1* repression (Toma et al., 2014). *Foxg1* is a nuclear-cytosolic transcription factor and its intracellular localization is controlled post translationally (Regad et al., 2007). Specifically, it is alternated between the nucleus and the cytoplasm: in areas of active neurogenesis *Foxg1* is predominantly confined in the nucleus while it localizes in the cytoplasm in early neuronal

differentiation areas. In the nucleus, Foxg1 act as a transcriptional repressor; targets examples include FGFs, Shh and cell-cycle inhibitors such as $p21^{Cip1}$ (Seoane et al., 2004). In the cytoplasm, Foxg1 inhibit TGF-β signalling by binding to Smad and FoxO transcription factor (Dou et al., 1999; Seoane et al., 2004).

Recent studies, started to provide insights on Foxg1 subcellular localization (Pancrazi et al., 2015). It has been shown that a fraction of Foxg1, having a unique domain responsible for its targeting, localizes in the mitochondria. Mitochondria have a role in controlling fundamental processes in neurodevelopment and neuroplasticity, including the differentiation of neurons, the growth of axons and dendrites, and finally formation and reorganization of synapse (Gioran et al., 2014; Mattson et al., 2008). Foxg1 may represent thus a key link between mitochondrial function and neuronal differentiation. Full-length Foxg1 forms (both mitochondrial and cytosolic) promotes mitochondrial fission and cellular proliferation, whereas mt-Foxg1 form (proteolized form, exclusively mitochondrial) favors mitochondrial fusion and an early phase of neuronal differentiation.

Besides, *Foxg1* overexpressed under the control of the neuronal lineage-specific Tubulin alpha 1 promoter (pTα1), it force to keep proliferating neural progenitors (NP). However, if the transgene is shut down, NPs exit cell cycle and the result is a remarkable increase of the neuronal output. Furthermore, these neurons show a prominent neurite overgrowth (Brancaccio et al., 2010).

Moreover, in experiments done using three-dimensional neural cultures derived from induced pluripotent stem cells (iPSCs) of individuals with severe idiopatic ASD, it has been found that *Foxg1* overexpression is correlated with an increase in proliferation and number of GABA precursors cells (Mariani et al., 2015). In addition to the GABAergic neuron overproduction, there were evidences of neurite overgrowth and increased spine density.

1.11 *Foxg1* in astrogenesis control

Recent studies revealed the implication of *Foxg1* in the astrogenesis. In particular, in vitro studies made by Brancaccio et al. (2010), demonstrated that overexpression of *Foxg1* in neural stem cells (NSCs) enlarge this compartment and halved their astroglial output possibly because of impaired commitment of these cells to glial fates and defective progression of early glia committed progenitors. Until now, in vertebrates no one reported anti-gliogenic activity of *Foxg1*, however this activity is not phylogenetically novel. Two Drosophila *Foxg1* orthologs, Sloppy paired-1 and -2 (*Slp1* and *Slp2*), have been shown to promote neurogenesis at the expenses of gliogenesis (Bhat et al., 2000) and *Foxg1* rescues the *Slp1&2* null phenotype (Mondal et al., 2007). An explanation to the behaviour of *Foxg1*-GOF NSCs could rely on the unbalanced expression of *Hes1*, a key promoter of NSC self-renewal (Ohtsuka et al., 2001) and key gliogenesis promoters such *Coup-tf1*, *Nf1a* and *Olig2* (Naka et al., 2008; Ono et al., 2008).

1.12 West Syndrome (WS)

West syndrome is a severe epilepsy syndrome composed of the triad of infantile spasms, an interictal electroencephalogram (EEG) pattern termed hypsarrhythmia, and mental retardation. However the diagnosis can be made even if one of the three elements is missing (according to the international classification) (Taghdiri and Nemati, 2014).

The syndrome's namesake, Dr W. J. West, gave the first detailed description of infantile spasms, which occurred in his own child, in the 1840s.

West syndrome is an age-dependent expression of a damaged brain, and most patients with infantile spasms have some degree of developmental delay. The term infantile spasm is used to describe the seizure type, the epilepsy syndrome, or both.

Epidemiology

Infantile spasm constitutes 2% of childhood epilepsies but 25% of epilepsy with onset in the first year of life. The rate of infantile spasm is estimated to be 2.5-6.0 cases per 10,000 live births (Hrachovy and Frost, 1989). Males are affected by infantile spasm slightly more often than females. Ninety percent of infantile spasms begin in infants younger than 12 months. Peak onset is at age 4-6 months (Zupanc, 2003).

Clinical manifestation

Spasms begin with a sudden, rapid, tonic contraction of trunk and limb musculature that gradually relaxes over 0.5-2 seconds. Contractions can last 5-10 seconds. The intensity of spasms may vary from a subtle head nodding to a powerful contraction of the body. Infantile spasms usually occur in clusters, often several dozen, separated by 5-30 seconds. Spasms frequently occur just before sleep or upon awakening. Spasms can be flexor, extensor, or a mixture of flexion and extension that is the most common type. In 70-95% of patients, the onset of spasms is accompanied by an arrest or regression of psychomotor development.

Moreover, patients may exhibit from moderate to severe growth delay, but this is a nonspecific finding as it could reflect the underlying brain injury. Besides, patients with infantile spasms demonstrates abnormalities in mental status function, specifically delays in developmental signs consistent with developmental delay or regression. EEG abnormalities consist in a pattern called ‘hypsarrhythmia’: high amplitude and irregular waves and spikes in a background of chaotic and disorganized activity. Basically, brain electrical activity is very chaotic and disorganized with no recognizable pattern, whereas a normal EEG shows clear separation between each signal and visible pattern. The ‘chaotic’ pattern becomes more organized with time and in most cases of infantile spasms, hypsarrhythmia either disappears or improves during a cluster of spasms and/or REM sleep. Hypsarrhythmia rarely persists beyond the age of 24 months.

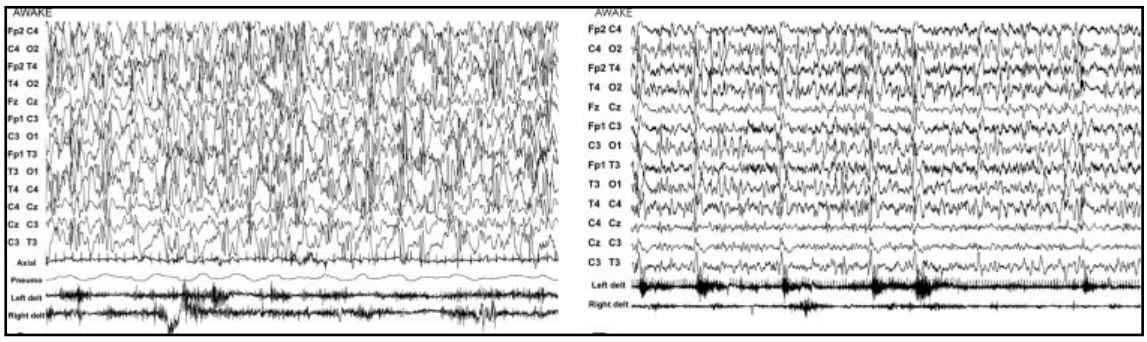

Fig. 1.19 EEG recordings in a West syndrome patient

Modified from (Bertossi et al., 2014)

Etiology

Infantile spasms are believed to reflect abnormal interactions between the cortex and brainstem structures. Focal lesions early in life may secondarily affect other sites in the brain, and hypsarrhythmia may represent this abnormal activity arising from multiple brain sites. The frequent onset of infantile spasms in infancy suggests that an immature central nervous system (CNS) may be important in the syndrome's pathogenesis.

Infantile spasms can be classified according to their suspected etiology as symptomatic, cryptogenic, or idiopathic. Patients are diagnosed with symptomatic infantile spasms if an identifiable factor is responsible for the syndrome (ILAE Task Force, 1989). Virtually any disorder that can produce brain damage can be associated with infantile spasms. If there is no cause identified but a cause is suspected and the epilepsy is presumed to be symptomatic, the infantile spasm is cryptogenic (Matsumoto et al., 1981; Vigevano et al., 1993). Patients may be considered to have idiopathic infantile spasms if there is a possible hereditary predisposition, such a family history of epilepsy (ILAE Task Force, 1992). Two specific genetic defects have a phenotypic presentation similar to that of the early onset of infantile spasms. The first is an abnormality in the short arm of chromosome X. The gene *ARX* is associated with a wide variety of structural abnormalities and early onset infantile spasms.

The second abnormality is in the cyclin-dependent kinase-like protein 5 (CDKL5) and has similar phenotypic presentations to those of *ARX* mutations.

1.13 Relationship between WS and FOXG1

Duplications of chromosome 14q12 harbouring *FOXG1* locus have been recently reported in patients with infantile spasm and developmental delay of variable severity (Brunetti-Pierri et al., 2011; Pontrelli et al., 2014; Yeung et al., 2009). Size of the duplication may differ, from 88 Kb to 84 Mb. To date, 15 patients with 14dup. including *FOXG1* have been reported and nine of them presented epilepsy with a mean age at onset 4.9 months. Therefore, a new theory is emerging regarding the potential role of *FOXG1* duplication in determining infantile spasm, developmental delay and severe epilepsy because of increased gene dosage. The contribution of *FOXG1* in the phenotype of reported patients is related to its key function in brain development.

However, there are some reports of individuals with 14q12 duplication, including *FOXG1*, with normal phenotype, intellect and no epilepsy (Amor et al., 2012; Shaikh et al., 2009). The explanation to these phenotypic variabilities could be an incomplete penetrance of *FOXG1* duplication, the variable involvement of its regulatory elements other genes in the duplicated regions and genetic mosaicism (Brunetti-Pierri et al., 2011; Falace et al., 2013; Tohyama et al., 2011).

Remarkably, *Foxg1* overexpression in neuronal cultures increase neuronal output while reducing the astroglial one and besides it promotes neurite growth (Brancaccio et al., 2010). Neurite outgrowth (including axons and dendrites) may determine the hyperexcitability of the cortex because of the enlarged afferent basin of neurons. Besides, if the ratio astrocytes/neurons is lowered, astrocytes function in neurotransmitter and potassium clearance upon neuronal firing will be impaired and again, this impact on

neuronal excitability. All these phenomena may contribute to abnormal electrical activities within the brain (like hypsarrhythmia) and support the role of *FOXG1* in the West syndrome.

2. AIM OF THE WORK

Aim of this study was to model etiopathogenetic mechanisms linking FOXG1 duplication to neurodevelopmental and neurological disorders peculiar to human patients affected by the FOXG1-duplication-associated variant of the West syndrome.

Such modeling was performed in mutant *Foxg1*-GOF mouse models as well in genetically engineered cultures of cortico-cerebral murine precursors.

3. MATERIAL AND METHODS

3.1 Mouse handling

Transgenic founders of *Foxg1*$^{+/+}$*;Tg:Tre-Foxg1-IRES-Egfp*$^{+/-}$ line E and *Foxg1*$^{+/+}$*;Tg:Tre-Foxg1-IRES-Egfp*$^{+/-}$ line D were generated at the Core Facility for Conditional Mutagenesis of the San Raffaele Scientific Institute, Milan, Italy. The "Tre-Foxg1-IRES-Egfp" transgene was delivered to CBA1xC57Bl6 zygotes by subzonal injection of the lentiviral vector LV_TREt-Foxg1-IRES-EGFP (Fig. 1A) (Brancaccio et al., 2010). Injected embryos were implanted in CD1 foster mothers. Three, PCR-positive, male founders were selected, in the Laboratory of Cerebral Cortex Development, at SISSA, Trieste, Italy. These mice and their transgenic progenies were repeteadly backcrossed against a CD1 outbred background (>15 generations), so obtaining three single-transgene insertion, CD1-congenic subfounders, "C", "D" and "E".

Foxg1$^{tTA/+}$ founders (Hanashima et al., 2002) were kindly provided by Dr. Ugo Borello, at Inserm U846, Stem Cell and Brain Research Institute, Bron, France

Wild type mice (strains CD1 purchased from Harlan-Italy) used in this study were maintained at the SISSA mouse facility.

Animals handling and subsequent procedures were in accordance with European laws [European Communities Council Directive of November 24, 1986 (86/609/EEC)] and with National Institutes of Health guidelines.

Embryos were staged by timed breeding and vaginal plug inspection.

3.2 Validation of *Foxg1*-GOF transgenic line "E" in vitro

Cortico-cerebral precursors were harvested from E12.5 *Tre-Foxg1-IRES-Egfp*$^{+/-}$mice, acutely infected by LV_Pgk1p-rtTAM2 at m.o.i = 8 and cultured as floating neurospheres in pro-proliferative medium [1:1 DMEM-F12, 1X Glutamax (Gibco), 1X N2 supplement (Invitrogen), 1mg/ml BSA, 0.6% w/v glucose, 2µg/ml heparin (Stemcell technologies), 20ng/ml bFGF (Invitrogen), 20ng/ml EGF (Invitrogen), 1X Pen/Strept (Gibco), 10pg/ml

fungizone (Gibco)] , under 2μg/ml doxycyclin, for 4 days. EGFP expression was firstly evaluated by fluorescence microscope at DIV 4. Subsequently, part of the culture was transferred to polylysinated coverslips and kept under pro-differentiative medium [1:1 DMEM-F12, 1X Glutamax, 1X N2 supplement, 1X B27 supplement, 6 mg/ml glucose, 1mg/ml BSA, 2.0 μg/ml heparin, 5% heat inactivated FBS], supplemented with 2μg/ml doxycyclin, when required, for 5 more days. EGFP/Tubβ3 immunoprofiling was performed at DIV 9.

3.3 Primary, neuronal, astroglial and mixed cultures

3.3.1 Cortico-cerebral neuronal and mixed cultures

Cortical tissue from E16.5 mice was chopped to small pieces for 5 minutes, in the smallest volume of ice-cold 1X PBS-0,6% glucose-0,1% DNaseI. The minced tissue was then resuspended and digested in 0.25mg/ml trypsin- 4mg/ml DNAseI for 5 minutes at 37°C. Digestion was stopped by adding ≥1.5 volumes of DMEM/F12/10%FBS. Cortices were spinned down and transferred to differentiative medium. The suspension was pipetted 5-8 times with a P1000 gilson pipette and undissociated tissue was left to sediment for 1-2 minutes. The supernatant was harvested and the living cells counted. 1x10^6 cells were plated on poly-L-Lysine coated 12 multiwell plates, in 600 μl of culturing medium: Neurobasal-A, 1X Glutamax (Gibco), 1X B27 supplement (Invitrogen), L-glutamate 25μM, 25μM β-Mercaptoethanol, 2% FBS, 10 μM Cytosine β-D-arabinofuranoside "AraC" (Sigma), 1X Pen/Strept (Gibco), 10 pg/ml fungizone (Gibco)]. Medium was half-replaced with fresh one every 3.5 days.

The same protocol was followed for mixed cultures, except for the addition of AraC which was omitted.

When required, neuronal and mixed cultures were infected with dominant negative LVs at day in vitro 1 (DIV1) as shown in Figure R13. Each LV was used at m.o.i = 8. 2 μg/ml of

doxycycline (Clontech) was added at DIV 5 except for the infection with LV_dn CREB and its relative control where doxycycline has been lowered to 0.062 µg/ml.

As for *Foxg1*-gain of function neuronal cultures, primary cortical precursors were harvested from E14.5 mice. The same neuronal culture procedure as previously described was followed. Infection has been made at E15.5 with LV_pTα1-rtTA2S-M2 and LV_Tre-Foxg1-EGFP or LV_Tre-EGFP. Each LV was used at m.o.i = 8.

3.3.2 Astroglial cultures

On day 0, neural precursors were isolated from E12.5 embryonic cortices and plated onto uncoated 24 multiwell (BD Falcon) after gentle mechanical dissociation to single cells. $3x10^5$ cortical precursors were plated for each well in 300µl of serum free pro-proliferative medium [1:1 DMEM-F12, 1X Glutamax (Gibco), 1X N2 supplement (Invitrogen), 1mg/ml BSA, 0.6% w/v glucose, 2µg/ml heparin (Stemcell technologies), 20ng/ml bFGF (Invitrogen), 20ng/ml EGF (Invitrogen), 1X Pen/Strept (Gibco), 10pg/ml fungizone (Gibco)] and cultured as floating neuropspheres. On day in vitro 2 (DIV2), if necessary neurospheres were harvested by centrifugation (300g for 3' at RT) and dissociated by trypsin 1X (Sigma) at RT for 2'. Trypsin was neutralized by adding 1 volume of DMEM/F12 medium containing Soy bean Trypsin Inhibitor140 µg/ml and DNAseI 10 µg/ml. Afterwards, the cells were centrifugated (200g for 7' at RT) resuspended and ri-plated at $3x10^5$ in pro-proliferative medium as on day 0. On day in vitro 4 (DIV4), the neurospheres were dissociated as previously described and resuspended in a differentiative – medium [1:1 DMEM, Glutamax (Gibco) , 10% FBS] at $3x10^5$ on 200 µg/ml poly-L-lysine-coated 12 multiwells. Medium was half-replaced with fresh one every 3.5 days.

When required, astroglial cultures were infected at day 0 with LV_dn as shown in figure R13. Each LV was used at m.o.i=8. 2 µg/ml of doxycycline (Clontech) was added at DIV 9 except for the infection with LV_dn CREB and its relative control where doxycycline has been lowered to 0.062 µg/ml.

3.4 Lentiviral production and titration

Third generation self-inactivating (SIN) lentiviral vectors were produced as previously described (Follenzi and Naldini, 2002) with some modifications. Briefly, 293T cells were co-transfected by LipoD (SignaGen) with the transfer vector plasmid together with the three auxiliary plasmids (pMD2 VSV.G, pMDLg/pRRE, pRSV-REV). The conditioned medium was collected after 24 and 48 hrs, filtered and ultracentrifugated at 50000 RCF on a fixed angle rotor (JA 25.50 Beckmann Coulter) for 150 min at 4°C. Viral pellets were resuspended in PBS without BSA (Gibco).

Lentiviral vectors were generally titrated by Real Time quantitative PCR after infection of HEK293T cells, as previously reported (Sastry et al., 2002). One end point fluorescence – titrated LV was included in eeach PCR titration session and PCR-titers were converted into fluorescence equivalent titers throught the study.

3.5 Lentiviral plasmids constructions

Basic DNA manipulations (extraction, purification, ligation) as well as bacterial cultures and transformation, media and buffer preparations were performed according to standard methods. Restriction enzymes were obtained from Promega and New England Biolabs; DNA fragments were purified from agarose gel by the QIAquick Gel Extraction Kit (QIAGEN). Plasmids were grown in E.Coli, Xl1-blue or ElectroMAX^{TM} Stbl4^{TM} Competent Cells (Invitrogen).

Lentiviral vectors employed in this study include:

-LV_pPgk1-rtTA2S-M2 is the “driver lentivirus” described in (Spigoni et al., 2010)

-LV_TREt-IRES2-EGFP derived from LV_TREt-luc-IRES2-EGFP (Brancaccio et al., 2010), via deletion of the luc cassette

-LV_pTα1-rtTA2S-M2 (Brancaccio et al., 2010)

-LV_Tre-Foxg1-EGFP (Brancaccio et al., 2010)

-LV_Tre-EGFP (Brancaccio et al., 2010)

Dominant negative (DN) constructs were builded from LV_TREt-IRES2-EGFP (Brancaccio et al., 2010) by replacing the EGFP cassette with the DN coding sequence (cds).

DN [ref]	DN cds
Fos-DN (A-Fos, JBC272(30): 18586–18594 Olive et al., 1997)	ATGGACTACAAGGACGACGATGACAAGCATATGGCTAG CATGACTGGTGGACAGCAAATGGGTCGGGATCCTGACC TGGAACAACGTGCTGAGGAACTGGCCCGTGAAAACGAA GAGCTGGAAAAAGAGGCCGAAGAGCTGGAGCAGGAACT GGCAGAACTGGAGGCGGAGACAGACCAACTAGAAGATG AGAAGTCTGCTTTGCAGACCGAGATTGCCAACCTGCTG AAGGAGAAGGAAAAACTAGAGTTCATCCTGGCAGCTCA CCGACCTGCCTGCAAGATCCCTGATTAA
Egr1-DN (Egr1/Zn, Endocrinology 149(12):6311–6325 Mayer et al., 2008)	ATGGTTGACTACAAGGACCACGACGGTGACTACAAGGA CCACGACATCGACTACAAGGACGACGACGACAAGCCAA AAAAGAAGAGAAAGGTGCCAAAAAAGAAGAGAAAGGTA TACCCCAACCGGCCCAGCAAGACACCCCCCCATGAACG CCCATATGCTTGCCCTGTCGAGTCCTGCGATCGCCGCT TTTCTCGCTCGGATGAGCTTACCCGCCATATCCGCATC CACACAGGCCAGAAGCCCTTCCAGTGTCGAATCTGCAT GCGTAACTTCAGTCGTAGTGACCACCTTACCACCCACA TCCGCACCCACACAGGCGAGAAGCCTTTTGCCTGTGAC ATTTGTGGGAGGAAGTTTGCCAGGAGTGATGAACGCAA GAGGCATACCAAAATCCATTTAAGACAGAAGGACAAGA

	AAGCAGACAAAAGTGTGGTGGCCTCCCCGGCTGCCTCT TCACTCTCTTCTTACCCATCCTGA
Cebp-DN (A-CebpA, JBC 274:211-217 Park et al., 1999)	ATGGACTACAAGGACGACGATGACAAGCATATGGCTAG CATGACTGGTGGACAGCAAATGGGTCGGGATCCTGACC TGGAACAACGTGCTGAGGAACTGGCCCGTGAAAACGAA GAGCTGGAAAAAGAGGCCGAAGAGCTGGAGCAGGAA**CT** **G**GCTGAACT**G**GAGCAGAAGGTGTTGGAGTTGACCAGTG ACAATGACCGCCTGCGCAAGCGGGTGGAACAGCTGAGC CGTGAACTGGACACGCTGCGGGGTATCTTCCGCCAGCT GCCTGAGAGCTCCTTGGTCAAGGCCATGGGCAACTGCG CGTGA
Nfkb-DN (mmu-IKBaM, Mol Cell Biol 16(7):3554–3559 Schwarz et al., 1996 & Science 274(5288):787-789 Van Antwerp et al., 1996)	ATGTTTCAGCCAGCTGGGCACGGCCAGGACTGGGCCAT GGAGGGCCCGCGGGATGGCCTCAAGAAGGAGCGCTTGG TGGACGATCGCCACGACGCTGGCCTGGACGCCATGAAG GACGAGGAGTACGAGCAAATGGTGAAGGAGCTGCGGGA GATCCGCCTGCAGCCGCAGGAGGCGCCGCTGGCCGCCG AGCCCTGGAAGCAGCAGCTCACGGAGGACGGAGACTCG TTCCTGCACTTGGCAATCATCCACGAAGAGAAGCCGCT GACCATGGAAGTCATTGGTCAGGTGAAGGGAGACCTGG CCTTCCTCAACTTCCAGAACAACCTGCAGCAGACTCCA CTCCACTTGGCTGTGATCACCAACCAGCCAGGAATTGC TGAGGCACTTCTGAAAGCTGGCTGTGATCCTGAGCTCC GAGACTTTCGAGGAAATACCCCTCTACATCTTGCCTGT GAGCAGGGCTGCCTGGCCAGTGTAGCAGTCTTGACGCA GACCTGCACACCCCAGCATCTCCACTCCGTCCTGCAGG CCACCAACTACAATGGCCACACGTGTCTGCACCTAGCC TCTATCCACGGCTACCTGGCCATCGTGGAGCACTTGGT GACTTTGGGTGCTGATGTCAACGCTCAGGAGCCCTGCA ATGGCCGGACAGCCCTCCACCTTGCGGTGGACCTGCAG AATCCTGACCTGGTTTCGCTCTTGTTGAAATGTGGGGC TGATGTCAACAGGGTAACCTACCAAGGCTACTCCCCCT ACCAGCTTACCTGGGGCCGCCCAAGTACCCGGATACAG CAGCAGCTGGGCCAGCTGACCCTGGAAAATCTCCAGAT GCTACCCGAGGCTGAGGATGAGGAGGCCTATGACGCTG AGGCCGAGTTCGCTGAGGATGAGCTGCCCTATGATGAC

	TGTGTGTTTGGAGGCCAGCGTCTGACATTATAA
Creb-DN (A-Creb, Mol Cell Biol 18(2):967-977 Ahn et al., 1998)	ATGGACTACAAGGACGACGATGACAAGCATATGGCTAG CATGACTGGTGGACAGCAAATGGGTCGGGATCCTGACC TGGAACAACGTGCTGAGGAACTGGCCCGTGAAAACGAA GAGCTGGAAAAAGAGGCCGAAGAGCTGGAGCAGGAA**CT** **G**GCAGAACT**G**GAGAACAGAGTGGCAGTGCTTGAAAACC AAAACAAAACATTGATTGAGGAGCTAAAAGCACTTAAG GACCTTTACTGCCACAAGTCAGATTAA

3.6 Quantitative RT-PCR

In each experimental session, $1x10^6$ cells were processed for RNA extraction by Trizol® Reagent (Ambion™) according to manufacturer's instructions. RNA preparations were treated by TURBO™DNase (2U/µl)(Ambion™) 1 hour at 37°C. At least 0.750 µg of genomic DNA-free total RNA from each sample was retro-transcribed by SuperScriptIII™ (Invitrogen) in the presence of random hexamers, according to manufacturer's instructions. 1/100 of the resulting cDNA was used as substrate of any qPCR reaction. Limited to intronless amplicons, negative controls PCRs were run on RT(-) RNA preparations. PCR reactions were performed by the SsoAdvanced STBR Green Supermix ™ platform (Biorad), according to manufacturer's instructions. Per each transcript under examination and each sample, cDNA was PCR-analyzed in technical triplicate and result averaged. Averages were further normalized against *Gapdh.* Experiments were performed in at least biological triplicates and analyzed by Student's t test.

Oligos were as follows:

mFoxg1cds/F 5′ CGA CCC TGC CCT GTG AGT CTT TAA G 3′

mFoxg1cds/R 5′ GGG TTG GAA GAA GAC CCC TGA TTT TGA TG 3′

mGapdh5/F 5′ ATC TTC TTG TGC AGT GCC AGC CTC GTC 3′

mGapdh5/R 5′ GAA CAT GTA GAC CAT GTA GTT GAG GTC AAT GAA GG 3′

mmuGluA1/F 5' TCC ATG TGA TCG AAA TGA AGC ATG ATG GAA TCC 3'

mmuGluA1/R 5' CGA TGT AGG TTC TAT TCT GGA CGC TTG AGT TG 3'

mmuGluN1/F 5' CGA GGA TAC CAG ATG TCC ACC AGA CTA AAG A 3'

mmuGluN1/R 5' CTT GAC AGG GTC ACC ATT GAC TGT GAA CT 3'

mmuGluD1/F 5' AAG GAC TGA CTC TCA AAG TGG TGA CTG TCT T 3'

mmuGluD1/R 5' CCT TAG CCA GTG CAT CCA GCA CAT CTA TG 3'

mmuGabra1/F 5' AAA CCA GTA TGA CCT TCT TGG ACA AAC AGT TGA C 3'

mmuGabra1/R 5' GTG GAA GTG AGT CGT CAT AAC CAC ATA TTC TC 3'

mmuvGluT1/F 5' CAT GGA GTT CCG GCA GGA GGA GTT TCG 3'

mmuvGluT1/R 5' CGT CGG CAC TCA GCT CCA GTG TCT C 3'

mmuvGluT2/F 5' TTT TGC TGG AAA ATC CCT CGG ACA GAT CTA CA 3'

mmuvGluT2/R 5' CTT ACC GTC CTC TGT CAG CTC GAT GG 3'

mFos/F1N 5' CTG ACA GAT ACA CTC CAA GCG GAG ACA G 3'

mFos/R1N 5' ACA TCT CCT CTG GGA AGC CAA GGT CAT C 3'

mEgr1/F1 5' AAC CCT ATG AGC ACC TGA CCA CAG AGT C 3'

mEgr1/R1 5' CGT TTG GCT GGG ATA ACT CGT CTC CAC 3'

mEgr2/F1 5' AGG CCC CTT TGA CCA GAT GAA CGG AGT 3'

mEgr2/R1 5' GTT TCT AGG TGC AGA GAT GGG AGC GAA G 3'

Protocol was as follows:

- Incubate at 98°C for 00:04:00
- Incubate at 98°C for 00:00:10
- Incubate at Ta°C for 00:00:15
- Incubate at 72°C for 00:00:20
- Incubate at 78°C for 00:00:03+ plate read
- Incubate at 80°C for 00:00:03+ plate read
- Incubate at 82°C for 00:00:03+ plate read
- Go to line 2 for 39 more times
- Melting curve from 60°C to 98°C, increment 0.5°C for 00:00:03 + plate read
- END

Ta	
60	*GluA1,GluN1, GluD1, Gabra1, vGluT1, vGluT2*
62	*Foxg1cds*
63	*Fos, Egr1, Egr2*

70	*Gapdh5*

3.7 Immunofluorescence

For immunocytofluorescence cells were fixed directly on poly-L-lysine coated 1 cm Ø glass coverslips in 24 multiwell plates with 4% paraformaldehyde (PFA) for 20 min at RT. Subsequently cells were washed 3 times in 1X PBS.

As for immunofluorescence on brain sections, slices were allowed to dry at least one hour at RT, they were post-fixed 5 minutes in 4% paraformaldehyde at RT, followed by three washes in 1X PBS. In all cases, samples were subsequently treated with blocking mix (1X PBS; 10% FBS; 1mg/ml BSA; 0.1% Triton X100) for at least 1 hour at RT. After that, incubation with primary antibody was performed in blocking mix, overnight at 4°C. The day after, samples were washed in "1X PBS-0.1% Triton X-100" 3 times for 5 minutes and then incubated with a secondary antibody in blocking mix, for 2 hours at RT. Samples were finally washed in 1X PBS for 5 minutes, 3 times and subsequently counterstained with DAPI (4', 6'-diamidino-2-phenylindole) and mounted in Vectashield Mounting Medium (Vector). In case of immunos with anti-Cux1, rabbit polyclonal (Santa Cruz, 1:20) antigen retrieval was performed by baking samples in 500 ml of 10 mM citrate buffer (pH 6.0), at 700 W for 5 min.

The following primary antibodies were used: anti-GFP, chicken polyclonal (Abcam ab13970, 1:400); anti-Foxg1, rabbit polyclonal (gift from G.Corte, 1;200); anti-Tubβ3, mouse monoclonal, (clone Tuj1, Covance MMS-435P, 1:1000); anti-NeuN, mouse monoclonal (clone A60, Millipore MAB 377, 1:80); anti-GFAP, rabbit polyclonal (DAKO Z0334, 1:500); anti-S100β, rabbit polyclonal (DAKO Z0311, 1:300); anti-Foxp2, rabbit polyclonal (Abcam, ab16046 1:800); anti-Ctip2, rat monoclonal (Abcam ab18465, 1:200); anti-PV, mouse monoclonal (Swant 235, 1:5000); anti-SST, rat monoclonal (Millipore MAB 354, 1:50); anti-CR, rabbit polyclonal (Swant 7697, 1:1000).

Secondary antibodies were conjugates of Alexa Fluor 488, and Alexa Fluor 594 (Invitrogen, 1:600).

3.8 Images acquisitions

Immunoprofiled cultured cells and brain sections were photographed on a Nikon TI-E microscope, equipped with 20X or 40X objectives and a Hamamatsu C4742-95 camera.

For figure R4 brain sections were photographed on a Nikon TI-E confocal microscope equipped with 20 or 40X objectives. Samples were collected as 6µm Z-stacks of 1024*1024 pixel images.

For figure R7 brain section has been photographed on Leica confocal microscope equipped with 40X objectives. Samples were collected as 6µm Z-stacks of 1024*1024 pixel images.

All images were processed using Adobe 9.0.2 Photoshop 2 CS2 software and ImageJ.

3.9 EEG recordings

EEG recordings were performed by Dr. Manuela Allegra in the laboratory of Dr. Matteo Caleo at the CNR Neuroscience Institute in Pisa.

Briefly, electrical activity of P41 Foxg1-GOF and WT controls (n=4,4) was monitored within the hippocampus. A bipolar electrode with its 500 placed µm-spaced pins ending in CA1 and DG/hilus regions was used. It was secured to the skull and electrical activity was monitored for three days, two hours per day. The temporal distribution of spikes, i.e voltage fluctuations with amplitude exceeding 4 standard deviations (SD) was analyzed. Spikes were categorised as "isolated" and "clustered", if alone or groupable in sets of at least two ones, spaced less than 0,5 sec, respectively. Spike clusters were further distinguished into interictal, if lasting <4sec, and ictal, i.e. lasting ≥4sec

3.10 Behavioral analysis, kainate-evoked seizures

Behavioral analysis was performed in collaboration with Prof. Yuri Bozzi and Dr. Giovanni Provenzano, at Centre for Integrative Biology (CIBIO), in Trent, and SISSA, in Trieste.

Each mouse, at the P35/40 stage, was weighted and kainic acid (SIGMA) was administered 20mg/kg by intraperitoneal injection. Subsequently mice were observed for 2 hours and a score, based on the Racine's stages, was given every ten minutes.

Racine's stages:

Stage 0: normal activity

Stage 1: immobility

Stage 2: forelimb and/or tail extension, rigid posture, "hunchback position"

Stage 3: repetitive movements, head bobbing

Stage 4: rearing and falling with forelimb clonus and "praying posture" (limbic motor seizure, LMS)

Stage 5: continuous rearing and falling

Stage 6: severe tonic-clonic seizures (TCS)

Stage 7: death

At the end of the behavioral observation mice were sacrificed, brains were dissected and included into Killik (Bio-Optica) and further analyzed by in situ hybridization performed by Dr. Giovanni Provenzano.

3.11 Statistical analysis

Generally, when not otherwise stated, experiments were performed at least in biological triplicate. Results were averaged and their statistical significance was evaluated by one-way ANOVA (* $p<0.5$; ** $p<0.01$; *** $p<0.001$) or χ-square test.

4. RESULTS

4.1 Generation and preliminary characterization of *Foxg1*-GOF mutant mice

To model etiopathogenetic mechanisms linking exaggerated *FOXG1* allele dosage to pronounced neuronal hyperexcitability peculiar to West syndrome patients, we generated mice gain of function for *Foxg1*, by lentiviral TetOFF transgenesis.

The *"Tre-Foxg1-IRES-Egfp"* transgene was delivered to CBA1xC57Bl6 zygotes by subzonal injection of the lentiviral vector LV_TREt-Foxg1-IRES-EGFP (Fig. 1A) (Brancaccio et al., 2010). Injected embryos were implanted in CD1 foster mothers. Three, PCR-positive, male founders were selected. These mice and their transgenic progenies were repeteadly backcrossed against a CD1 outbred background (>15 generations), so obtaining three single-transgene insertion, CD1-congenic subfounders, "C", "D" and "E".

To preliminarly assess transgene functionality, we dissected out cortico-cerebral precursors from E12.5 *Foxg1*$^{+/+}$*;Tg:Tre-Foxg1-IRES-Egfp*$^{+/-}$ embryos, acutely infected them by LV_Pgk1p-rtTA^{M2} (driving constitutive expression of a doxycycline-activatable rtTA^{M2} transactivator) and cultured them as floating neurospheres in pro-proliferative medium, under 2μg/ml doxycyclin. 4 days later, we inspected them for EGFP fluorescence (Fig. 1B). The transgene was silent in the "C" line. A signal was only detectable in case of D (weaker) and E (stronger) lines. To get preliminary hints about the articulation of the transgene expression domain, we dissociated DIV4, LV_Pgk1p-rtTA^{M2}-infected, *Foxg1*$^{+/+}$*;Tg:Tre-Foxg1-IRES-Egfp*$^{+/-}$ neurospheres to single cells and transferred them onto polylysinated coverslips, under a prodifferentiative, doxycycline-containing medium. 5 days later, we coimmunoprofiled the resulting cultures for EGFP and Tubβ3 immunoreactivity. We found that the almost totality of the EGFP signal was restricted to juvenile Tubβ3^{+} neurons (Fig. 1C).

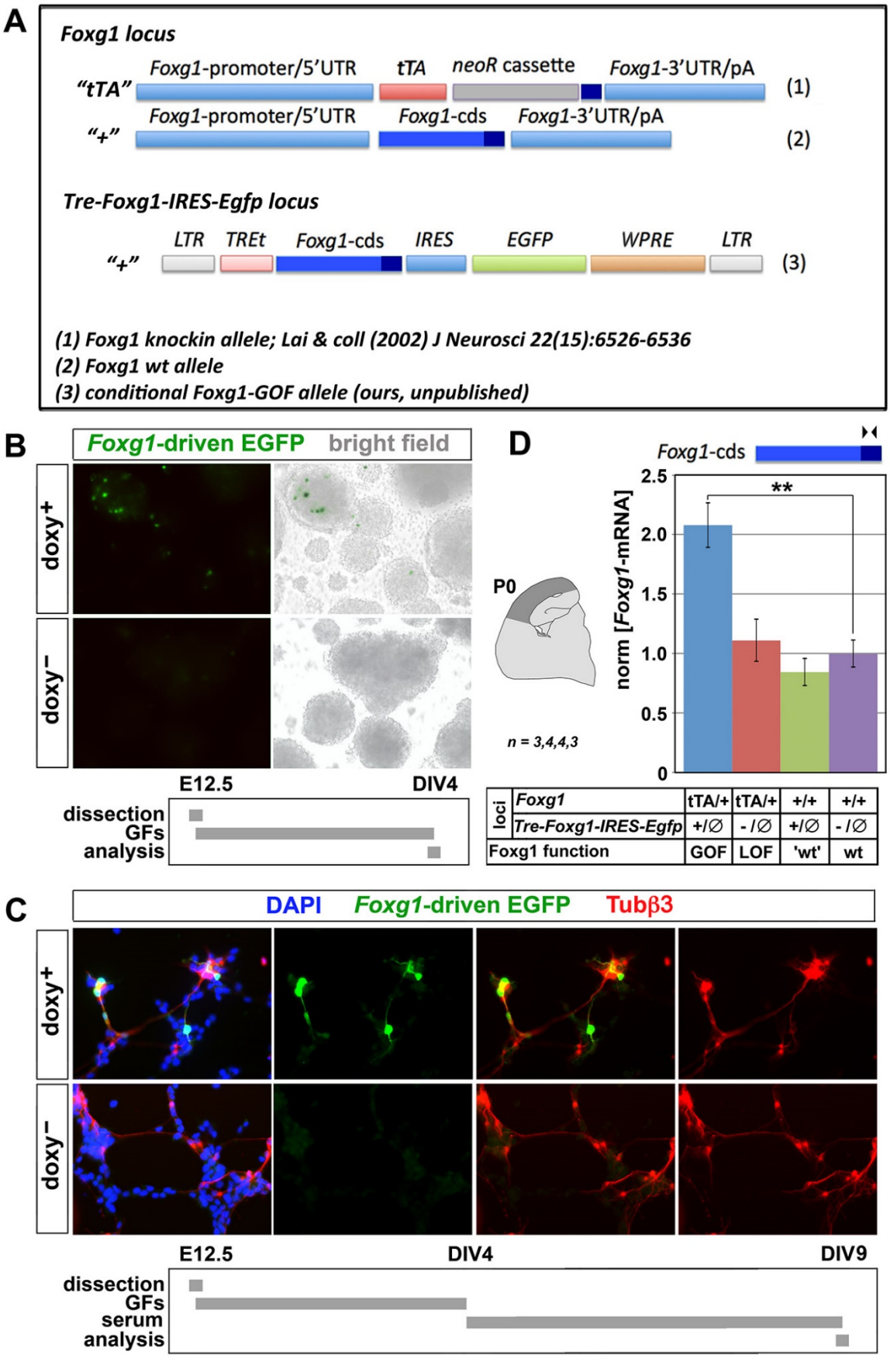
A
Foxg1 locus
"tTA"
Foxg1-promoter/5'UTR
tTA
neoR cassette
Foxg1-3'UTR/pA
(1)
"+"
Foxg1-promoter/5'UTR
Foxg1-cds
Foxg1-3'UTR/pA
(2)
Tre-Foxg1-IRES-Egfp locus
"+"
LTR
TREt
Foxg1-cds
IRES
EGFP
WPRE
LTR
(3)
(1) Foxg1 knockin allele; Lai & coll (2002) J Neurosci 22(15):6526-6536
(2) Foxg1 wt allele
(3) conditional Foxg1-GOF allele (ours, unpublished)
B
Foxg1-driven EGFP
bright field
doxy+
doxy–
E12.5
DIV4
dissection
GFs
analysis
D
Foxg1-cds
P0
n = 3,4,4,3
norm [Foxg1-mRNA]
2.5
2.0
1.5
1.0
0.5
0
**
loci
Foxg1
Tre-Foxg1-IRES-Egfp
Foxg1 function
tTA/+
+/∅
GOF
tTA/+
- /∅
LOF
+/+
+/∅
'wt'
+/+
- /∅
wt
C
DAPI
Foxg1-driven EGFP
Tubβ3
doxy+
doxy–
E12.5
DIV4
DIV9
dissection
GFs
serum
analysis

Figure R1. Generation and preliminary characterization of the *Foxg1-GOF* transgenic line "E" (A) Schematics of the two *Foxg1* locus alleles and the *Tre-Foxg1-IRES-Egfp* transgene employed in this study. **(B)** EGFP fluorescence profiling of *Foxg1*$^{+/+}$*;Tg:Tre-Foxg1-IRES-Egfp*$^{+/-}$ cortico-cerebral precursors dissected out at E12.5, acutely infected by LV_Pgk1p-rtTA^{M2} and cultured as floating neurospheres in pro-proliferative medium, under 2µg/ml doxycyclin, for 4 days. **(C)** EGFP/Tubβ3 immunoprofiling of precursors referred to in (B), further transferred at DIV4 to polylysinated coverslips and kept under pro-differentiative medium 5 more days. **(D)** *Foxg1*-mRNA levels in neocortex of *Foxg1*-GOF, *Foxg1*-LOF and wild type (WT), *Foxg1*$^{(tTA\text{-}or\text{-}+)/+}$*;Tg:Tre-Foxg1-IRES-Egfp*$^{\pm/-}$ P0 mice, as measured by qRTPCR. Data double normalized against *Gapdh*-mRNA and WT controls. Statistical significance (*p*) evaluated by t-test (one-tailed, unpaired). *n* is the number of biological replicates.

To confirm transgene functionality in vivo, we crossed *Foxg1*$^{+/+}$*;Tg:Tre-Foxg1-IRES-Egfp*$^{+/-}$ founders to *Foxg1*$^{tTA/+}$ mutants, expressing the tTA TetOFF transactivator within the *Foxg1* expression domain (Hanashima et al., 2002) and kept pregnant female under doxycycline-free diet. We harvested neocortices from P0 progenies originating from this crossing, genotyped them by PCR and evaluated their cumulative *Foxg1*-mRNA content. This was done by quantifying an amplicon within the 3'-most *Foxg1*-cds, shared by all *Foxg1* alleles employed in this study. As expected, this content was very similar in wild type (*Foxg1*$^{+/+}$*;Tg:Tre-Foxg1-IRES-Egfp*$^{-/-}$), congenic "wild type" (*Foxg1*$^{+/+}$*;Tg:Tre-Foxg1-IRES-Egfp*$^{+/-}$), and *Foxg1*-LOF (*Foxg1*$^{tTα/+}$*;Tg:Tre-Foxg1-IRES-Egfp*$^{-/-}$) mice. Moreover, it was upregulated by 2.08±0.18 in *Foxg1*-GOF (*Foxg1*$^{tTα/+}$*;Tg:Tre-Foxg1-IRES-Egfp*$^{+/-}$) pups, compared to wild type pups ($p<0.002$ and $n=3,3$), so corroborating previous in vitro results. (Fig. 1D).

4.2 Analysis of the *Foxg1*-GOF transgene expression profile

We took advantage of EGFP immunoreactivity of cells expressing *Tg:Tre-Foxg1-IRES-Egfp* to reconstruct the transgene expression profile and compare its spatio-temporal articulation with the expression pattern of the endogenous *Foxg1* gene, spanning the entire telencephalon.

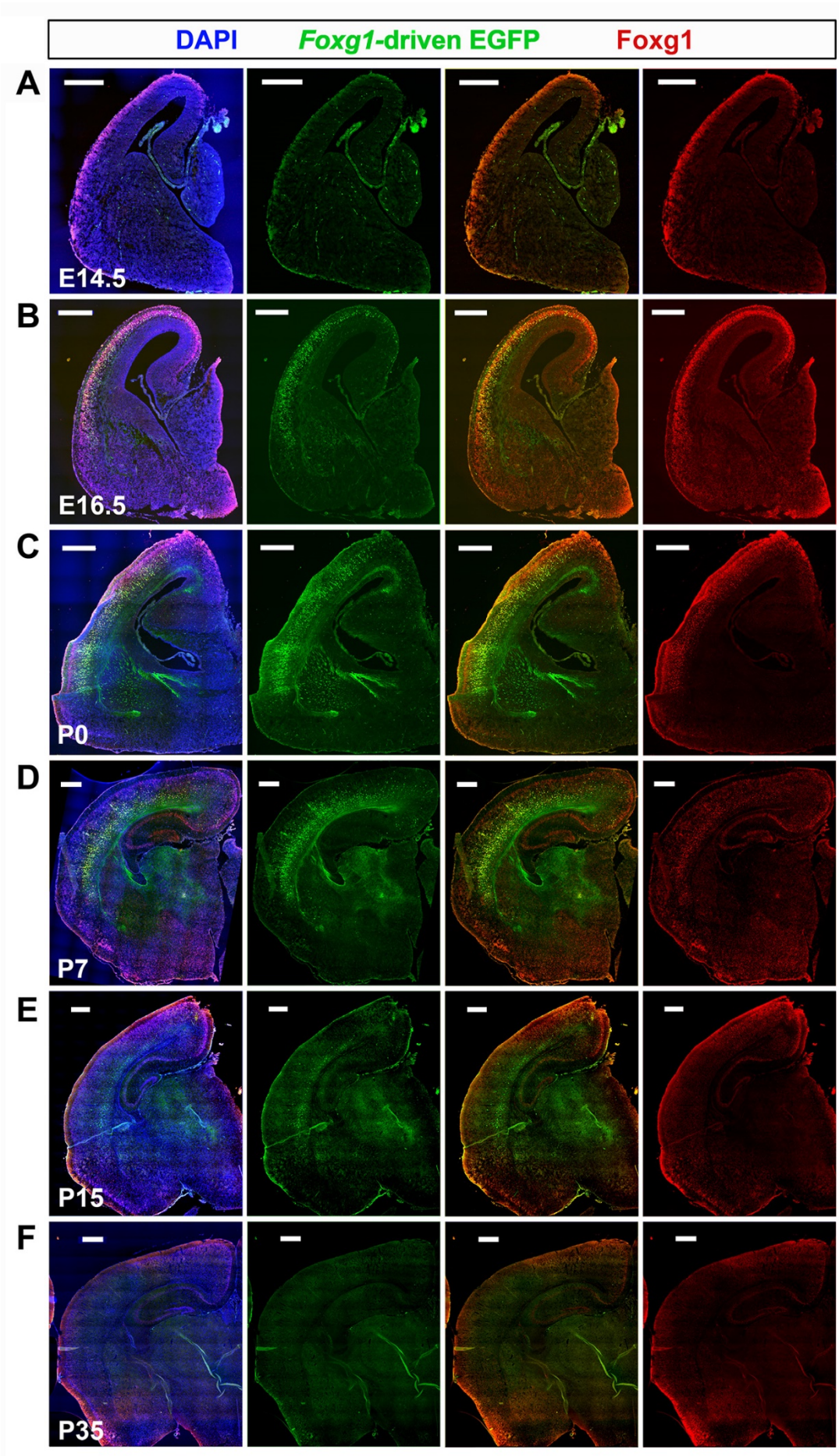
DAPI
Foxg1-driven EGFP
Foxg1
A
E14.5
B
E16.5
C
P0
D
P7
E
P15
F
P35

Figure R2 EGFP expression profile in *Foxg1-GOF*, *Foxg1$^{tTA/+}$;Tg:Tre-Foxg1-IRES-Egfp$^{+/-}$* mutants, at different embryonic and postnatal stages: mid-coronal telencephalic sections. E14.5 **(A)**, E16.5 **(B)**, P0 **(C)**, P7 **(D)**, P15 **(E)**, and P35 **(F)** samples. *Foxg1-promoter*-driven EGFP is revealed in green, total Foxg1 in red. Scale bars: 500µm.

We found that at E14.5, a weak transgene expression was only detectable within the neocortical field. (Fig. R2A). A similar tangential restriction was found at E16.5, when - although much stronger - the transgene was active within neocortex but not in hippocampus, paleocortex and basal ganglia (Fig. R2B). This pattern remained substantially immutated at later developmental ages. Transgene expression level reached its peak at P7 and started to decline around P15. By P35 no EGFP could be detected anymore (Fig. R2C-F).

Specifically within neocortex, transgene products showed a higly dynamic radial distribution. At E14.5, a faint signal was only detectable within a few cells located in the uppermost cortical plate (Fig. R3A, arrowheads). At E16.5 a large fraction of presumptive pyramidal neurons populating the cortical plate was strongly immunoreactive for EGFP, which also stained large bundles of cortico-fugal fibers running within the subplate and below it (Fig. R3B). A similar radial pattern was retained at P0 and P7, when - however - the cortical plate signal was mainly limited to deeper layers and the EGFP-positive fibers clustered just above subventricular zone and ependyma (Fig. R3C,D). [At the same ages, these bundles could be easily recognized while crossing the striatal field (Fig. R3F, arrows)]. Neocortical transgene activity declined substantially at P15, when a few EGFP^{+} cells could be only detected within presumptive layer VI. Remarkably, at no developmental age analyzed any transgene activity could be detectable within periventricular proliferative layers, where the endogenous *Foxg1* wild type allele is normally active, albeit at low levels (Fig. R3A-F).

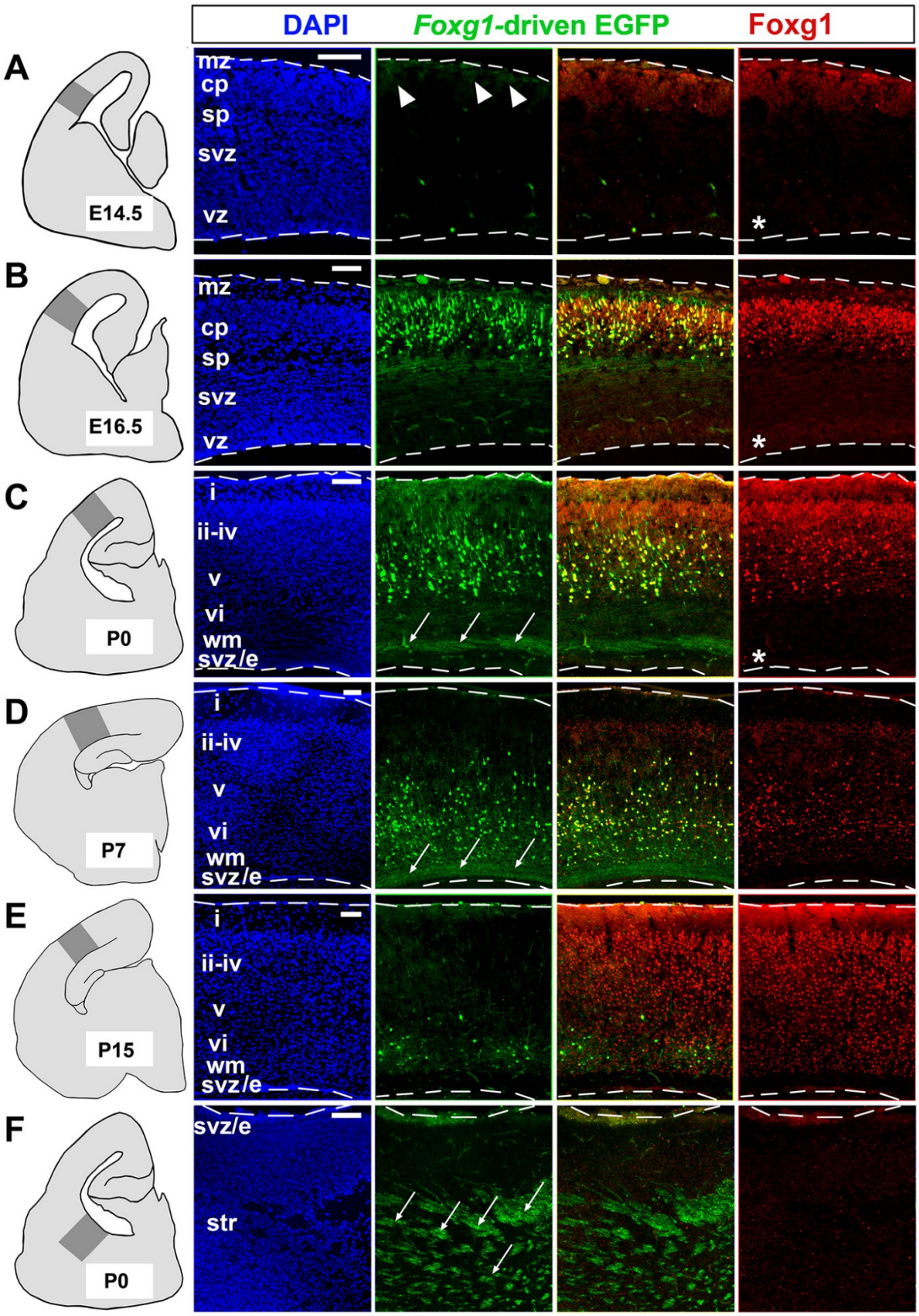
DAPI
Foxg1-driven EGFP
Foxg1
A
E14.5
mz
cp
sp
svz
vz
B
E16.5
mz
cp
sp
svz
vz
C
P0
i
ii-iv
v
vi
wm
svz/e
D
P7
i
ii-iv
v
vi
wm
svz/e
E
P15
i
ii-iv
v
vi
wm
svz/e
F
P0
svz/e
str

Figure R3 EGFP expression profile in *Foxg1-GOF*, *Foxg1$^{tTA/+}$;Tg:Tre-Foxg1-IRES-Egfp$^{+/-}$* mutants, at different embryonic and postnatal stages: high power fields. (A-E) E14.5, E16.5, P0, P7 and P15 neocortical sectors, and **(F)** P0 striatum. Arrowheads in (A) point to early EGFP expression in superficial cortical plate. Arrows in (C,D,F) point to presumptive cortico-fugal fibers within white matter (C,D) and striatum (F). Stars in (A,B,C) label periventricular precursors weakly expressing Foxg1. Abbreviations: mz, marginal zone; cp, cortical plate; sp, subplate; svz, subventricular zone; vz, ventricular zone; i,ii-iv,v,vi refers to cortical layers; wm, white matter; svz/e, subventricular zone/ependyma; str,striatum. Scale bars: 100µm.

Next, we addressed the histological identity of neural cells expressing the transgene. We confirmed our previous suspicion that a large fraction of them were postmitotic neurons, by extensively colocalizing EGFP with established pan-neuronal markers, Tubβ3 and NeuN, at E16.5 through P7. Based on obvious morphological criteria (a thin apical dendrite emerging from a radially oriented soma, see Fig. R4A,B), these cells turned out to be prototypical pyramidal neurons.

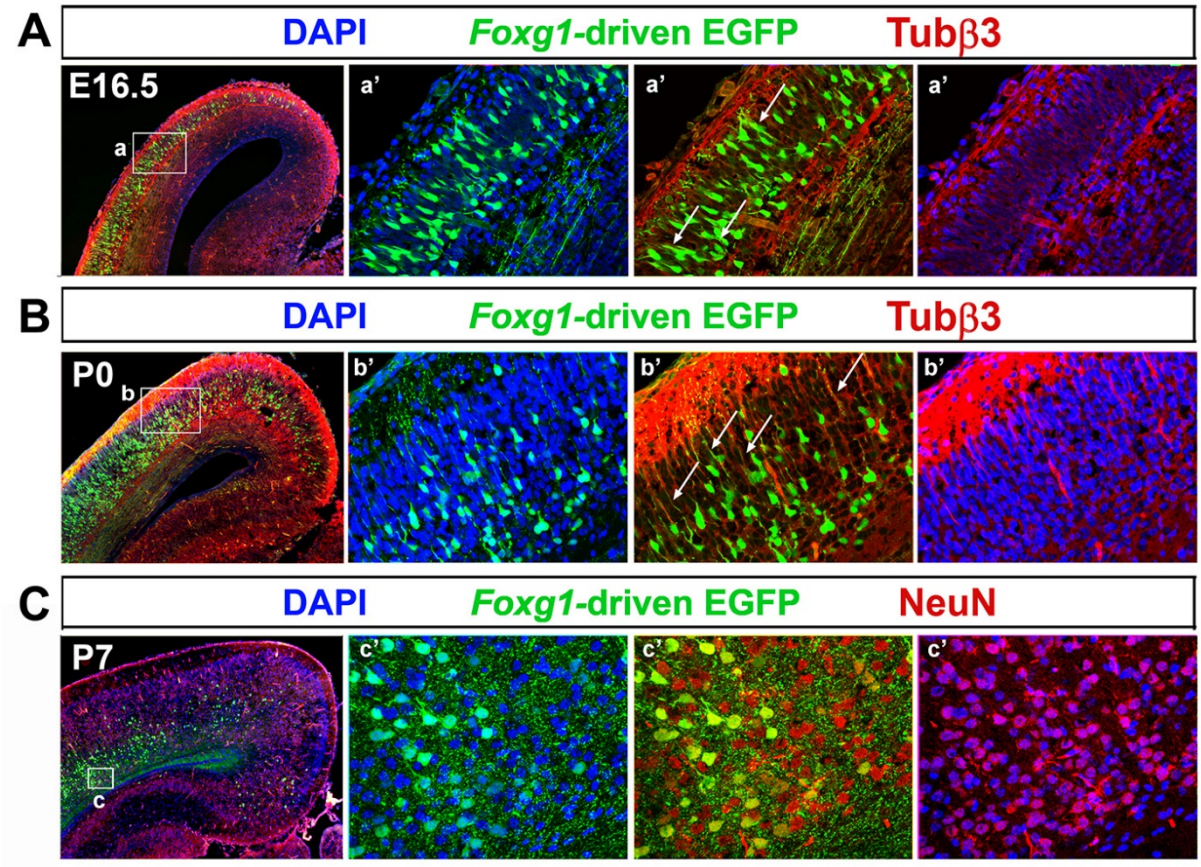

Figure R4 Colocalization of *Foxg1-promoter*-driven EGFP with pan-neuronal markers. (A,B) EGFP/Tubβ3 immunoprofiling of E16.5 and P0 neocortices. **(Aa') and (Bb')** are confocal magnifications of boxed regions in (A) and (B), respectively. Arrows in (a') and (b') point to EGFP/Tubβ3 colocalization in presumptive apical dendrites of pyramidal neurons. **(C)** EGFP/NeuN immunoprofiling of P7 neocortex. **(Cc')** is a confocal magnification of the boxed region in (C).

Comparison of their radial distribution at P7 with $DAPI^{+}$ nuclear packaging profile and radial activation pattern of three established layer-specific markers, FoxP2 (layer VI), Ctip2 (layer V) and Cux1 (layers IV-II), suggested a presumptive layer VI/V identity (Fig. R5A-C).

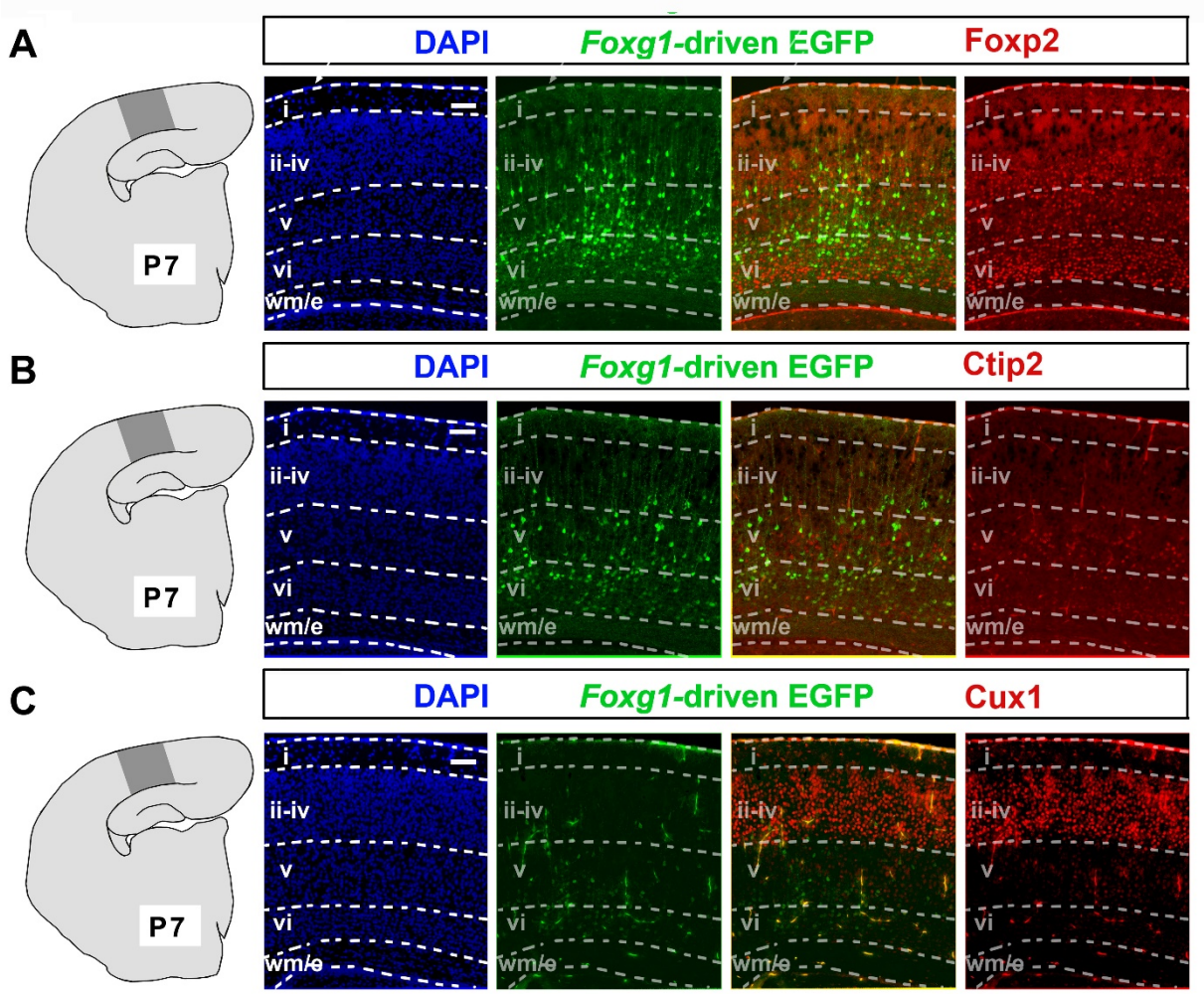

Figure R5 Neocortical laminar distribution of cells expressing *Foxg1-promoter*-driven EGFP. Here the distribution of EGFP is compared with that of laminar markers Foxp2 **(A)**, Ctip2 **(B)** and Cux1 **(C)** in

the P7 neocortex. Abbreviations: i,ii-iv,v,vi refers to cortical layers; wm/e, white matter/ependyma. Scale bars: 100μm.

To corroborate *glutamatergic* identity of these cells, we coimmunoprofiled P7 and P15 brains for EGFP and three calcium-binding proteins brightly labelling the majority of gabaergic interneurons at these developmental ages, parvalbumin (PV), somatostatin (SST) and calretinin (CR). As expected, no colocalization could be detected at all (Fig. R6A-F).

Finally, we wondered if transgene-expressing cells might include non-neuronal elements, such as astrocytes. To address this issue, we co-immunoprofiled transgenic P7 brains for EGFP and the mature astrocyte marker S100β. No colocalization was detected at all, suggesting that transgene-expressing cells were to large extent - if not all - neurons (Fig. R7).

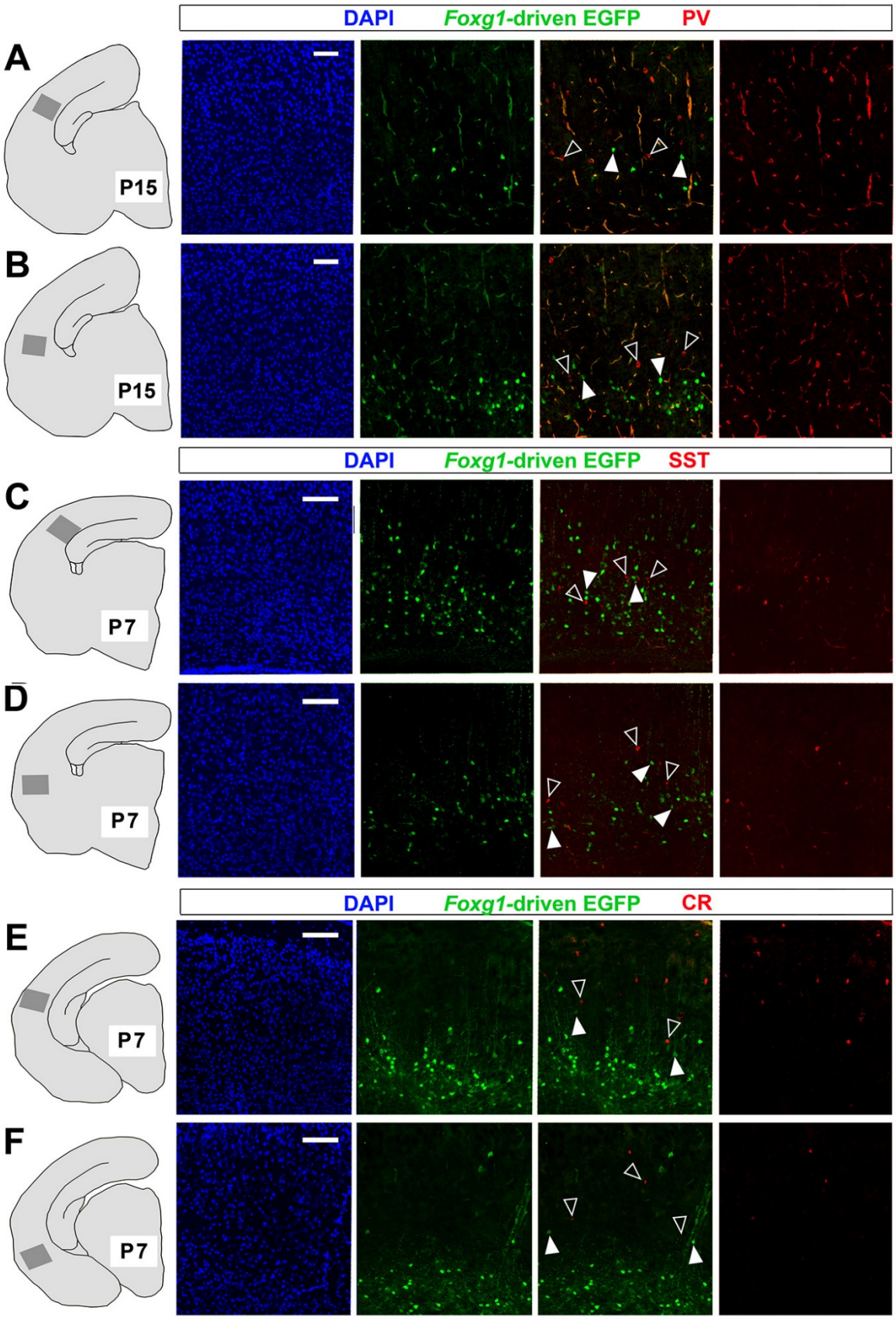
DAPI
Foxg1-driven EGFP
PV
A
P15
B
P15
DAPI
Foxg1-driven EGFP
SST
C
P7
D
P7
DAPI
Foxg1-driven EGFP
CR
E
P7
F
P7

Figure R6 Coimmunoprofiling of *Foxg1*-GOF brains for *Foxg1-promoter*-driven EGFP and inter-neuronal markers. Distribution of EGFP and Parvalbumin (PV) in P15 neocortex **(A,B)**, EGFP and Somatostatin (SST) in P7 neocortex **(C,D)**, and EGFP and Calretinin (CR) in P7 neocortex **(E)** and paleocortex **(F)**. Solid arrowheads point to $EGFP^+$ cells, empty arrowheads to PV^+, SST^+ and CR^+ cells. Scale bars: 100μm.

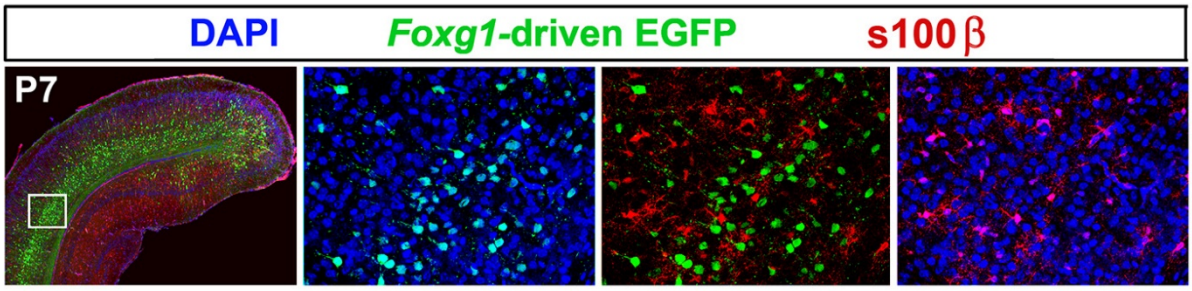

Figure R7 Coimmunoprofiling of *Foxg1*-GOF brains for *Foxg1-promoter*-driven EGFP and the astrocyte marker S100β. (a') is a confocal magnification of the boxed region (a).

4.3 Assaying neuronal excitability of *Foxg1*-GOF mutants

As mentioned above, *Foxg1*-GOF mutants were generated as a model for dissecting neurodevelopmental and neurophysiological abnormalities of human patients affected by *FOXG1*-duplication-linked West syndrome. To preliminarly assess the suitability of these mutants for such purpose, these animals were subject of two dedicated sets of experiments.

First, electrical activity of their brains was profiled by electroencephalography (EEG) in basal awake conditions. Electrical activity was monitored within the hippocampus. This structure was selected, as receiving and integrating afferences coming from all the cortex, via the entorhino-hippocampal bundle, and so acting as a comfortable proxy of entire brain electrical activity. A bipolar electrode was placed into the hippocampus of P41 *Foxg1*-GOF mutants (*Foxg1*$^{tTA/+}$*;Tg:Tre-Foxg1-IRES-Egfp*$^{+/-}$) and wild type controls (*Foxg1*$^{+/+}$*;Tg:Tre-Foxg1-IRES-Egfp*$^{-/-}$), with its two 500μm-spaced pins ending in CA1 and DG/hilus regions (Fig. R8A). It was secured to the skull and electrical activity was monitored for three days, two hours

per day. The EEG was inspected, paying special attention to temporal distribution of spikes, i.e. voltage fluctuations with amplitude exceeding 4 standard deviations (SD). Spikes were categorised as "isolated" and "clustered", if alone or groupable in sets of at least two ones, spaced less than 0,5 sec, respectively. Spike clusters were further distinguished into interictal, if lasting <4sec, and ictal, i.e. lasting ≥4sec (Fig. R8B). Interestingly, both total spike frequency and interictal cluster frequency were increased by about 50% in *Foxg1*-GOF mutants as compared to controls (with n=4,4, and p<0.01). Isolated spike frequency was unaffected. Ictal cluster frequency was increased >3 times, however this did not result statistically significant (Fig. R8C). Altogether, these data point to a appreciable increase of neuronal activity occurting in *FOXG1*-GOF mutants compared to controls.

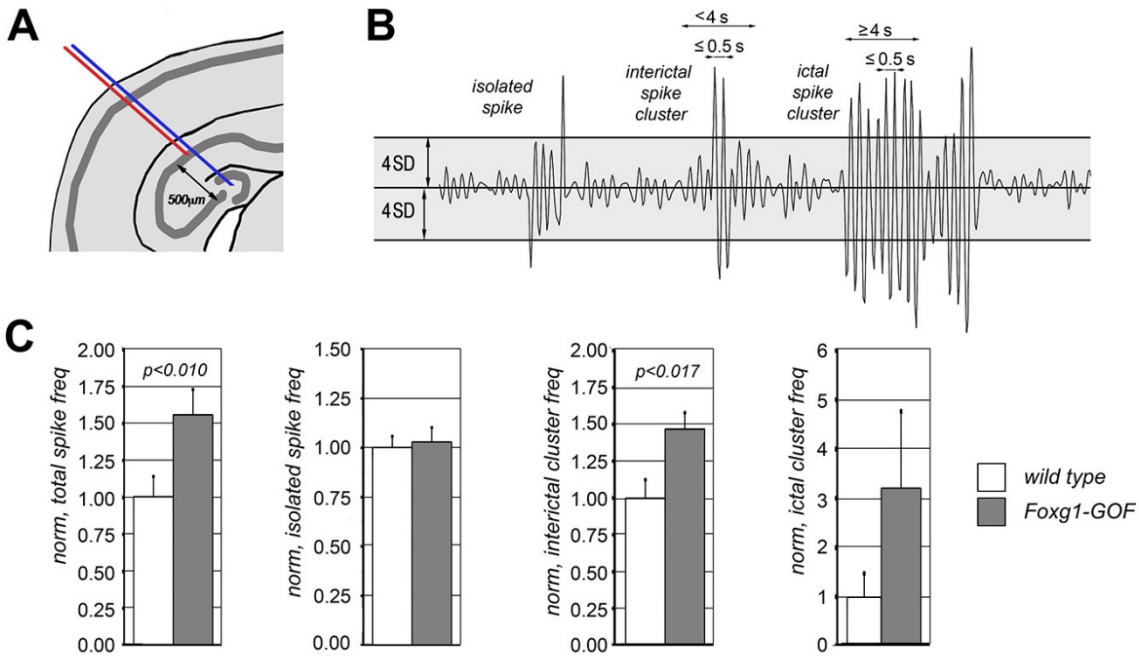

Figure R8 EEG recordings of P35 *Foxg1*-GOF (*Foxg1*$^{tTA/+}$;*Tg:Tre-Foxg1-IRES-Egfp*$^{+/-}$) and WT (*Foxg1*$^{+/+}$;*Tg:Tre-Foxg1-IRES-Egfp*$^{-/-}$) mice. (A) Schematics of bipolar electrodes placement into the hippocampal field. **(B)** Classification of isolated spikes, interictal spike clusters and ictal spike clusters (or seizures). **(C)** Graphical summary of control-normalized, (1) total spike frequency, (2) isolated spike frequency, (3) interictal spike cluster frequency and (4) ictal spike cluster frequency, in *Foxg1*-GOF and control mice. Absolute control average values were 500, 150, 95 and 0.25 events/10 min, respectively.

Encouraged by these results, to confirm the suitability of *FOXG1*-GOF mutants for our purposes, we challenged them (as well as *FOXG1*-LOF and control mice) with an established proconvulsant agent promoting glutamatergic transmission, kainic acid (KA). We administered P35 animals with 20 mg of KA per kg of body weight, by intraperitoneal injection, and monitored their behaviour over the following two hours, paying attention to specific signs of altered brain activity (e.g., immobility, rigid posture, head bobbing, forelimb clonus with rearing and falling, etc). Every 10 min, a score was given, according to Racine's staging criteria (Fig. R9A).

The majority of animals did not go beyond Racine stage (RS) 3, *repetitive movements & head bobbing* (5/14, 12/17 and 7/9, in case of GOF, WT and LOF, respectively), a subset of them reached RS4, *limbic motor seizure* (4/14, 4/17 and 2/9, as for GOF, WT and LOF, respectively). Only a few got up to RS5, *continuous rearing and falling*, and beyond (5/14, 1/17 and 0/9 in case of GOF, WT and LOF, respectively) ($p<0.073$, χ-square test; Fig. R9B). Longitudinal analysis of data showed that, for each group, RS increased progressively from the onset of the experiment to about 1 hour later, then smothly declining. The RS(t) curve of the GOF group was on average 1.3 units above WT controls (this average gap resulted to be only 0.3 between LOF and WT animals). In particular, the distance between the GOF and the WT curves peaked at 90 and 100 min, reaching 1.7 and 1.9, respectively, with $p<0.01$ (ANOVA) in both cases (Fig. R9C). Altogether, these data point to an remarkable increase of neuronal excitability, occurring in GOF models compared to control, and rule out that such effect may stem from dominant negative effects.

Upon completion of Racine tests, mice were sacrificed and their brains snap-frozen for subsequent analysis. Brains from animals which reached different Racine's stages, from different groups, were processed. They were sliced and profiled by not-radioactive in situ hybridization, for expression of the ieg-gene c-fos. Within GOF brains, c-fos was strongly activated throughout the hippocampus, including the dentate gyrus (DG), as well as in scattered neocortical cells. In case of WT brains, a cFos signal was present in Cornu Ammonis fields 1-3 (CA1) and, to a lesser extent, in the DG. Finally, cFos activation in LOF brains was very weak, or not detectable at all (Fig. R9D). This scenario is nicely consistent with behaviourial data reported above and strenghtens the hypothesis that a specific increase of neuronal excitability occurred in *FOXG1*-GOF mutants compared to controls.

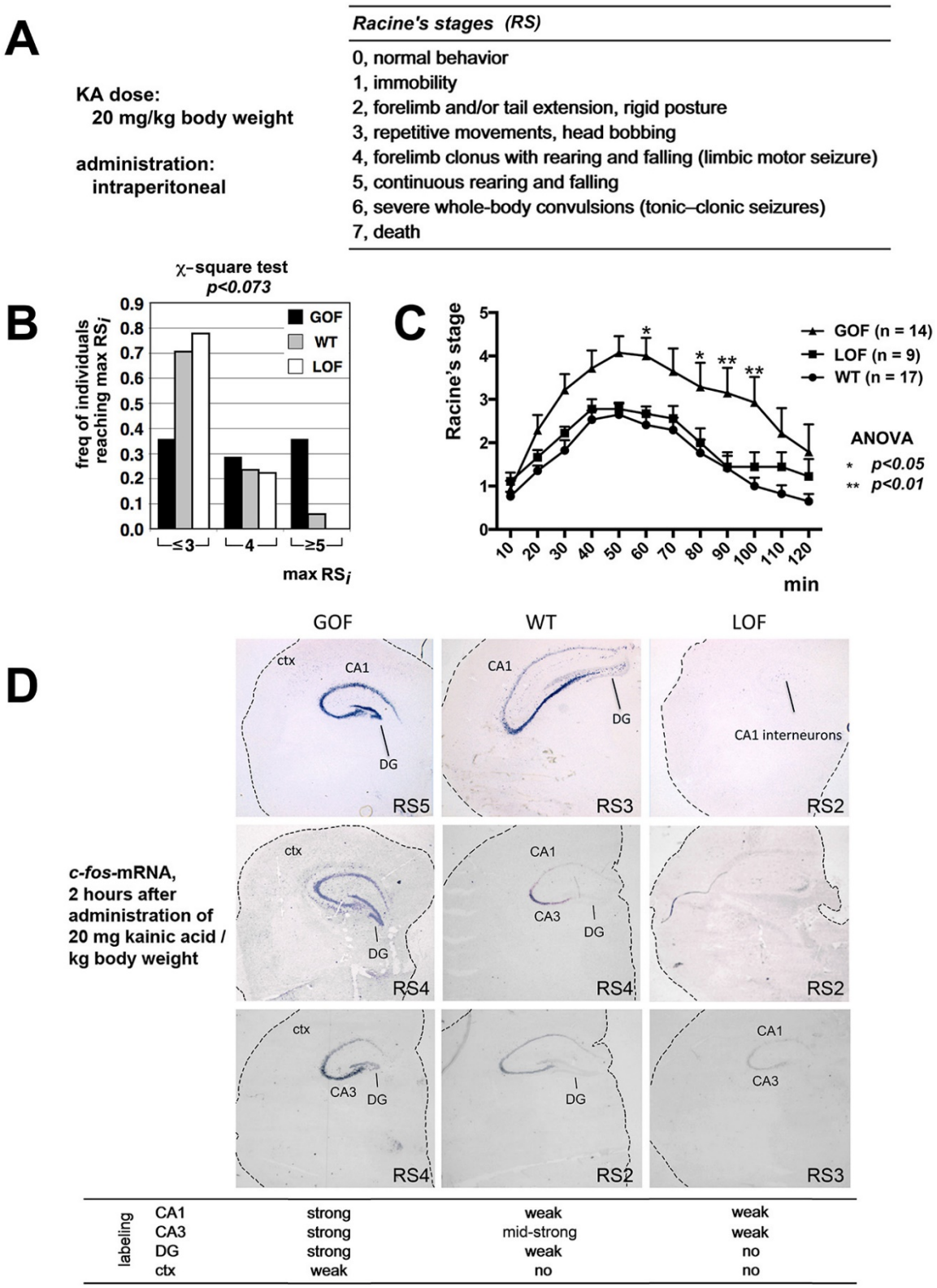

Figure R9 Behavioral analysis in *Foxg1*-GOF, *Foxg1*-LOF and WT, *Foxg1*$^{(tTA\text{-}or\text{-}+)/+}$;*Tg:Tre-Foxg1-IRES-Egfp*$^{\pm/-}$ mice at P35-40. (A) Temporal Racine profiling of *Foxg1*-GOF, *Foxg1*-LOF and WT mice, upon administration of 20 mg Kainic acid/kg body weight, over 2 hours. Here wt refers to data from pooled

Foxg1$^{+/+}$*;Tre-Foxg1-IRES-Egfp*$^{-/-}$ and *Foxg1*$^{+/+}$*;Tre-Foxg1-IRES-Egfp*$^{+/-}$, among which no statistically significant differences were previously found. **(B)** Cumulative/non-parametric (χ-square test) and **(C)** timed/parametric (ANOVA) evaluation of the resulting Racine profiling **(D)** Acute *c-fos* in situ hybridization of KA-treated mice, upon completion of Racine profiling, mid-frontal brain sections. Abbreviations: RS, Racine stage, maximal animal-specific value; ctx, cortex; DG, dentate gyrus; CA1-3, Cornu Ammonis 1-3 fields.

4.4 Putative mechanisms underlying neuronal hyperexcitability: abnormal neuronal histogenesis and differentiation

To cast light on possible histogenetic abnormalities triggered by *Foxg1* overexpression, we scored P0 and P7, GOF and WT neocortices for their neuronal packaging profile, as evaluated by DAPI staining, and the expression profiles of FoxP2, Ctip2 and Cux1, layer VI, V and II-IV markers, respectively. At P0 (Fig. R10A), FoxP2 was slightly down-regulated, and Ctip2, which is normally confined to the intermediate third of the cortical plate (corresponding to presumptive V layer) spread into the deeper third of it (corresponding to putative VI layer). Cux1, normally labelling the superficial third of cortical plate (with layer IV-II identity) was dramatically downregulated and hardly detectable. At P7 (Fig. R10B), FoxP2^{+} cells, which were closely packaged in VI layer of WT neocortex, were more loosely distributed through layer VI, V and - to some extent - IV of the GOF neocortex. Conversely, Ctip2^{+} cells, normally limited to layer V, partially spread into layer VI of mutant neocortex (Fig. R10B, arrows). Finally, the Cux1^{+} layer IV-II was halved in its radial extension. All that points to a defective segregation of layer V and layer VI neurons as well as to a pronounced suppression of layer IV-II programs (Fig. R10C).

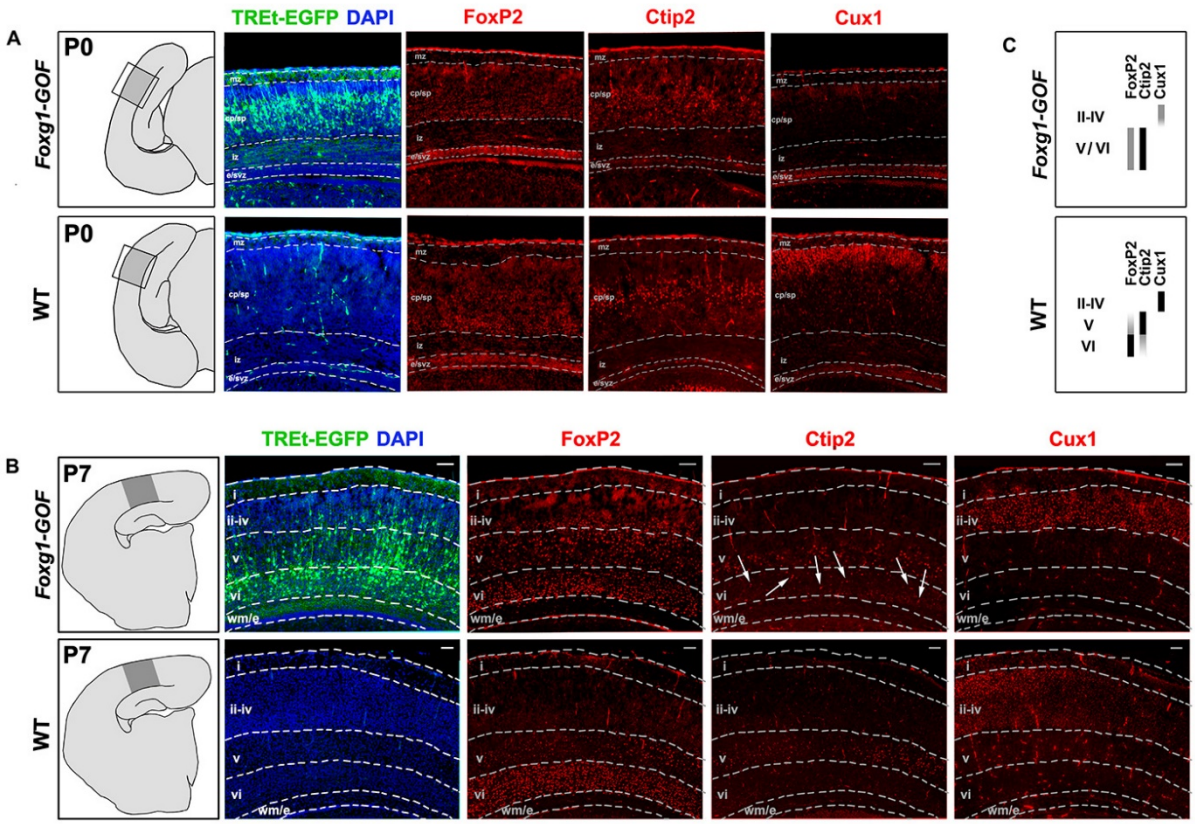

Figure R10 Comparison of neocortical lamination in *Foxg1*-GOF mutants and WT mice. (A,B) Here presumptive radial extension of neocortical layers is inferred on the basis of the neuronal packaging profile, as evaluated by DAPI staining, and the expression profiles of FoxP2, Ctip2 and Cux1, layer VI, V and II-IV markers, respectively, at two different stages, P0 and P7. Arrows point the spreading of Ctip2^{+} cells into layer VI. **(C)** Synopsis of laminar profile changes occurring in *Foxg1*-GOF mutants. Abbreviations: mz, marginal zone; cp/sp, cortical plate/subplate; iz, intermediate zone; e/svz, ependyma/subventricular zone; i,ii-iv,v,vi refers to cortical layers; wm/e, white matter/ependyma; Scale bars: 100µm.

Next, we inspected the mutant P35 GOF neocortex for distribution and spatial frequency of gabaergic interneurons expressing the three main Ca2^{+}-binding proteins, parvalbumin (PV), somatostatin (SST) and calretinin (CR). We detected a robust and specific reduction of PV^{+} cells spatial frequency throughout layers VI-II of the mutant neocortex. This phenomenon was expecially pronounced within the rostral-medial neocortical sector, where interneurons decreased by >40% (n=3,3, p<0.004) (Fig. R11A,B). No major changes of SST^{+} and CR^{+} interneurons were conversely detectable (data not shown).

A wt-normalized densities of PV$^+$ cells in *Foxg1*-mutant murine cortices

P35	R		I		C	
	l	*m*	*l*	*m*	*l*	*m*
I	gof: 0.378±0.378 wt: 1.000±0.711 p< 0.260	gof: 1.048± 1.049 wt: 1.000± 1.000 p< 0.488	gof: 3.899± 2.488 wt: 1.000± 1.000 p< 0.140	gof: 1.805± 0.815 wt: 1.000± 0.660 p< 0.143	gof: 0.372± 0.372 wt: 1.000± 0.676 p< 0.248	gof: 2.646± 1.335 wt: 1.000± 1.000 p< 0.179
II-VI	gof: 0.607± 0.055 wt: 1.000± 0.091 p< 0.010	gof: 0.582± 0.095 wt: 1.000± 0.052 p< 0.004	gof: 0.676± 0.070 wt: 1.000± 0.127 p< 0.050	gof: 0.712± 0.043 wt: 1.000± 0.110 p< 0.043	gof: 0.612± 0.107 wt: 1.000± 0.079 p< 0.015	gof: 0.604± 0.130 wt: 1.000± 0.120 p< 0.039
WM/E	gof: 1.521± 0.918 wt: 1.000± 0.637 p< 0.324	gof: 0.960± 0.488 wt: 1.000± 0.292 p< 0.472	gof: 0.739± 0.739 wt: 1.000± 0.595 p< 0.396	gof: 4.128± 2.347 wt: 1.000± 0.602 p< 0.097	gof: 1.508± 0.775 wt: 1.000± 0.200 p< 0.247	gof: 0.813± 0.456 wt: 1.000± 0.345 p< 0.376

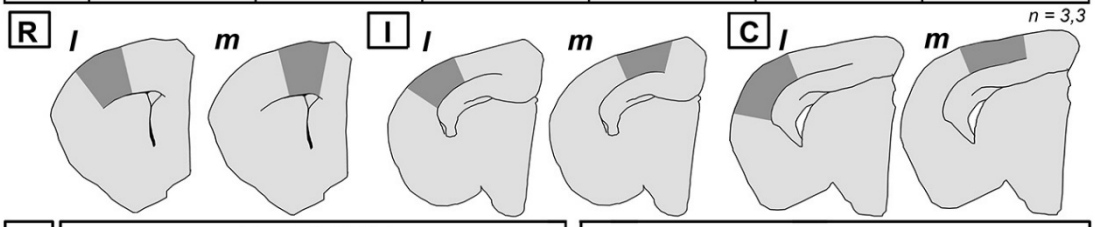

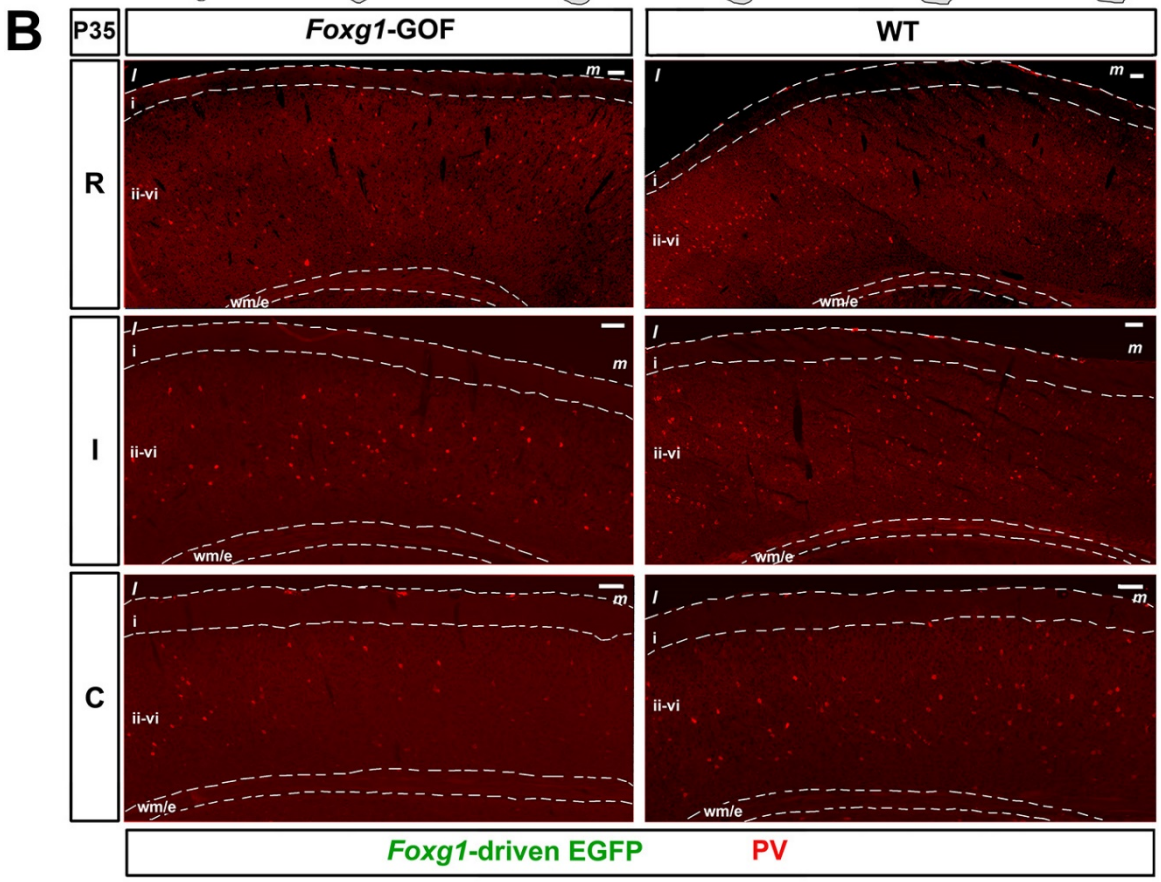

Figure R11 Comparative quantification of neocortical PV$^+$ interneurons in *Foxg1*-GOF and WT P35 mice. (A) wt-normalized densities of PV$^+$ cells at rostral (R), intermediate (I) and caudal (C), lateral (*l*)

and medial (*m*), neocortical sectors at P35 (dark grey in silhouettes). Presumptive radial extension of layer I (i), layers II-VI (ii-vi) and white matter/ependyma (wm/e) was inferred on the basis of the neuronal packaging profile, evaluated by DAPI staining (not shown). Absolute PV^+ cell densities in wild type animals are reported in Fig. S1 **(B)** Examples of PV immunofluorescences referred to in (A). Scale bars: 100μm.

Finally, to get insights into aberrant molecular mechanisms possibly contributing to neural tissue hyperexcitability, we profiled RNA from *Foxg1*-GOF, *Foxg1*-LOF and WT P0 neocortices for a small gene panel tuning the proper neuronal excitatory/inhibitory balance. These included: *Gria1*, encoding for the major GluA1 subunit of AMPA receptors, *Grin1*, encoding for the major GluN1 subunit of NMDA receptors, *Slc17a6* and *Slc17a7*, encoding for the vGluT1 and vGluT2 vesicular glutamate transporters, *Grid1*, encoding for the GluD1 subunit of ionotropic glutamate delta receptors, and *Gabra1*, encoding for the major GABA receptor subunit α1. We found that Gabra1 was down-regulated in GOF cortices by more than 50% ($p<0.05$). An apparent, pronounced decrease was also detectable for *Slc17a6* and *Grid1* in both GOF and LOF samples, however it dit not reach statistical significance (Fig. R12A). To assess if these expression changes specifically occur within the neuronal complement, we evaluated the effect of *Foxg1*-GOF manipulations on pure neuronal cultures established from E14.5 neocortical tissue, engineered by lentiviral vectors (Fig. R12C). Similarly and even more than in acute tissue, *Gabra1* as well as *Grid1* and *Slc17a6* were all down-regulated, in a statistically significant way (Fig. R12B). Because of the amplitude of *Gabra1*-mRNA downregulation and the deep impact that it might have on neocortical excitability, we monitored the distribution of its protein product in *Foxg1*-GOF neocortices. Remarkably, Gabra1 immunoreactivity, which normally gives rise to three stripes in layers I, II-IV and V, was here dramatically lowered (Fig. R13A-C), so corroborating the down-regulation of its mRNA.

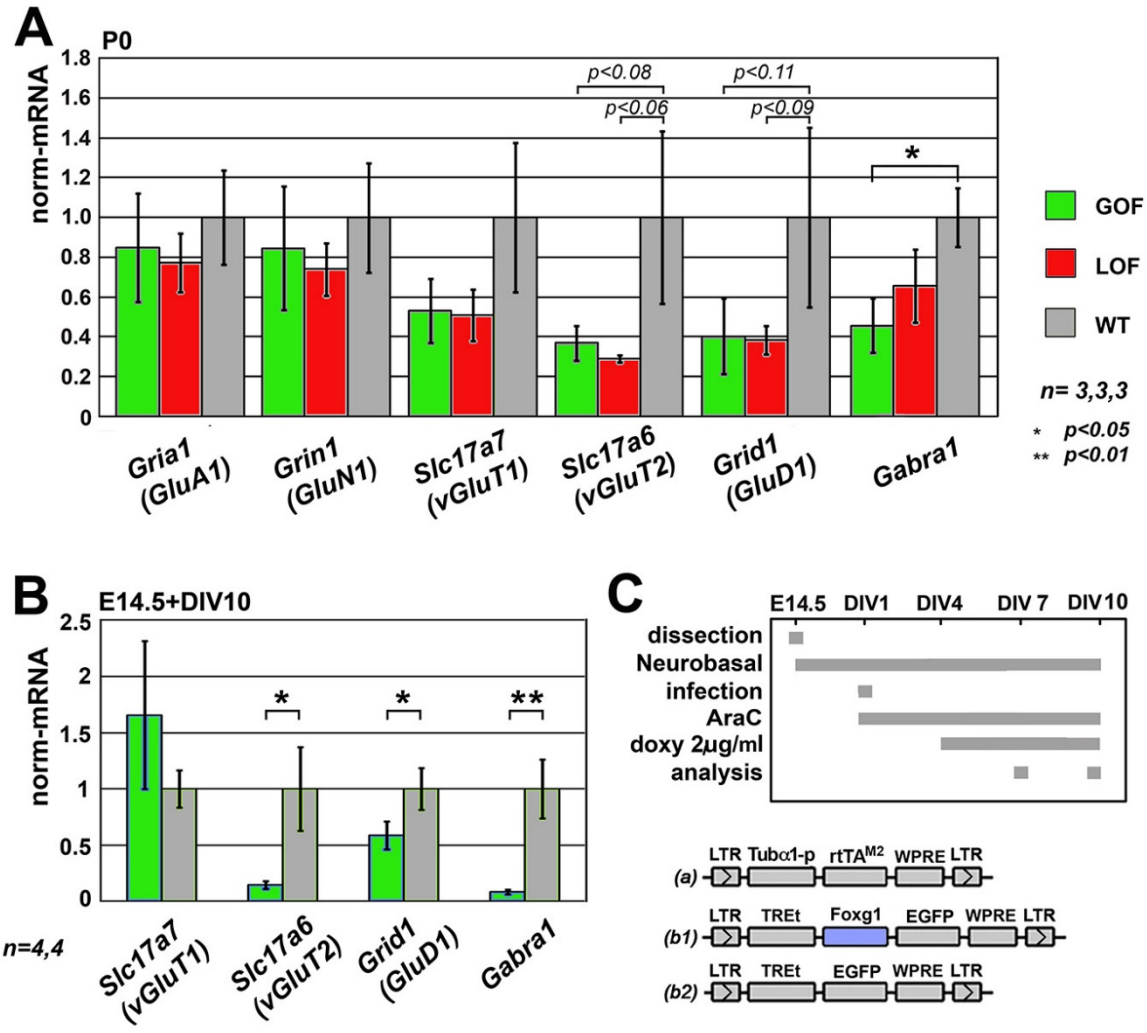

Figure R12 Preliminary molecular characterization of *Foxg1*-GOF, *Foxg1*-LOF and WT, *Foxg1*$^{(tTA\text{-}or\text{-}+)/+}$;*Tg:Tre-Foxg1-IRES-Egfp*$^{\pm/-}$ cortico-cerebral neural cells. (A) mRNA levels of a selection of genes essential for proper neuronal excitatory/inhibitory balance, as measured by qRTPCR on P0 neocortical samples from *Foxg1*-GOF (*Foxg1*$^{tTA/+}$;*Tg:Tre-Foxg1-IRES-Egfp*$^{+/-}$), *Foxg1*-LOF (*Foxg1*$^{tTA/+}$;*Tg:Tre-Foxg1-IRES-Egfp*$^{-/-}$) and wt (*Foxg1*$^{+/+}$;*Tg:Tre-Foxg1-IRES-Egfp*$^{-/-}$) mice. Data double normalized against *Gapdh*-mRNA and WT controls. Statistical significance (*p*) evaluated by t-test (one-tailed, unpaired). *n* is the number of biological replicates. **(B)** mRNA levels of a subset of genes shown in (A), as measured by qRTPCR in neocortical precursors dissected at E14.5, infected with LV_Ptα1-rtTA^{M2} and, alternatively, LV_TREt-Foxg1-IRES-Egfp (*Foxg1-GOF*) or LV_TREt-EGFP (controls) and cultured in pro-differentiative medium, under 2µg/ml doxycyclin and 10mM AraC, for 10 days. Statistical significance (*p*) evaluated by t-test (one-tailed, unpaired). *n* is the number of biological replicates. **(C)** Graphical abstract and temporal articulation of the culture procedure analyzed in (B).

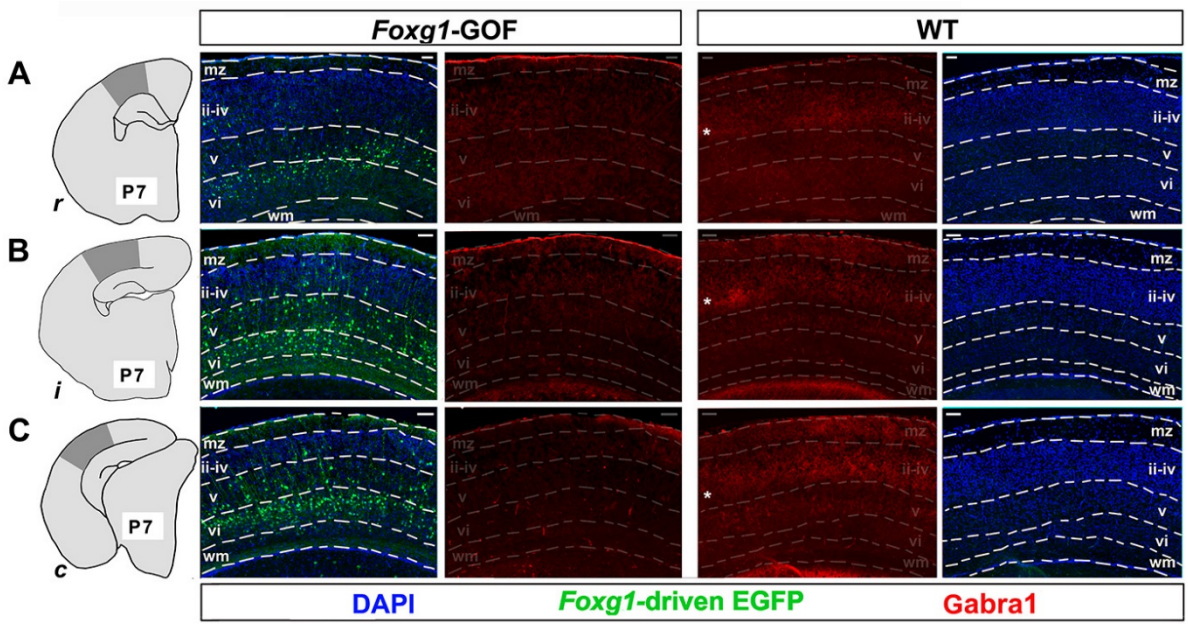

Figure R13 Comparison of Gabra1 expression in *Foxg1*-GOF mutants and WT P7 neocortex. Rostral **(A)**, intermediate **(B)** and caudal **(C)** neocortical sections immunoprofiled for *Foxg1*-driven-EGFP/Gabra1. Presumptive radial extension of neocortical layers was inferred on the basis of the neuronal packaging profile, evaluated by DAPI staining. Abbreviations: r, rostral; i, intermediate; c, caudal; mz, marginal zone; ii-iv, v, vi, refers to cortical layers; wm, white matter; Scale bars: 100µm.

4.5 Putative mechanisms underlying neuronal hyperexcitability: defective astrogenesis

We showed that our *Foxg1*-GOF transgene is selectively activated within the neuronogenic lineage, only after the exit of neuronal cells from cell cycle, so precluding any cell-autonomous effect by this transgene on the astrocytic complement. Nevertheless, neurons exert a deep influence on astrocyte generation and maturation, which makes a non-cell-autonomous impact of our mutation on this lineage still possible. To address this issue, we scored *Foxg1*-GOF cortices for spatio-temporal distribution of cells immunoreactive for a key astrocyte marker, S100β. At P0, neocortical spatial frequency of these cells was reduced by about 20% ($p<0.064$). At the same age *Foxg1*-LOF mutants showed an opposite trend ($p<0.03$), ruling out any possible dominant-negative effects. (Fig. R14A-C).

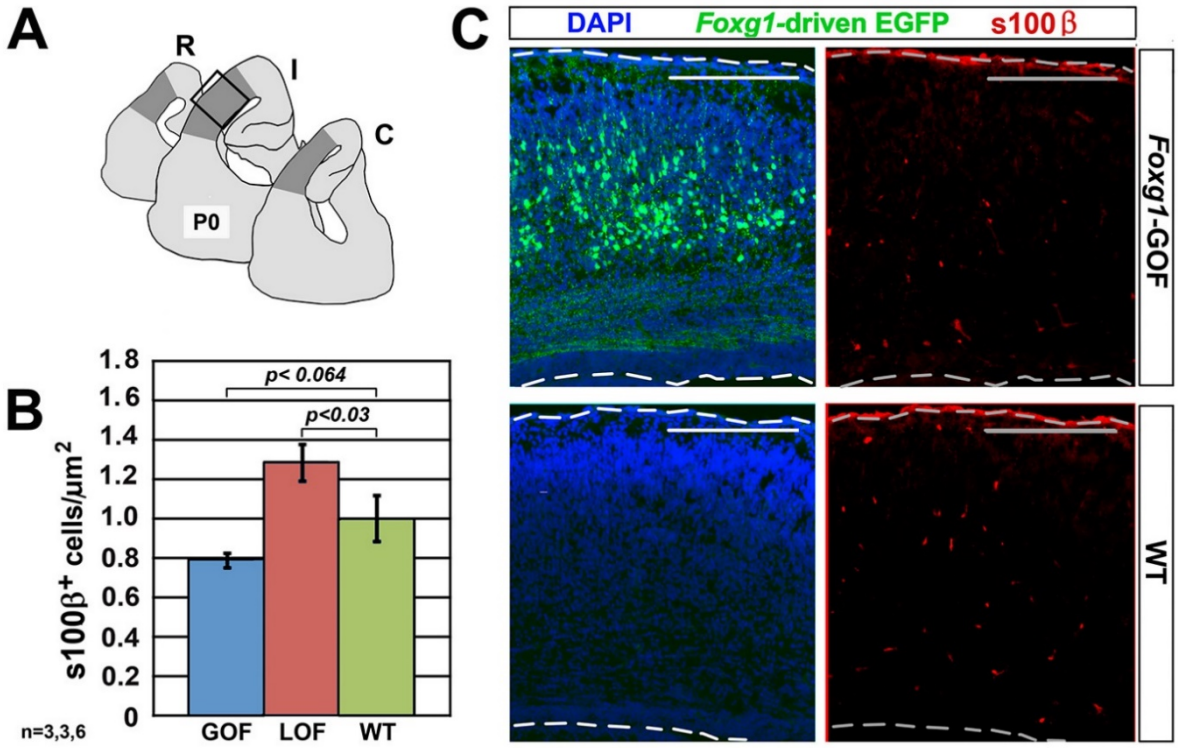

Figure R14 Comparative quantification of S100β$^+$ astrocytes in *Foxg1*-GOF and WT P0 pups. (A) Cell counting was performed throughout neocortex (dark grey). **(B)** wt-normalized, superficial density of S100β$^+$ astrocytes in *Foxg1*-GOF, *Foxg1*-LOF and control mice. Here wt refers to data from pooled *Foxg1*$^{+/+}$*;Tre-Foxg1-IRES-Egfp*$^{-/-}$ and *Foxg1*$^{+/+}$*;Tre-Foxg1-IRES-Egfp*$^{+/-}$, among which no statistically significant differences were previously found. [Absolute, average wt frequence on 16mm-thick sections was 2,124 cells/mm^2]. Statistical significance (*p*) evaluated by t-test (one-tailed, unpaired). *n* is the number of biological replicates. **(C)** Examples of *Foxg1*-driven-EGFP and S100b immunolocalizations in neocortical sectors approximately corresponding to the boxed area in (A). Scale bars: 100µm.

At P7, *Foxg1*-GOF mutants showed again an overall reduction of S100β$^+$ astrocytes (-14.0±2.4%, p<0.080, n=3,3). Frequency of these cells was diminished both in medial and lateral neocortex (-12.0±2.4%, p<0.150, and -15.9±2.4%, p<0.051, respectively). Moreover it was specifically downregulated in layer I and II-IV (-33.0±2.3%, p<0.025, and -23.2±4.6%, p<0.054, respectively), as well as slightly upregulated in layer VI (+14.4±4.0%, p<0.029). These tangential and radial trends combine so that a pronounced and more statistically robust decrease of astrocyte density could be found at specific neocortical locations (Fig. R15A,B).

A wt-normalized densities of S100β⁺ cells in *Foxg1*-mutant murine cortices

P7	R		I		C	
	l	*m*	*l*	*m*	*l*	*m*
I	gof: 0.576±0.113 wt: 1.000±0.082 p<0.019	gof: 0.611±0.037 wt: 1.000±0.074 p<0.005	gof: 0.621±0.012 wt: 1.000±0.085 p<0.006	gof: 0.727±0.131 wt: 1.000±0.190 p<0.151	gof: 0.912±0.149 wt: 1.000±0.112 p<0.330	gof: 0.659±0.050 wt: 1.000±0.215 p<0.098
II-IV	gof: 0.798±0.102 wt: 1.000±0.102 p<0.117	gof: 0.779±0.102 wt: 1.000±0.126 p<0.122	gof: 0.707±0.024 wt: 1.000±0.079 p<0.012	gof: 0.729±0.068 wt: 1.000±0.095 p<0.041	gof: 0.796±0.023 wt: 1.000±0.115 p<0.079	gof: 0.854±0.037 wt: 1.000±0.172 p<0.227
V	gof: 0.991±0.073 wt: 1.000±0.162 p<0.482	gof: 0.952±0.135 wt: 1.000±0.172 p<0.418	gof: 1.032±0.031 wt: 1.000±0.039 p<0.281	gof:0.957±0.010 wt: 1.000±0.054 p<0.240	gof: 0.774±0.053 wt: 1.000±0.098 p<0.056	gof:0.899±0.010 wt: 1.000±0.128 p<0.237
VI	gof:1.129±0.137 wt: 1.000±0.196 p<0.309	gof: 1.377±0.043 wt: 1.000±0.138 p<0.030	gof: 1.176±0.036 wt: 1.000±0.068 p<0.042	gof: 1.311±0.123 wt: 1.000±0.068 p<0.046	gof:0.932±0.154 wt: 1.000±0.085 p<0.360	gof: 1.073±0.110 wt: 1.000±0.141 p<0.352
WM/E	gof: 1.089±0.128 wt: 1.000±0.258 p<0.387	gof: 1.178±0.111 wt: 1.000±0.106 p<0.155	gof: 1.140±0.260 wt: 1.000±0.125 p<0.326	gof: 1.101±0.089 wt: 1.000±0.071 p<0.213	gof: 0.872±0.172 wt: 1.000±0.140 p<0.297	gof: 1.194±0.251 wt: 1.000±0.096 p<0.255

n = 3,3

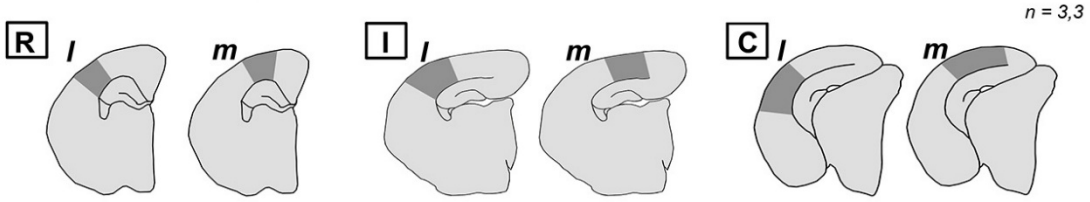

B

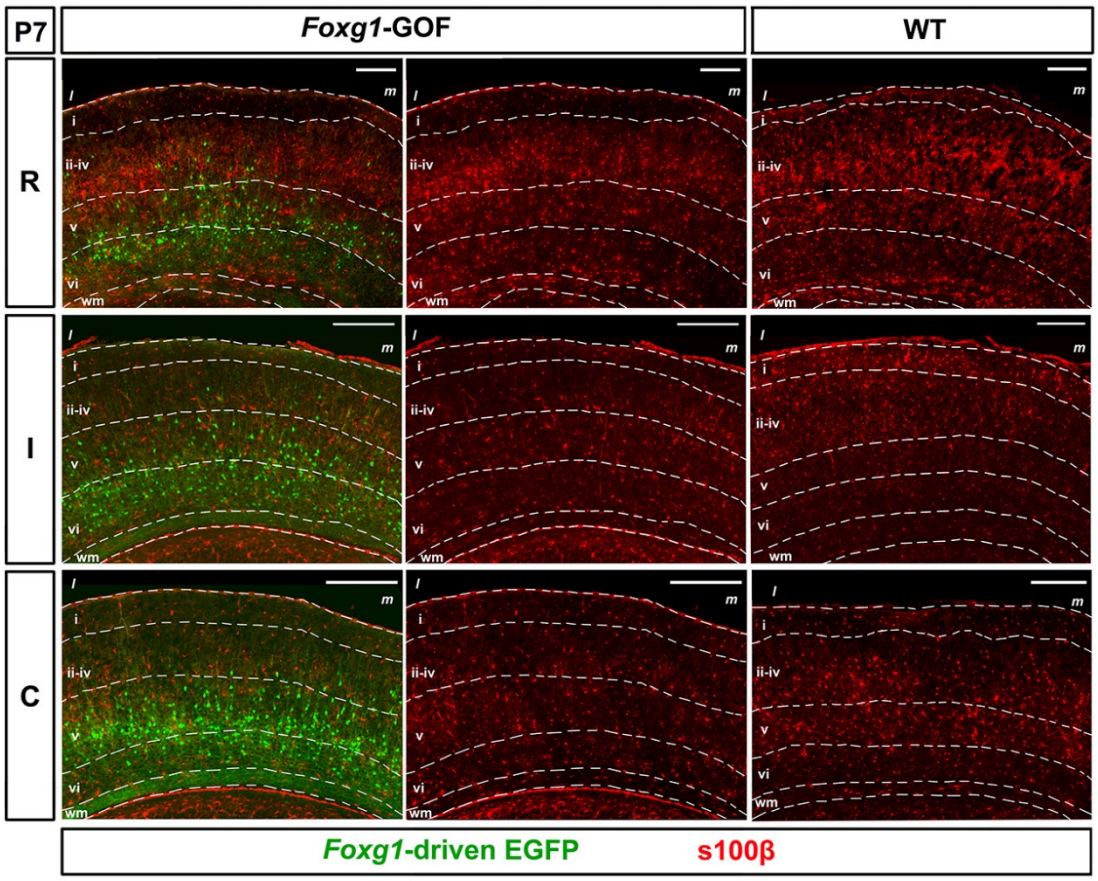

Figure R15 Comparative quantification of S100β$^+$ astrocytes in *Foxg1*-GOF and WT P7 pups. (A) wt-normalized densities of S100β $^+$ cells at rostral (R), intermediate (I) and caudal (C), lateral (*l*) and medial (*m*), neocortical sectors at P7 (dark grey in silhouettes). Presumptive radial extension of layer I (i), layers II-IV (ii-iv), layer V (v), layer VI (vi) and white matter (wm) was inferred on the basis of the neuronal packaging profile, evaluated by DAPI staining (not shown). Absolute S100β $^+$ cell densities in wild type animals are reported in Fig. S2. **(B)** Examples of *Foxg1*-driven-EGFP and S100β immunofluorescences referred to in (A). Scale bars: 100μm.

4.6 Putative mechanisms underlying neuronal hyperexcitability: activity-linked *Foxg1*-modulation

Until now, we have seen that exaggerated *Foxg1* expression leads to increased neuronal activity, possibly mediated by complex neurodevelopmental disorders. Next, we wondered if increased neuronal activity might - in turn - upregulate neuronal expression of *Foxg1*. In patient cells harboring *FOXG1* duplications, in fact, this phenomenon might ignite a harmful vicious circle, leading to further exacerbated neuronal hyperactivity and contributing to unique EEG aberrancies of these patients.

To this aim, we set up mixed cocultures of cortico-cerebral neurons and astrocytes from wild type E16.5 mouse donors (Fig. R16A,B) and challenged them by 25mM extracellular K^+, as an inducer of neuronal hyperactivity. Potassium stimulation was delivered for different times and time-course progression of *Foxg1*-mRNA was profiled. We found that *Foxg1* was transiently upregulated. It reached its peak value 3 hours after K^+ administration (2.7±0.2 folds compared to baseline, n = 3,4, $p<0.001$) and then smoothly declined, getting back to baseline by one day (Fig. R17). mRNA levels of *cFos*, *Egr1* and *Egr2* iegs were also monitored, as positive controls. As expected, they displayed a transient elevation around 1 hour and declined to baseline by 12 hours (Fig. R17).

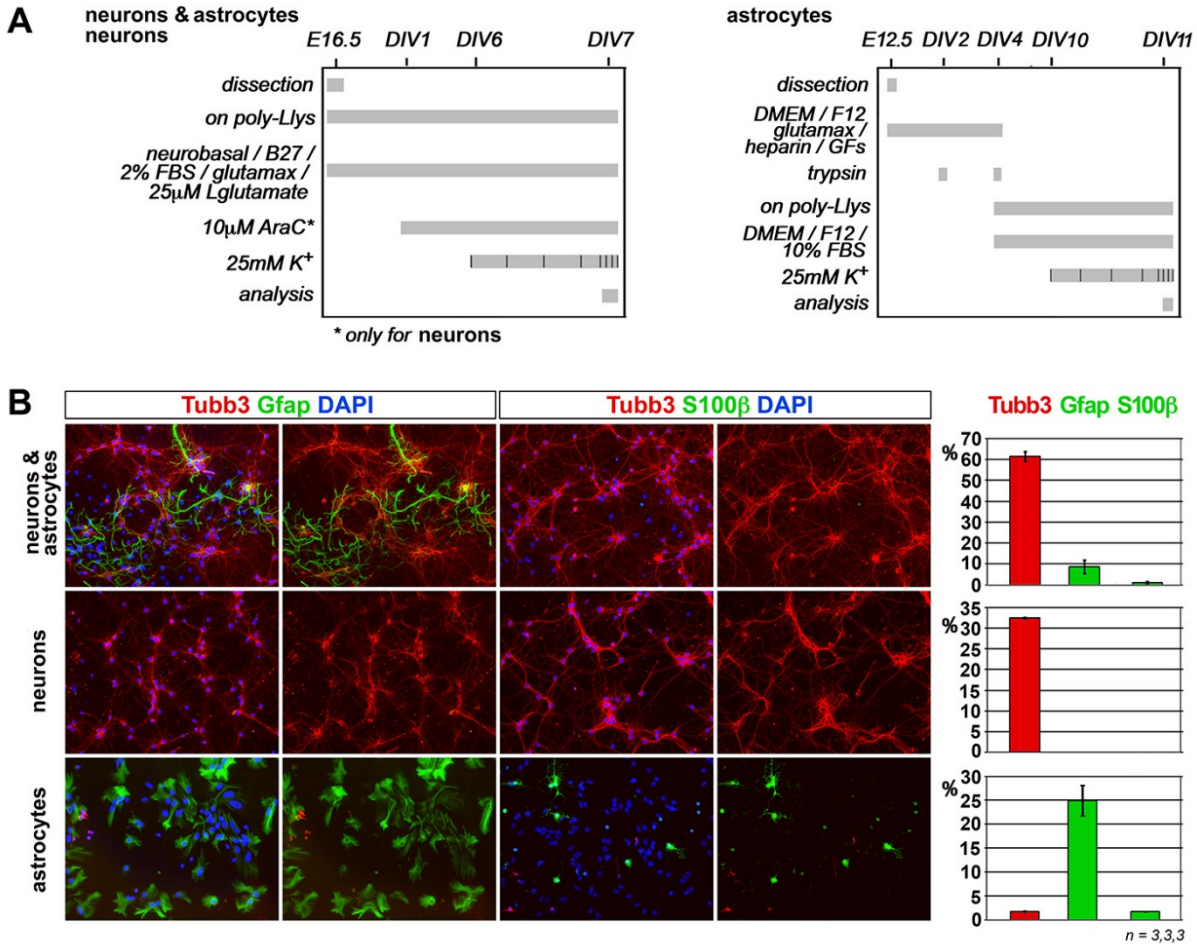

Figure R16 Immunoprofiling of primary, neuronal, astroglial and mixed cultures originating from murine pallial precursors. (A) Graphical abstract and temporal articulation of the culturing procedures. **(B)** Tubβ3/Gfap and Tubβ3/S100β co-immunoprofiling of neuronal, astroglial and mixed cultures and relative percentages of each cell subpopulation at the time of analysis.

Next, to preliminarly dissect neuronal and astroglial contributions to this phenomena, we set up isochronous, "pure", neuronal or astroglial cultures from the same source (Fig. R16A,B) and repeated the assays on them. *Foxg1* displayed a smooth and transient upregulation in astrocytes. Here it peaked up around 2 hours (1.7±0.2 folds compared to baseline, n = 4,4, $p<0.01$) and got back to baseline around 12 hours. In case of neurons, it only displayed small oscillations, which did not reach statistical significance (Fig. R17). As a reference, *cFos*, *Egr1* and *Egr2* generally displayed a transient upregulation in pure cultures at 1-2 hours, except *cFos* in neuronal cultures, unaffected (Fig. R17).

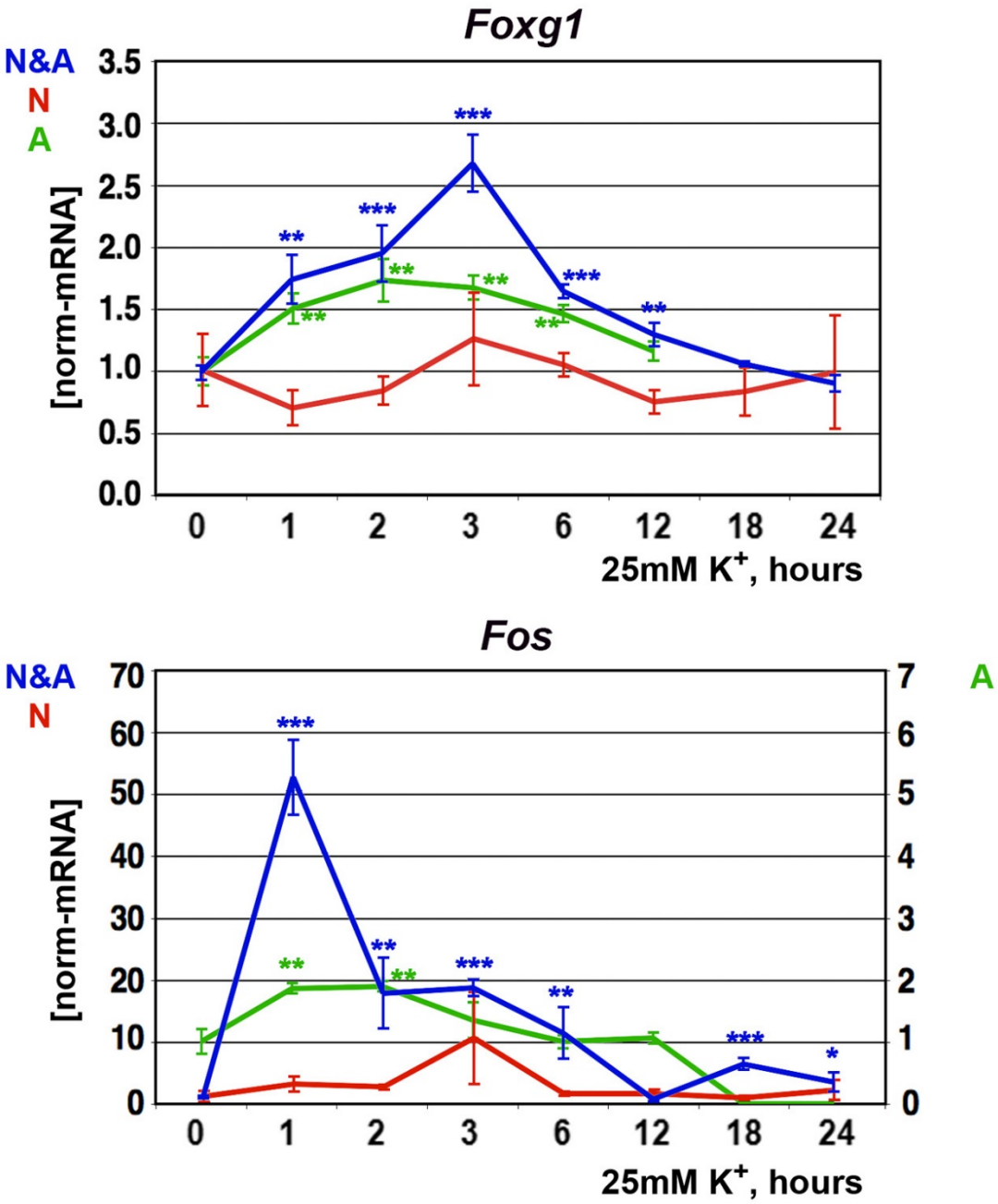
Foxg1
N&A
N
A
[norm-mRNA]
3.5
3.0
2.5
2.0
1.5
1.0
0.5
0.0
0
1
2
3
6
12
18
24
25mM K+, hours
Fos
N&A
N
A
[norm-mRNA]
70
60
50
40
30
20
10
0
7
6
5
4
3
2
1
0
0
1
2
3
6
12
18
24
25mM K+, hours

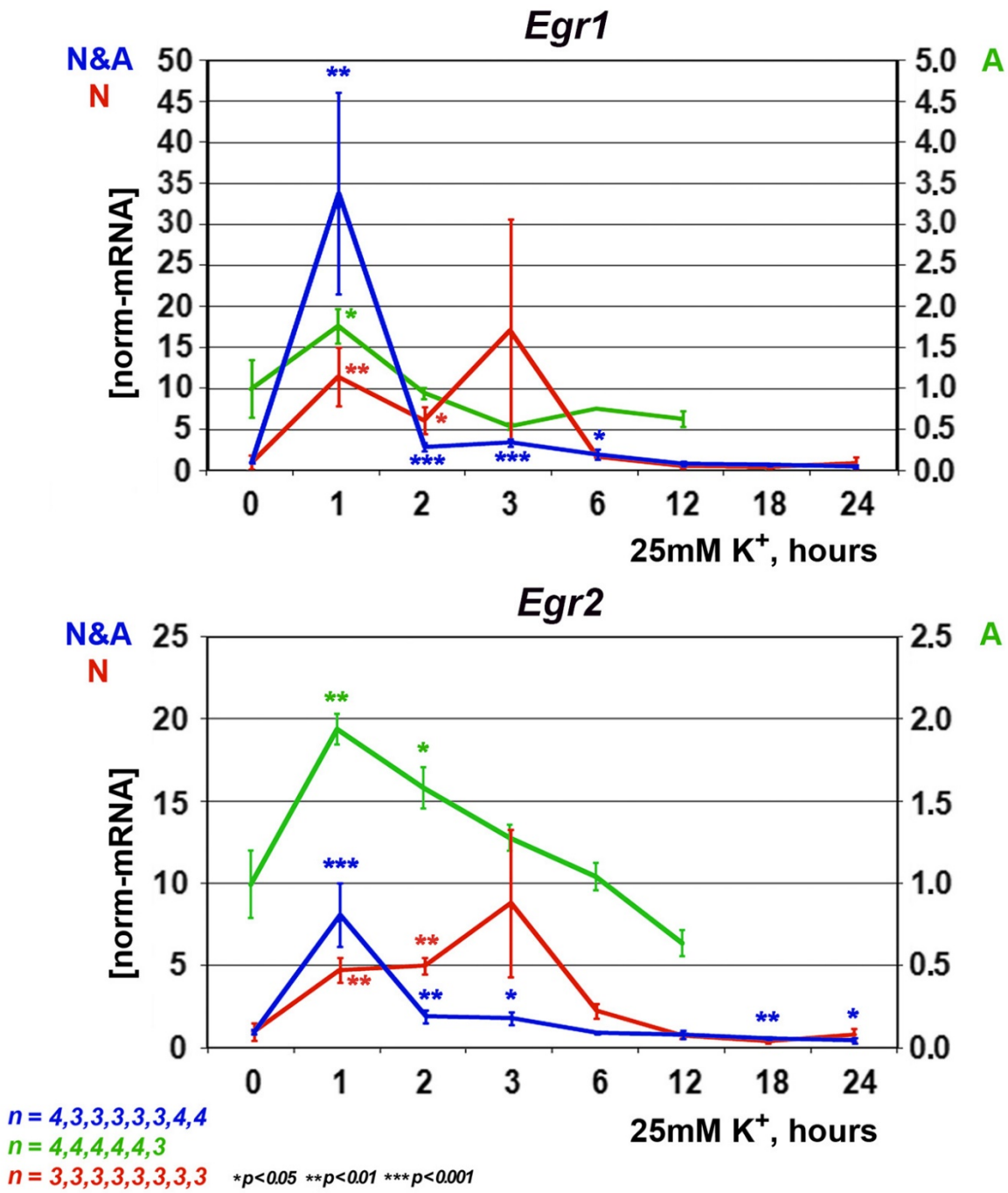

Figure R17 Time course of *Foxg1* and immediate early genes (ieg) mRNA levels in primary, neuronal, astroglial and mixed cultures challenged by 25mM of K^+. Analysis of *Foxg1*- **(A)**, *Fos*- **(B)**, *Egr1*- **(C)**, *Egr2*- **(D)** mRNA levels in primary neuronal (N), astroglial (A) and mixed cultures (N&A), prepared as in Figure R16A, following culture exposure to 25mM extracellular K^+ for different times. Gene expression levels were measured by qRTPCR and double-normalized against *Gapdh*-mRNA and t=0 controls. Statistical significance (*p*) evaluated by t-test (one-tailed, unpaired). *n* is the number of biological replicates.

We wondered which molecular mechanisms mediate activity-dependent *Foxg1* modulation in mixed neural cultures. For this purpose, we inspected the human *FOXG1* locus for binding sites recognized by transcription factors (TFs) stimulated by neuronal activity, including those encoded by immediate-early genes. We scored chromatin immunoprecipitation data from a variety of human cell lines, as well as *in silico* TF-binding site predictions, all available from a publicly accessible repository (https://genome.ucsc.edu). We focussed on ieg-TF-binding sites (BSs) falling in the ±5.0kb interval around the *FOXG1*-transcriptional start site (TSS). Among them, we found BSs for FOS, EGR1, NFKB, CEBP and CREB (Fig. R18). *Foxg1* locus sequence is highly conserved among primates and rodents, suggesting that similar BSs may be present on the *mouse Foxg1* locus, at orthologous locations.

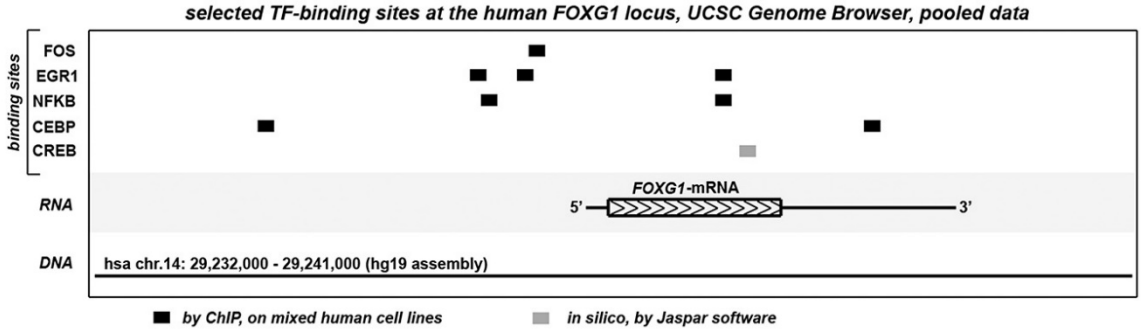

Figure R18 Selected TF-binding sites at the human *FOXG1* locus, UCSC Genome Borwser. Data, harvested from UCSC Genome Borwser, were obtained by ChIP, on mixed human cell lines, and in silico, by Jaspar software.

To assay the dependence of *Foxg1* expression on each of these factors, we challenged mixed neuronal-astrocytic cultures prepared as above with lentiviral vectors driving TetON-regulated expression of dedicated dominant negative (DN) effectors. We monitored the impact of these manipulations in baseline conditions, as well as in samples exposed to 25 mM K^+ for three hours (Fig. R19A,C). We found that in both cases DN constructs antagonizing activity stimulated-TFs elicited a pronounced, statistically significant downregulation of *Foxg1*-mRNA levels. The only exceptions were Egr1-DN, uneffective in baseline samples, as well as Nfkb-DN, uneffective in K^+ challenged samples. The amplitude of such downregulation was dramatic in case of Creb-DN, which halved *Foxg1* level in baseline

conditions and reduced it by about 9/10 under K^+ (Fig. R19E,F). Actually, Creb-assays required a far lower doxycycline concentration, as TetON Creb-DN activation elicited by standard concentrations was often lethal (R19D). These data suggest that - to different extents - cFos, Egr1, Nfkb, Cebp and Creb sustain baseline neuronal *Foxg1* transcription and contribute to its elevation associated to electrical activity.

To preliminarly dissect the distinct contributions that these activity stimulated-TFs provide to *Foxg1* regulation in mixed neural cultures, we repeated the DN assays in pure neuronal and astrocytic populations (Fig. R19A-C). We found that functional knock-down of these TFs in pure neuronal cultures not supplemented with K^+ depressed *Foxg1* expression to different extents, similar to mixed cultures. This confirms the pivotal role that these factors play in sustaining neuronal baseline *Foxg1* expression. Unexpectedly, however, we also found that ieg-TF-DNs *upregulated Foxg1* in pure astrocyte cultures, both in baseline conditions and, even more, under 25mM K^+. This effect was specifically pronounced in case of Egr1-DN, which increased *Foxg1* by >50% under high potassium ($p<0.01$). This does not apply to Creb-DN, whose impact on astrocytes was negligible (Fig. R19E,F). These data suggest that, within astrocytes, activity stimulated-TFs *inhibit* rather than promote *Foxg1* expression and contribute to dampen the smooth activation wave that this gene displays upon K^+ stimulation. Finally, we found that a substantial *Foxg1* upregulation was also achieved by Egr1-DN, Cebp-DN and Nfkb-DN overexpression in pure neuronal cultures stimulated by K^+ (Fig. R19F). These last phenomena are puzzling. It is really difficult to provide simple explanations for them.

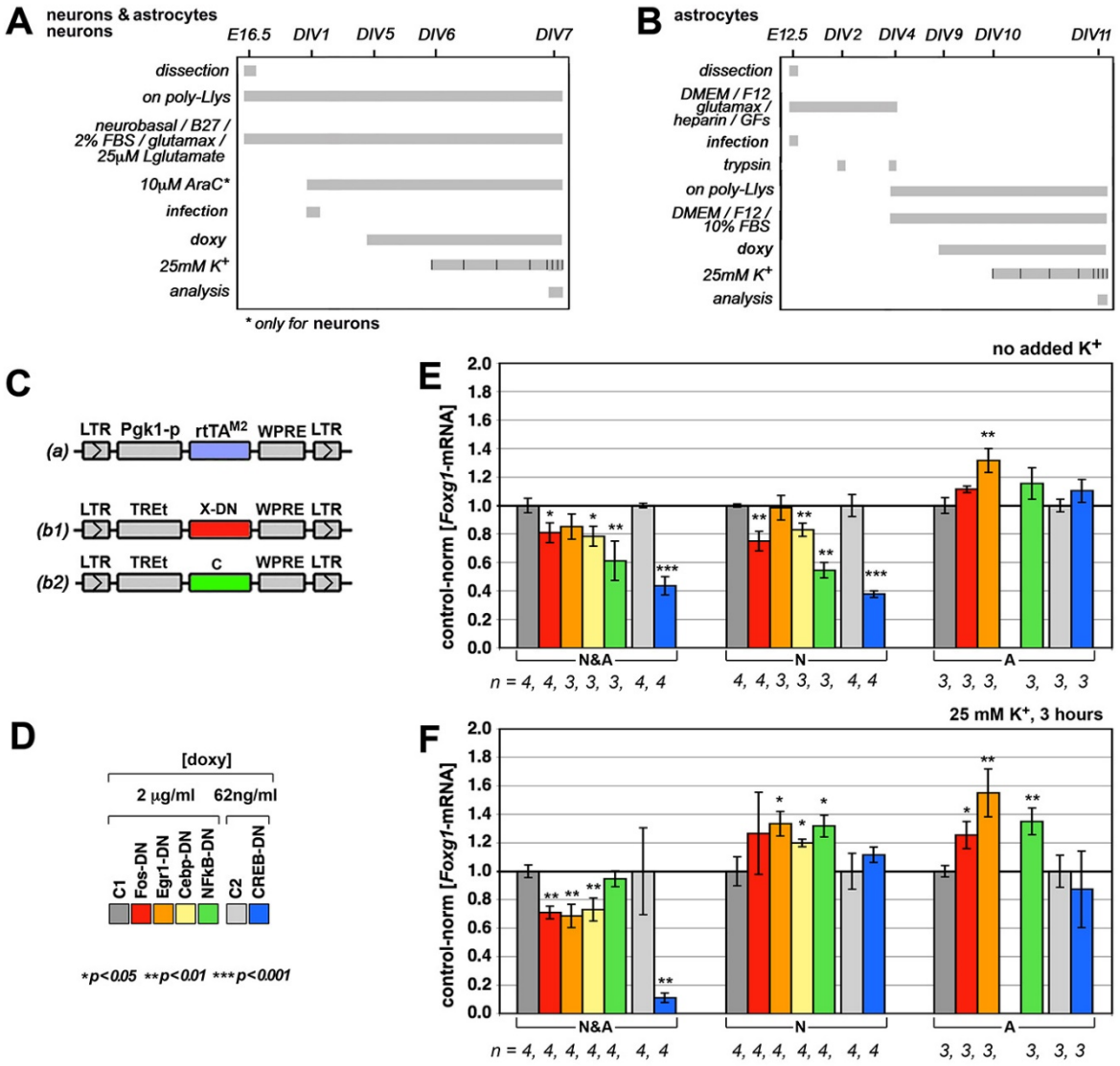

Figure R19 Fluctuations of *Foxg1* mRNA levels in primary, neuronal, astroglial and mixed cultures, upon chronic overexpression of immediate early gene- (ieg)-dominant negative (DN) LV effectors and/or 3 hours exposure to 25mM extracellular K^+. Culturing procedures followed for mixed and neuronal **(A)** as well as astroglial **(B)** preparations subject of RNA profiling. **(C,D)** TetON lentiviral vector sets and doxycycline concentrations employed for DN (a,b1) and control (a,b2) manipulations. **(E,F)** Graphical synopsis of results, obtained under 25mM extracellular K^+ (F) and control conditions (E).

5. DISCUSSION

5.1 A synopsis of major findings

Here we describe a characterization of a novel *Foxg1*-GOF model we created to dissect the role of *Foxg1* in postmitotic neuronal differentiation and reconstruct pathogenetic mechanisms which underlie the *FOXG1* duplication-linked West syndrome. This is a devastating neurological disorder, triggered by a complex variety of pathogenic conditions. It is characterized by infantile spasms, abnormal EEG with hypsarrhytmia and seizures and dramatic cognitive impairment, for which only symptomatic treatments are presently available.

As expected, these *Foxg1*-GOF mice showed increased neuronal activity in baseline conditions and were more prone to limbic motor seizures upon kainic acid administration.

A preliminary developmental profiling of their cerebral cortex unveiled four major histogenetic anomalies, likely contributing to their hyperexcitability. These anomalies were: (1) an altered neocortical laminar blueprint with impaired layer VI/layer V segregation and defective activation of layer IV-II programs; (2) a substantial reduction of PV^+ interneurons; (3) a patterned, area- and lamina-specific astrocyte deprivation; (4) a defective expression of the Gabra1 receptor subunit. Similar phenomena might concur to neurological anomalies of West syndrome patients harboring *FOXG1* duplications.

A parallel in vitro study, run on dissociated cortico-cerebral cultures, revealed that a substantial *Foxg1* upregulation occurred upon delivery of depolarizing stimuli. Neuronal, activity-linked *Foxg1* elevation required the presence of astrocytes. Activity-linked *Foxg1* fluctuations were inter-twinned with immediate-early genes fluctuations and depended on them, according to distinct, neuron- and astrocyte-specific patterns. In West syndrome patients with augmented *FOXG1* dosage, a *FOXG1*-mRNA increase evoked by depolarizing stimuli might ignite a vicious circle, exacerbating neuronal hyperactivity and contributing to interictal EEG anomalies and seizures.

5.2 Generation of *Foxg1* gain-of-function mouse models

Foxg1-GOF models employed for this study were generated by combining a *TREt*-driven *Foxg1-IRES-Egfp* transgene and a tTA-TetOFF-transactivator encoding allele, knocked into the endogenous *Foxg1* locus by homologous recombination (Fig. R1A). According to the experimental design, they were expected to faithfully reproduce the expression pattern of the endogenous gene. Conversely, transgene activation was restricted to the neocortical field. No transgene product was detected in archicortex, paleocortex, subpallium, eye, anterior hypothalamus and their derivatives, all expressing the endogenous gene (Fig. R2 and R6). Moreover, within neocortex, transgene products were absent in periventricular proliferative layers, expressing the endogenous gene at low levels. They were only detectable in embryonic cortical plate and deep layers of perinatal/juvenile neocortex, characterized by a robust activation of the endogenous gene (Fig. R3 and R5). Here, as expected, the transgene was specifically expressed in postmitotic pyramidal neurons (Fig. R4), but not at all in astrocytes (Fig. R7). Transgene confinement to a subset of the canonical *Foxg1* expression domain reasonably reflects the "landing" of the transgene into a poorly permissive "chromatin environment", inhibiting tTA from driving transgene transcription in extra-neocortical territories. In particular, delayed transgene activation in postmitotic neurons (Fig. R1C), might specifically originate from its integration into an L1 LINE element, as detected by splinkerette-assisted mapping (Ochman et al., 1988) of transgene insertion (data not shown). It has been shown - in fact - that L1 elements are specifically silenced in neural stem cells, by a dedicated Sox2/MeCP2/HDAC1-dependent mechanism, getting permissive for transcription only in their neuronal derivatives (Coufal et al., 2009).

Total mRNA originating from the *Foxg1* and transgene loci was quantified by cumulative qRTPCR evaluation of a diagnostic amplicon shared by the $Foxg1^{+}$, $Foxg1^{tTA}$ and $TREt\text{-}Foxg1\text{-}IRES\text{-}Egfp^{+}$ alleles (Fig. 1A,D). Compared to wt, "wt" and LOF animals, GOF mice showed a 2.1x mRNA content (Fig. 1D). 0.5x of this content comes from the $Foxg1^{tTA}$ allele, 1.6x really encodes for *Foxg1*-cds (Fig. 1A), so suggesting that a net +60% average expression gain may characterize GOF mutants compared to controls. However, at P0 (the time at which qRTPCR was done), only a fraction of pyramidal neurons forming the normal *Foxg1*

expression domain activates the transgene. Cautiously, such fraction might be close to 1/3. This means that such neurons might give rise to a real *Foxg1*-mRNA expression gain around +3*60%, i.e. +180%.

Summing up, our "*Foxg1*-GOF" mutants are "functionally *Foxg1*-LOF" within their proliferating neural precursors and display an approximate 3x *Foxg1* expression gain in a large subset of their deep neocortical neurons. As such, they are not a "perfect" model for dissecting pathogenetic mechanisms triggered by exaggerated *FOXG1* dosage. However, they offer the unique opportunity to study a subset of them in a far simplified and tractable context.

5.3 Hyperexcitability of *Foxg1*-GOF mice

To unveil a possible hyperexcitability of *Foxg1*-GOF tissue, mutant mice were challenged with the powerful glutamatergic agonist kainic acid. As expected, GOF mutants gave a Racine's score higher than pooled WT (*Foxg1*$^{+/+}$*;Tg:Tre-Foxg1-IRES-Egfp*$^{-/-}$) and "WT" (*Foxg1*$^{+/+}$*;Tg:Tre-Foxg1-IRES-Egfp*$^{+/-}$) controls, which resulted statistically significant upon both cumulative/non-parametric and timed/parametric evaluation of results (Fig. R9A-C). Interestingly, LOF mutants scored very close to controls and no statistically significant difference was appreciable (Fig. R9A-C). This rules out that the GOF genotype could arise form a dominant negative effect. Moreover, comparison of performances of WT and "WT" groups (both cumulative/non parametric and parametric at times of stronger GOF/controls discrepancy) did not display any significant change (data not shown). This further implies that GOF hyperexcitability is due to transgene activity itself and not to consequences of insertional mutagenesis, associated to lentiviral integration. In situ analysis of brains taken from KA-treated animals showed a patterned activation of the ieg *cFos*, nicely correlating with the animal Racine's scoring. It pointed to the hippocampus as the source of epileptogenic electric perturbations (Fig. R9D).

Preferential involvement of the hippocampus in epileptogenic events largely originates from neurocircuital connections of this structure, receiving neocortical and paleocortical afferences through the entorhino-hippocampal bundle and reverberating them through the CA3 autoassociator (Neves et al., 2008; Wilson and Rennaker, 2010). As such,

the hippocampus acts as a "high gain antenna" collecting afferences from all over the cortex and providing a relatively simplified proxy for their evaluation. We took advantage of that in KA assays, but also in EEG evaluation of animals, in "baseline" conditions. Here an electrode placed between CA1 and DG (Fig. R8A) provided us with a "comprehensive overview" of the whole brain electrical activity (Fig. R8C), substantially corroborating conclusions of KA assays. In this context, it is to note the differences of *cFos* activation evoked by KA, in DG, more refractory, versus CA3, more permissive. Self-reverberating connections of CA3 neurons likely undelie this phenomenon. Such differences allow to neatly discriminate among *Foxg1*-GOF and other mice (Fig. 9D).

5.4 Histogenetic disorders underlying *Foxg1*-GOF mice hyperexcitability

Then we studied a number of histogenetic anomalies occurring to *Foxg1*-GOF mice and possibly underlying their neural hyperexcitability.

A subset of them admit a cell autonomous explanation. This is the case of defective segregation among layer VI and layer V pyramidal neurons, both expressing the transgene at high frequency (Fig. 10A,B). This applies to Gabra1 downregulation, which takes place to large extent in cerebral neurons (Fig. R12 and R13). This can also be the case of shrunken upper layer neurons.

Actually, the interpretation of this last phenotype requires some special caution. In fact, a similar phenomenon has been described in *Foxg1*-LOF mice, possibly due to precocious exhaustion of the periventricular proliferating pool (Eagleson et al., 2007). Our "GOF" mice are functionally LOF within this pool, which opens the possibility that what we observe has not a real GOF origin. However, it has been firmly shown that the occurrence of this phenomenon in LOF mice does require the presence of a specific "*cre*" allele within the *null Foxg1* locus and does not appear in the presence of *LacZ* and *tTA* alleles. Moreover, it only occurs in mice of pure C57Bl6 strain, while disappearing in CBA1xC57Bl6 hybrids (Eagleson et al., 2007). Our mice do not harbor a *cre* allele and moreover they were generated on a C57Bl6xCD1 background. Therefore we are strongly confident that what we see has a genuine GOF origin.

How may this layer IV-II shrinkage arise in *Foxg1*-GOF animals? Mutual exclusion of Cux1 and EGFP in mutant neocortices suggests that Foxg1 might trans-repress Cux1 in late newborn neurons, channelling them toward deep rather than upper layer identities. Actually, laminar specification of upper layer neurons specifically relies on an intricate network of cross-inhibitory interactions among patterned transcription factors active in proliferating precursors and/or their post-mitotic derivatives. In particular, Tbr1 indirectly permits the activation of layer IV-II programs, via inhibition of their inhibitor, the layer V promoter Fezf2 (Han et al., 2011; McKenna et al., 2011; Srinivasan et al., 2012). In this context, *Foxg1* could dampen upper layer specification indirectly, by repressing *Tbr1* transcription (Toma et al., 2014).

Even if we favor this hypothesis, we are aware that a different, not-cell-autonomous mechanism may contribute to upper layer shrinkage. Hanashima and coll. (Toma et al., 2014) have shown that deep layer neurons send an (unknown) signal to periventricular layers, pushing them to transit to upper layer generation. It is tempting to speculate that *Foxg1* overexpression in deep layer neurons might jeopardize the transmission of this signal or could force progenitors to precociously leave cell cycle, ultimately resulting in upper layers hypoplasia

Besides lamination defects, our *Foxg1*-GOF models exhibit two other major histogenetic disorders, which occur in clonal compartments not originating from transgene-expressing cells. These are reduced PV^+ interneurons and astrocytes. These anomalies may obviously provide a major causative contribution to neuronal hyperexcitability. As both PV^+ cells and astrocytes are not born by transgene-expressing cells, molecular mechanisms linking transgene activation to their scarcity reasonably include not-cell autonomous ones. In particular, defective signals from neocortical periventricular layers promoting interneuron influx from subpallium (Sessa et al., 2010) might account for the former phenomenon. Unbalanced signals coming from pyramidal neurons and tuning astrogenic rates might account for the latter. A preliminary survey of these signals (Barnabé-Heider et al., 2005; Seuntjens et al., 2009; Sardi et al., 2006) did not revealed any change. Further dedicated assays will be required to clarify these issues.

5.5 Activity-dependent *Foxg1* regulation

Finally, we have seen that exaggerated *Foxg1* expression results in a number of neurodevelopmental anomalies leading to an increase of neural tissue excitability. We wondered if electrical activity in turn modulates *Foxg1* activation. We addressed this point by evaluating the impact that exposure to high extracellular potassium, an established tool for promoting neuronal discharge, can have on *Foxg1*-mRNA levels, in mixed neuronal/astroglial cultures, originating from cerebral cortex of late gestation embryos. We found that *Foxg1* was upregulated starting from 1 hour, peaked at 3 hours and got back to baseline by 24 hours (Fig. R17).

The presence of a number binding sites for activity-regulated TFs (cFos, Egr1, Egr2, Cebp, Nfkb, Creb) within the *Foxg1* promoter (Fig. R18) suggested that these TFs might be involved in controlling such dynamics. To verify this prediction, we functionally knocked down these TFs by chronic overexpression of DN mutant versions of them. In all cases, this treatment led to an attenuation of *Foxg1* expression, *both in baseline conditions and under chronic* K^+. As expected (REF: Minichiello-Kein), three of these factors, cFos, Egr1 and Egr2, displayed a peak of mRNA expression 1 hour after K^+ supplementation (Fig. R17). This dynamics hardly accounts for a role of these genes in early *Foxg1*-mRNA elevation and rather helps explain further upregulation of this gene at around 3 hours and later. Conversely, a pivotal role in early *Foxg1* activation might be played by activity-dependent activation of Cebp, Nfkb and Creb, which mainly relies on *fast* post-translational regulation. This is achieved by neurotrophin-dependent recruitment to chromatine (Cebp) (Calella et al., 2007), extra-cellular signal-modulated cytoplasm-to-nucleus translocation (Nfkb)(Gutierrez and Davies, 2011), and Ca^{2+}/cAMP-triggered phosphorylation (Creb) (de la Torre-Ubieta and Bonni, 2011). As such, Cebp, Nfkb and Creb may promote both early and later *Foxg1*-mRNA elevation.

As for late *Foxg1* decline, different mechanisms may account for it. Such decline may reflect the parallel decrease of presumptive *Foxg1* transactivators cFos and Egr (Fig R19E,F and R17), the canonical autoinhibitory loop intrinsic to Nfkb signalling (Chiao et al., 1994), and a *Foxg1* self-inhibitory loop relying on the Foxg1 protein (data not shown).

To dissect neuronal and astrocytic contributions to the *Foxg1* dynamics in mixed cultures under K^+ stimulation, we run *Foxg1* time course analysis on pure neuronal or astrocytic cultures. Astrocytes gave rise to an activation profile similar to mixed cultures, however missing the pronounced peak at 3 hours. Conversely, neurons displayed only small changes, not statistically relevant (Fig. R17). This is particularly intriguing as our mixed cultures differred from neuronal cultures only for a small percentage of astrocytes (about 1/12) present in the former and absent in the latter (Fig. R16). This suggests that either an event of the chain leading to neuronal *Foxg1* transactivation takes place in astrocytes, or astrocytes provide neurons with a specific input needed for its implementation. Further hints came from functional inhibition of activity-regulated TFs in (1) pure astroglial and (2) neuronal populations. In the former case (Fig. R19E,F), such manipulation paradoxycally resulted in *Foxg1* upregulation, both in baseline conditions and under high potassium. In other words, within astrocytes, these TFs seem to inhibit *Foxg1*. Differential expression of lineage-specific cofactors, synergizing with them on the *Foxg1* promoter (Calella et al., 2007), might undelie this discrepancy, determining the distinct outcomes of their activity. In the latter case (Fig. R19E,F), transduction of DN constructs resulted in *Foxg1* downregulation and its upregulation, in baseline conditions and under K^+, respectively. In other words, neurons, deprived of their astrocyte companions, adopt an astrocyte-like "behaviour", specifically if exposed to conditions triggering electrical hyperactivity. Molecular mechanics underlying such neuronal behaviour and its biological meaning, if any, are at the moment obscure.

6. SUPPLEMENTARY MATERIAL

wt-absolute averages of PV$^+$cells/1mm^2 on 16μm thick sections

P35	R		I		C	
	l	*m*	*l*	*m*	*l*	*m*
I	3.1 ± 2.2	2.5 ± 2.5	1.0 ± 1.0	0.0 ± 0.0	3.7 ± 2.5	1.5 ± 1.5
II-VI	80.5 ± 7.3	89.7 ± 4.7	100.0 ± 12.7	118.3 ± 13.0	101.2 ± 8.0	117.3 ± 14.1
WM/E	5.1 ± 3.2	9.6 ± 2.8	4.7 ± 2.8	3.3 ± 2.0	15.5 ± 3.1	26.8 ± 9.2

Supplementary Figure S1.

wt-absolute averages of S100β$^+$cells/1000μm^2 on 16μm thick sections

P7	R		I		C	
	l	*m*	*l*	*m*	*l*	*m*
I	1.5 ± 0.1	1.2 ± 0.1	1.2 ± 0.1	1.0 ± 0.2	1.0 ± 0.1	1.3 ± 0.3
II-IV	1.3 ± 0.1	1.3 ±0.2	1.3 ± 0.1	1.3 ± 0.1	1.0 ± 0.1	0.9 ± 0.2
V	1.0 ± 0.2	1.1 ± 0.2	1.1 ± 0.0	1.2 ± 0.1	1.3 ± 0.1	1.2 ± 0.1
VI	1.0 ± 0.2	0.9 ± 0.1	1.0 ± 0.1	1.1 ± 0.1	1.2 ± 0.1	1.1 ± 0.2
WM/E	1.2 ± 0.3	1.1 ± 0.1	1.0 ± 0.1	1.2 ± 0.1	1.5 ± 0.2	1.3 ± 0.1

Supplementary Figure S2.

Acknowledgments:

Thanks to Dr. Manuela Allegra and Dr. Matteo Calleo for the EEG recordings performed at CNR Neuroscience Institute in Pisa.

Thanks to Prof.Yuri Bozzi and Dr.Giovanni Provenzano for the collaboration on behavioral experiments at Centre for Integrative Biology (CIBIO), in Trent, and SISSA, in Trieste.

Thanks to Simone Chiola for the *Foxg1*-gain of function *in vitro* cultures.

REFERENCES

Ahn, S., Olive, M., Aggarwal, S., Krylov, D., Ginty, D.D., and Vinson, C. (1998). A dominant-negative inhibitor of CREB reveals that it is a general mediator of stimulus-dependent transcription of c-fos. Mol. Cell. Biol. *18*, 967–977.

Alcamo, E.A., Chirivella, L., Dautzenberg, M., Dobreva, G., Fariñas, I., Grosschedl, R., and McConnell, S.K. (2008). Satb2 regulates callosal projection neuron identity in the developing cerebral cortex. Neuron *57*, 364–377.

Altmann, C.R., and Brivanlou, A.H. (2001). Neural patterning in the vertebrate embryo. Int. Rev. Cytol. *203*, 447–482.

Amor, D.J., Burgess, T., Tan, T.Y., and Pertile, M.D. (2012). Questionable pathogenicity of FOXG1 duplication. Eur. J. Hum. Genet. EJHG *20*, 595–596; author reply 596–597.

Anderson, D.J., Groves, A., Lo, L., Ma, Q., Rao, M., Shah, N.M., and Sommer, L. (1997). Cell lineage determination and the control of neuronal identity in the neural crest. Cold Spring Harb. Symp. Quant. Biol. *62*, 493–504.

Anderson, S.A., Marín, O., Horn, C., Jennings, K., and Rubenstein, J.L. (2001). Distinct cortical migrations from the medial and lateral ganglionic eminences. Dev. Camb. Engl. *128*, 353–363.

Anderson, S.A., Kaznowski, C.E., Horn, C., Rubenstein, J.L.R., and McConnell, S.K. (2002). Distinct origins of neocortical projection neurons and interneurons in vivo. Cereb. Cortex N. Y. N 1991 *12*, 702–709.

Ang, E.S.B.C., Haydar, T.F., Gluncic, V., and Rakic, P. (2003). Four-dimensional migratory coordinates of GABAergic interneurons in the developing mouse cortex. J. Neurosci. Off. J. Soc. Neurosci. *23*, 5805–5815.

Angevine, J.B., and Sidman, R.L. (1961). Autoradiographic study of cell migration during histogenesis of cerebral cortex in the mouse. Nature *192*, 766–768.

Anthony, T.E., Klein, C., Fishell, G., and Heintz, N. (2004). Radial glia serve as neuronal progenitors in all regions of the central nervous system. Neuron *41*, 881–890.

Araque, A., Sanzgiri, R.P., Parpura, V., and Haydon, P.G. (1999). Astrocyte-induced modulation of synaptic transmission. Can. J. Physiol. Pharmacol. *77*, 699–706.

Barnabé-Heider, F., Wasylnka, J.A., Fernandes, K.J.L., Porsche, C., Sendtner, M., Kaplan, D.R., and Miller, F.D. (2005). Evidence that embryonic neurons regulate the onset of cortical gliogenesis via cardiotrophin-1. Neuron *48*, 253–265.

Barnes, A.P., Lilley, B.N., Pan, Y.A., Plummer, L.J., Powell, A.W., Raines, A.N., Sanes, J.R., and Polleux, F. (2007). LKB1 and SAD kinases define a pathway required for the polarization of cortical neurons. Cell *129*, 549–563.

Bertossi, C., Cassina, M., De Palma, L., Vecchi, M., Rossato, S., Toldo, I., Donà, M., Murgia, A., Boniver, C., and Sartori, S. (2014). 14q12 duplication including FOXG1: is there a common age-dependent epileptic phenotype? Brain Dev. *36*, 402–407.

Bhat, K.M., van Beers, E.H., and Bhat, P. (2000). Sloppy paired acts as the downstream target of wingless in the Drosophila CNS and interaction between sloppy paired and gooseberry inhibits sloppy paired during neurogenesis. Dev. Camb. Engl. *127*, 655–665.

Bielle, F., Griveau, A., Narboux-Nême, N., Vigneau, S., Sigrist, M., Arber, S., Wassef, M., and Pierani, A. (2005). Multiple origins of Cajal-Retzius cells at the borders of the developing pallium. Nat. Neurosci. *8*, 1002–1012.

Brancaccio, M., Pivetta, C., Granzotto, M., Filippis, C., and Mallamaci, A. (2010). Emx2 and Foxg1 inhibit gliogenesis and promote neuronogenesis. Stem Cells Dayt. Ohio *28*, 1206–1218.

Britanova, O., de Juan Romero, C., Cheung, A., Kwan, K.Y., Schwark, M., Gyorgy, A., Vogel, T., Akopov, S., Mitkovski, M., Agoston, D., et al. (2008). Satb2 is a postmitotic determinant for upper-layer neuron specification in the neocortex. Neuron *57*, 378–392.

Brunetti-Pierri, N., Paciorkowski, A.R., Ciccone, R., Della Mina, E., Bonaglia, M.C., Borgatti, R., Schaaf, C.P., Sutton, V.R., Xia, Z., Jelluma, N., et al. (2011). Duplications of FOXG1 in 14q12 are associated with developmental epilepsy, mental retardation, and severe speech impairment. Eur. J. Hum. Genet. EJHG *19*, 102–107.

Bystron, I., Blakemore, C., and Rakic, P. (2008). Development of the human cerebral cortex: Boulder Committee revisited. Nat. Rev. Neurosci. *9*, 110–122.

Calegari, F., and Huttner, W.B. (2003). An inhibition of cyclin-dependent kinases that lengthens, but does not arrest, neuroepithelial cell cycle induces premature neurogenesis. J. Cell Sci. *116*, 4947–4955.

Calella, A.M., Nerlov, C., Lopez, R.G., Sciarretta, C., von Bohlen und Halbach, O., Bereshchenko, O., and Minichiello, L. (2007). Neurotrophin/Trk receptor signaling mediates C/EBPalpha, -beta and NeuroD recruitment to immediate-early gene promoters in neuronal cells and requires C/EBPs to induce immediate-early gene transcription. Neural Develop. *2*, 4.

Cavanagh, M.E., and Parnavelas, J.G. (1989). Development of vasoactive-intestinal-polypeptide-immunoreactive neurons in the rat occipital cortex: a combined immunohistochemical-autoradiographic study. J. Comp. Neurol. *284*, 637–645.

Chen, B., Wang, S.S., Hattox, A.M., Rayburn, H., Nelson, S.B., and McConnell, S.K. (2008). The Fezf2-Ctip2 genetic pathway regulates the fate choice of subcortical projection neurons in the developing cerebral cortex. Proc. Natl. Acad. Sci. U. S. A. *105*, 11382–11387.

Chenn, A., and McConnell, S.K. (1995). Cleavage orientation and the asymmetric inheritance of Notch1 immunoreactivity in mammalian neurogenesis. Cell *82*, 631–641.

Cherubini, E., and Conti, F. (2001). Generating diversity at GABAergic synapses. Trends Neurosci. *24*, 155–162.

Chiao, P.J., Miyamoto, S., and Verma, I.M. (1994). Autoregulation of I kappa B alpha activity. Proc. Natl. Acad. Sci. U. S. A. *91*, 28–32.

Coufal, N.G., Garcia-Perez, J.L., Peng, G.E., Yeo, G.W., Mu, Y., Lovci, M.T., Morell, M., O'Shea, K.S., Moran, J.V., and Gage, F.H. (2009). L1 retrotransposition in human neural progenitor cells. Nature *460*, 1127–1131.

Danesin, C., and Houart, C. (2012). A Fox stops the Wnt: implications for forebrain development and diseases. Curr. Opin. Genet. Dev. *22*, 323–330.

Danesin, C., Peres, J.N., Johansson, M., Snowden, V., Cording, A., Papalopulu, N., and Houart, C. (2009). Integration of telencephalic Wnt and hedgehog signaling center activities by Foxg1. Dev. Cell *16*, 576–587.

DeFelipe, J. (1993). Neocortical neuronal diversity: chemical heterogeneity revealed by colocalization studies of classic neurotransmitters, neuropeptides, calcium-binding proteins, and cell surface molecules. Cereb. Cortex N. Y. N 1991 *3*, 273–289.

DeFelipe, J. (1997). Types of neurons, synaptic connections and chemical characteristics of cells immunoreactive for calbindin-D28K, parvalbumin and calretinin in the neocortex. J. Chem. Neuroanat. *14*, 1–19.

Dehay, C., and Kennedy, H. (2007). Cell-cycle control and cortical development. Nat. Rev. Neurosci. *8*, 438–450.

Desai, A.R., and McConnell, S.K. (2000). Progressive restriction in fate potential by neural progenitors during cerebral cortical development. Dev. Camb. Engl. *127*, 2863–2872.

Djukic, B., Casper, K.B., Philpot, B.D., Chin, L.-S., and McCarthy, K.D. (2007). Conditional knock-out of Kir4.1 leads to glial membrane depolarization, inhibition of potassium and glutamate uptake, and enhanced short-term synaptic potentiation. J. Neurosci. Off. J. Soc. Neurosci. *27*, 11354–11365.

Doetsch, F., Caillé, I., Lim, D.A., García-Verdugo, J.M., and Alvarez-Buylla, A. (1999). Subventricular zone astrocytes are neural stem cells in the adult mammalian brain. Cell *97*, 703–716.

Dou, C.L., Li, S., and Lai, E. (1999). Dual role of brain factor-1 in regulating growth and patterning of the cerebral hemispheres. Cereb. Cortex N. Y. N 1991 *9*, 543–550.

Eagleson, K.L., Schlueter McFadyen-Ketchum, L.J., Ahrens, E.T., Mills, P.H., Does, M.D., Nickols, J., and Levitt, P. (2007). Disruption of Foxg1 expression by knock-in of cre recombinase: effects on the development of the mouse telencephalon. Neuroscience *148*, 385–399.

Edlund, T., and Jessell, T.M. (1999). Progression from extrinsic to intrinsic signaling in cell fate specification: a view from the nervous system. Cell *96*, 211–224.

Falace, A., Vanni, N., Mallamaci, A., Striano, P., and Zara, F. (2013). Do regulatory regions matter in FOXG1 duplications? Eur. J. Hum. Genet. EJHG *21*, 365–366.

Fasano, C.A., Phoenix, T.N., Kokovay, E., Lowry, N., Elkabetz, Y., Dimos, J.T., Lemischka, I.R., Studer, L., and Temple, S. (2009). Bmi-1 cooperates with Foxg1 to maintain neural stem cell self-renewal in the forebrain. Genes Dev. *23*, 561–574.

Fellin, T., and Carmignoto, G. (2004). Neurone-to-astrocyte signalling in the brain represents a distinct multifunctional unit. J. Physiol. *559*, 3–15.

Fietz, S.A., and Huttner, W.B. (2011). Cortical progenitor expansion, self-renewal and neurogenesis-a polarized perspective. Curr. Opin. Neurobiol. *21*, 23–35.

Flames, N., and Marín, O. (2005). Developmental mechanisms underlying the generation of cortical interneuron diversity. Neuron *46*, 377–381.

Follenzi, A., and Naldini, L. (2002). Generation of HIV-1 derived lentiviral vectors. Methods Enzymol. *346*, 454–465.

Fox, I.J., and Kornblum, H.I. (2005). Developmental profile of ErbB receptors in murine central nervous system: implications for functional interactions. J. Neurosci. Res. *79*, 584–597.

Franco, S.J., Gil-Sanz, C., Martinez-Garay, I., Espinosa, A., Harkins-Perry, S.R., Ramos, C., and Müller, U. (2012). Fate-restricted neural progenitors in the mammalian cerebral cortex. Science *337*, 746–749.

Frantz, G.D., and McConnell, S.K. (1996). Restriction of late cerebral cortical progenitors to an upper-layer fate. Neuron *17*, 55–61.

Gioran, A., Nicotera, P., and Bano, D. (2014). Impaired mitochondrial respiration promotes dendritic branching via the AMPK signaling pathway. Cell Death Dis. *5*, e1175.

Gonchar, Y., Wang, Q., and Burkhalter, A. (2007). Multiple distinct subtypes of GABAergic neurons in mouse visual cortex identified by triple immunostaining. Front. Neuroanat. *1*, 3.

Gorski, J.A., Talley, T., Qiu, M., Puelles, L., Rubenstein, J.L.R., and Jones, K.R. (2002). Cortical excitatory neurons and glia, but not GABAergic neurons, are produced in the Emx1-expressing lineage. J. Neurosci. Off. J. Soc. Neurosci. *22*, 6309–6314.

Götz, M., and Huttner, W.B. (2005). The cell biology of neurogenesis. Nat. Rev. Mol. Cell Biol. *6*, 777–788.

Greig, L.C., Woodworth, M.B., Galazo, M.J., Padmanabhan, H., and Macklis, J.D. (2013). Molecular logic of neocortical projection neuron specification, development and diversity. Nat. Rev. Neurosci. *14*, 755–769.

Grove, E.A., Tole, S., Limon, J., Yip, L., and Ragsdale, C.W. (1998). The hem of the embryonic cerebral cortex is defined by the expression of multiple Wnt genes and is compromised in Gli3-deficient mice. Dev. Camb. Engl. *125*, 2315–2325.

Guruharsha, K.G., Kankel, M.W., and Artavanis-Tsakonas, S. (2012). The Notch signalling system: recent insights into the complexity of a conserved pathway. Nat. Rev. Genet. *13*, 654–666.

Gutierrez, H., and Davies, A.M. (2011). Regulation of neural process growth, elaboration and structural plasticity by NF-κB. Trends Neurosci. *34*, 316–325.

Gutin, G., Fernandes, M., Palazzolo, L., Paek, H., Yu, K., Ornitz, D.M., McConnell, S.K., and Hébert, J.M. (2006). FGF signalling generates ventral telencephalic cells independently of SHH. Dev. Camb. Engl. *133*, 2937–2946.

Han, W., Kwan, K.Y., Shim, S., Lam, M.M.S., Shin, Y., Xu, X., Zhu, Y., Li, M., and Sestan, N. (2011). TBR1 directly represses Fezf2 to control the laminar origin and development of the corticospinal tract. Proc. Natl. Acad. Sci. U. S. A. *108*, 3041–3046.

Hanashima, C., Shen, L., Li, S.C., and Lai, E. (2002). Brain factor-1 controls the proliferation and differentiation of neocortical progenitor cells through independent mechanisms. J. Neurosci. Off. J. Soc. Neurosci. *22*, 6526–6536.

Hanashima, C., Li, S.C., Shen, L., Lai, E., and Fishell, G. (2004). Foxg1 suppresses early cortical cell fate. Science *303*, 56–59.

Hanashima, C., Fernandes, M., Hebert, J.M., and Fishell, G. (2007). The role of Foxg1 and dorsal midline signaling in the generation of Cajal-Retzius subtypes. J. Neurosci. Off. J. Soc. Neurosci. *27*, 11103–11111.

Hansen, D.V., Lui, J.H., Parker, P.R.L., and Kriegstein, A.R. (2010). Neurogenic radial glia in the outer subventricular zone of human neocortex. Nature *464*, 554–561.

Haubensak, W., Attardo, A., Denk, W., and Huttner, W.B. (2004). Neurons arise in the basal neuroepithelium of the early mammalian telencephalon: a major site of neurogenesis. Proc. Natl. Acad. Sci. U. S. A. *101*, 3196–3201.

Heinrich, P.C., Behrmann, I., Müller-Newen, G., Schaper, F., and Graeve, L. (1998). Interleukin-6-type cytokine signalling through the gp130/Jak/STAT pathway. Biochem. J. *334 (Pt 2)*, 297–314.

Hevner, R.F., Shi, L., Justice, N., Hsueh, Y., Sheng, M., Smiga, S., Bulfone, A., Goffinet, A.M., Campagnoni, A.T., and Rubenstein, J.L. (2001). Tbr1 regulates differentiation of the preplate and layer 6. Neuron *29*, 353–366.

Higashi, K., Fujita, A., Inanobe, A., Tanemoto, M., Doi, K., Kubo, T., and Kurachi, Y. (2001). An inwardly rectifying K(+) channel, Kir4.1, expressed in astrocytes surrounds synapses and blood vessels in brain. Am. J. Physiol. Cell Physiol. *281*, C922–C931.

Houart, C., Westerfield, M., and Wilson, S.W. (1998). A small population of anterior cells patterns the forebrain during zebrafish gastrulation. Nature *391*, 788–792.

Houser, C.R., Hendry, S.H., Jones, E.G., and Vaughn, J.E. (1983). Morphological diversity of immunocytochemically identified GABA neurons in the monkey sensory-motor cortex. J. Neurocytol. *12*, 617–638.

Hrachovy, R.A., and Frost, J.D. (1989). Infantile spasms. Pediatr. Clin. North Am. *36*, 311–329.

John Rubenstein and Pasko Rakic (2013). Patterning and Cell type specification in the developing Cns and Pns.

Juliandi, B., Abematsu, M., and Nakashima, K. (2010). Chromatin remodeling in neural stem cell differentiation. Curr. Opin. Neurobiol. *20*, 408–415.

Kaestner, K.H., Lee, K.H., Schlöndorff, J., Hiemisch, H., Monaghan, A.P., and Schütz, G. (1993). Six members of the mouse forkhead gene family are developmentally regulated. Proc. Natl. Acad. Sci. U. S. A. *90*, 7628–7631.

Kawaguchi, Y., and Kondo, S. (2002). Parvalbumin, somatostatin and cholecystokinin as chemical markers for specific GABAergic interneuron types in the rat frontal cortex. J. Neurocytol. *31*, 277–287.

Kimelberg, H.K., and Kettenmann, H. (1990). Swelling-induced changes in electrophysiological properties of cultured astrocytes and oligodendrocytes. I. Effects on membrane potentials, input impedance and cell-cell coupling. Brain Res. *529*, 255–261.

Kippin, T.E., Martens, D.J., and van der Kooy, D. (2005). p21 loss compromises the relative quiescence of forebrain stem cell proliferation leading to exhaustion of their proliferation capacity. Genes Dev. *19*, 756–767.

Kofuji, P., and Newman, E.A. (2004). Potassium buffering in the central nervous system. Neuroscience *129*, 1045–1056.

Kopan, R., and Ilagan, M.X.G. (2009). The canonical Notch signaling pathway: unfolding the activation mechanism. Cell *137*, 216–233.

Kowalczyk, T., Pontious, A., Englund, C., Daza, R.A.M., Bedogni, F., Hodge, R., Attardo, A., Bell, C., Huttner, W.B., and Hevner, R.F. (2009). Intermediate neuronal progenitors (basal progenitors) produce pyramidal-projection neurons for all layers of cerebral cortex. Cereb. Cortex N. Y. N 1991 *19*, 2439–2450.

Kriegstein, A., and Alvarez-Buylla, A. (2009). The glial nature of embryonic and adult neural stem cells. Annu. Rev. Neurosci. *32*, 149–184.

Krimer, L.S., and Goldman-Rakic, P.S. (2001). Prefrontal microcircuits: membrane properties and excitatory input of local, medium, and wide arbor interneurons. J. Neurosci. Off. J. Soc. Neurosci. *21*, 3788–3796.

Krubitzer, L., and Kaas, J. (2005). The evolution of the neocortex in mammals: how is phenotypic diversity generated? Curr. Opin. Neurobiol. *15*, 444–453.

Kucheryavykh, Y.V., Kucheryavykh, L.Y., Nichols, C.G., Maldonado, H.M., Baksi, K., Reichenbach, A., Skatchkov, S.N., and Eaton, M.J. (2007). Downregulation of Kir4.1 inward rectifying potassium channel subunits by RNAi impairs potassium transfer and glutamate uptake by cultured cortical astrocytes. Glia *55*, 274–281.

Kuschel, S., Rüther, U., and Theil, T. (2003). A disrupted balance between Bmp/Wnt and Fgf signaling underlies the ventralization of the Gli3 mutant telencephalon. Dev. Biol. *260*, 484–495.

Lavdas, A.A., Grigoriou, M., Pachnis, V., and Parnavelas, J.G. (1999). The medial ganglionic eminence gives rise to a population of early neurons in the developing cerebral cortex. J. Neurosci. Off. J. Soc. Neurosci. *19*, 7881–7888.

Lehre, K.P., Levy, L.M., Ottersen, O.P., Storm-Mathisen, J., and Danbolt, N.C. (1995). Differential expression of two glial glutamate transporters in the rat brain: quantitative and immunocytochemical observations. J. Neurosci. Off. J. Soc. Neurosci. *15*, 1835–1853.

Leone, D.P., Srinivasan, K., Chen, B., Alcamo, E., and McConnell, S.K. (2008). The determination of projection neuron identity in the developing cerebral cortex. Curr. Opin. Neurobiol. *18*, 28–35.

Malatesta, P., Hartfuss, E., and Götz, M. (2000). Isolation of radial glial cells by fluorescent-activated cell sorting reveals a neuronal lineage. Dev. Camb. Engl. *127*, 5253–5263.

Mallamaci, A., and Stoykova, A. (2006). Gene networks controlling early cerebral cortex arealization. Eur. J. Neurosci. *23*, 847–856.

Mariani, J., Coppola, G., Zhang, P., Abyzov, A., Provini, L., Tomasini, L., Amenduni, M., Szekely, A., Palejev, D., Wilson, M., et al. (2015). FOXG1-Dependent Dysregulation of GABA/Glutamate Neuron Differentiation in Autism Spectrum Disorders. Cell *162*, 375–390.

Marín, O., and Rubenstein, J.L.R. (2003). Cell migration in the forebrain. Annu. Rev. Neurosci. *26*, 441–483.

Markram, H., Toledo-Rodriguez, M., Wang, Y., Gupta, A., Silberberg, G., and Wu, C. (2004). Interneurons of the neocortical inhibitory system. Nat. Rev. Neurosci. *5*, 793–807.

Martynoga, B., Morrison, H., Price, D.J., and Mason, J.O. (2005). Foxg1 is required for specification of ventral telencephalon and region-specific regulation of dorsal telencephalic precursor proliferation and apoptosis. Dev. Biol. *283*, 113–127.

Matsumoto, A., Watanabe, K., Negoro, T., Sugiura, M., Iwase, K., Hara, K., and Miyazaki, S. (1981). Infantile spasms: etiological factors, clinical aspects, and long term prognosis in 200 cases. Eur. J. Pediatr. *135*, 239–244.

Mattson, M.P., Gleichmann, M., and Cheng, A. (2008). Mitochondria in neuroplasticity and neurological disorders. Neuron *60*, 748–766.

Mayer, S.I., Dexheimer, V., Nishida, E., Kitajima, S., and Thiel, G. (2008). Expression of the transcriptional repressor ATF3 in gonadotrophs is regulated by Egr-1, CREB, and ATF2 after gonadotropin-releasing hormone receptor stimulation. Endocrinology *149*, 6311–6325.

McKenna, W.L., Betancourt, J., Larkin, K.A., Abrams, B., Guo, C., Rubenstein, J.L.R., and Chen, B. (2011). Tbr1 and Fezf2 regulate alternate corticofugal neuronal identities during neocortical development. J. Neurosci. Off. J. Soc. Neurosci. *31*, 549–564.

Miyata, T., Kawaguchi, A., Saito, K., Kawano, M., Muto, T., and Ogawa, M. (2004). Asymmetric production of surface-dividing and non-surface-dividing cortical progenitor cells. Dev. Camb. Engl. *131*, 3133–3145.

Miyoshi, G., and Fishell, G. (2011). GABAergic interneuron lineages selectively sort into specific cortical layers during early postnatal development. Cereb. Cortex N. Y. N 1991 *21*, 845–852.

Miyoshi, G., and Fishell, G. (2012). Dynamic FoxG1 expression coordinates the integration of multipolar pyramidal neuron precursors into the cortical plate. Neuron *74*, 1045–1058.

Miyoshi, G., Butt, S.J.B., Takebayashi, H., and Fishell, G. (2007). Physiologically distinct temporal cohorts of cortical interneurons arise from telencephalic Olig2-expressing precursors. J. Neurosci. Off. J. Soc. Neurosci. *27*, 7786–7798.

Molyneaux, B.J., Arlotta, P., Menezes, J.R.L., and Macklis, J.D. (2007). Neuronal subtype specification in the cerebral cortex. Nat. Rev. Neurosci. *8*, 427–437.

Mondal, S., Ivanchuk, S.M., Rutka, J.T., and Boulianne, G.L. (2007). Sloppy paired 1/2 regulate glial cell fates by inhibiting Gcm function. Glia *55*, 282–293.

Muzio, L., and Mallamaci, A. (2005). Foxg1 confines Cajal-Retzius neuronogenesis and hippocampal morphogenesis to the dorsomedial pallium. J. Neurosci. Off. J. Soc. Neurosci. *25*, 4435–4441.

Naka, H., Nakamura, S., Shimazaki, T., and Okano, H. (2008). Requirement for COUP-TFI and II in the temporal specification of neural stem cells in CNS development. Nat. Neurosci. *11*, 1014–1023.

Namihira, M., Kohyama, J., Semi, K., Sanosaka, T., Deneen, B., Taga, T., and Nakashima, K. (2009). Committed neuronal precursors confer astrocytic potential on residual neural precursor cells. Dev. Cell *16*, 245–255.

Nery, S., Fishell, G., and Corbin, J.G. (2002). The caudal ganglionic eminence is a source of distinct cortical and subcortical cell populations. Nat. Neurosci. *5*, 1279–1287.

Neves, G., Cooke, S.F., and Bliss, T.V.P. (2008). Synaptic plasticity, memory and the hippocampus: a neural network approach to causality. Nat. Rev. Neurosci. *9*, 65–75.

Nielsen, S., Nagelhus, E.A., Amiry-Moghaddam, M., Bourque, C., Agre, P., and Ottersen, O.P. (1997). Specialized membrane domains for water transport in glial cells: high-resolution immunogold cytochemistry of aquaporin-4 in rat brain. J. Neurosci. Off. J. Soc. Neurosci. *17*, 171–180.

Nieto, M., Schuurmans, C., Britz, O., and Guillemot, F. (2001). Neural bHLH genes control the neuronal versus glial fate decision in cortical progenitors. Neuron *29*, 401–413.

Noctor, S.C., Flint, A.C., Weissman, T.A., Dammerman, R.S., and Kriegstein, A.R. (2001). Neurons derived from radial glial cells establish radial units in neocortex. Nature *409*, 714–720.

Noctor, S.C., Martínez-Cerdeño, V., Ivic, L., and Kriegstein, A.R. (2004). Cortical neurons arise in symmetric and asymmetric division zones and migrate through specific phases. Nat. Neurosci. *7*, 136–144.

Ochman, H., Gerber, A.S., and Hartl, D.L. (1988). Genetic applications of an inverse polymerase chain reaction. Genetics *120*, 621–623.

Ohkubo, Y., Chiang, C., and Rubenstein, J.L.R. (2002). Coordinate regulation and synergistic actions of BMP4, SHH and FGF8 in the rostral prosencephalon regulate morphogenesis of the telencephalic and optic vesicles. Neuroscience *111*, 1–17.

Ohtsuka, T., Sakamoto, M., Guillemot, F., and Kageyama, R. (2001). Roles of the basic helix-loop-helix genes Hes1 and Hes5 in expansion of neural stem cells of the developing brain. J. Biol. Chem. *276*, 30467–30474.

O'Leary, D.D.M., and Nakagawa, Y. (2002). Patterning centers, regulatory genes and extrinsic mechanisms controlling arealization of the neocortex. Curr. Opin. Neurobiol. *12*, 14–25.

O'Leary, D.D.M., Chou, S.-J., and Sahara, S. (2007). Area patterning of the mammalian cortex. Neuron *56*, 252–269.

Olive, M., Krylov, D., Echlin, D.R., Gardner, K., Taparowsky, E., and Vinson, C. (1997). A dominant negative to activation protein-1 (AP1) that abolishes DNA binding and inhibits oncogenesis. J. Biol. Chem. *272*, 18586–18594.

Ono, K., Takebayashi, H., Ikeda, K., Furusho, M., Nishizawa, T., Watanabe, K., and Ikenaka, K. (2008). Regional- and temporal-dependent changes in the differentiation of Olig2 progenitors in the forebrain, and the impact on astrocyte development in the dorsal pallium. Dev. Biol. *320*, 456–468.

Otis, T.S., and Jahr, C.E. (1998). Anion currents and predicted glutamate flux through a neuronal glutamate transporter. J. Neurosci. Off. J. Soc. Neurosci. *18*, 7099–7110.

Paek, H., Gutin, G., and Hébert, J.M. (2009). FGF signaling is strictly required to maintain early telencephalic precursor cell survival. Dev. Camb. Engl. *136*, 2457–2465.

Pancrazi, L., Di Benedetto, G., Colombaioni, L., Della Sala, G., Testa, G., Olimpico, F., Reyes, A., Zeviani, M., Pozzan, T., and Costa, M. (2015). Foxg1 localizes to mitochondria and coordinates cell differentiation and bioenergetics. Proc. Natl. Acad. Sci. U. S. A. *112*, 13910–13915.

Park, E.A., Song, S., Vinson, C., and Roesler, W.J. (1999). Role of CCAAT enhancer-binding protein beta in the thyroid hormone and cAMP induction of phosphoenolpyruvate carboxykinase gene transcription. J. Biol. Chem. *274*, 211–217.

Parri, H.R., Gould, T.M., and Crunelli, V. (2001). Spontaneous astrocytic Ca2+ oscillations in situ drive NMDAR-mediated neuronal excitation. Nat. Neurosci. *4*, 803–812.

Pilaz, L.-J., Patti, D., Marcy, G., Ollier, E., Pfister, S., Douglas, R.J., Betizeau, M., Gautier, E., Cortay, V., Doerflinger, N., et al. (2009). Forced G1-phase reduction alters mode of division, neuron number, and laminar phenotype in the cerebral cortex. Proc. Natl. Acad. Sci. U. S. A. *106*, 21924–21929.

Polleux, F., Whitford, K.L., Dijkhuizen, P.A., Vitalis, T., and Ghosh, A. (2002). Control of cortical interneuron migration by neurotrophins and PI3-kinase signaling. Dev. Camb. Engl. *129*, 3147–3160.

Pontrelli, G., Cappelletti, S., Claps, D., Sirleto, P., Ciocca, L., Petrocchi, S., Terracciano, A., Serino, D., Fusco, L., Vigevano, F., et al. (2014). Epilepsy in patients with duplications of chromosome 14 harboring FOXG1. Pediatr. Neurol. *50*, 530–535.

Pow, D.V., and Robinson, S.R. (1994). Glutamate in some retinal neurons is derived solely from glia. Neuroscience *60*, 355–366.

Privat, A. (1995). [Treatment of the future for spinal cord injuries]. Rev. Prat. *45*, 2051–2056.

Rakic, P. (1972). Mode of cell migration to the superficial layers of fetal monkey neocortex. J. Comp. Neurol. *145*, 61–83.

Rakic, P. (1974). Neurons in rhesus monkey visual cortex: systematic relation between time of origin and eventual disposition. Science *183*, 425–427.

Rakic, P. (2003). Developmental and evolutionary adaptations of cortical radial glia. Cereb. Cortex N. Y. N 1991 *13*, 541–549.

Rallu, M., Machold, R., Gaiano, N., Corbin, J.G., McMahon, A.P., and Fishell, G. (2002). Dorsoventral patterning is established in the telencephalon of mutants lacking both Gli3 and Hedgehog signaling. Dev. Camb. Engl. *129*, 4963–4974.

Rash, B.G., and Grove, E.A. (2006). Area and layer patterning in the developing cerebral cortex. Curr. Opin. Neurobiol. *16*, 25–34.

Regad, T., Roth, M., Bredenkamp, N., Illing, N., and Papalopulu, N. (2007). The neural progenitor-specifying activity of FoxG1 is antagonistically regulated by CKI and FGF. Nat. Cell Biol. *9*, 531–540.

Rothstein, J.D., Martin, L., Levey, A.I., Dykes-Hoberg, M., Jin, L., Wu, D., Nash, N., and Kuncl, R.W. (1994). Localization of neuronal and glial glutamate transporters. Neuron *13*, 713–725.

Sardi, S.P., Murtie, J., Koirala, S., Patten, B.A., and Corfas, G. (2006). Presenilin-dependent ErbB4 nuclear signaling regulates the timing of astrogenesis in the developing brain. Cell *127*, 185–197.

Sasai, Y., and De Robertis, E.M. (1997). Ectodermal patterning in vertebrate embryos. Dev. Biol. *182*, 5–20.

Schwarz, E.M., Van Antwerp, D., and Verma, I.M. (1996). Constitutive phosphorylation of IkappaBalpha by casein kinase II occurs preferentially at serine 293: requirement for degradation of free IkappaBalpha. Mol. Cell. Biol. *16*, 3554–3559.

Seoane, J., Le, H.-V., Shen, L., Anderson, S.A., and Massagué, J. (2004). Integration of Smad and forkhead pathways in the control of neuroepithelial and glioblastoma cell proliferation. Cell *117*, 211–223.

Sessa, A., Mao, C.-A., Colasante, G., Nini, A., Klein, W.H., and Broccoli, V. (2010). Tbr2-positive intermediate (basal) neuronal progenitors safeguard cerebral cortex expansion by controlling amplification of pallial glutamatergic neurons and attraction of subpallial GABAergic interneurons. Genes Dev. *24*, 1816–1826.

Seuntjens, E., Nityanandam, A., Miquelajauregui, A., Debruyn, J., Stryjewska, A., Goebbels, S., Nave, K.-A., Huylebroeck, D., and Tarabykin, V. (2009). Sip1 regulates sequential fate decisions by feedback signaling from postmitotic neurons to progenitors. Nat. Neurosci. *12*, 1373–1380.

Shaikh, T.H., Gai, X., Perin, J.C., Glessner, J.T., Xie, H., Murphy, K., O'Hara, R., Casalunovo, T., Conlin, L.K., D'Arcy, M., et al. (2009). High-resolution mapping and analysis of copy number variations in the human genome: a data resource for clinical and research applications. Genome Res. *19*, 1682–1690.

Shigeri, Y., Seal, R.P., and Shimamoto, K. (2004). Molecular pharmacology of glutamate transporters, EAATs and VGLUTs. Brain Res. Brain Res. Rev. *45*, 250–265.

Shimamura, K., and Rubenstein, J.L. (1997). Inductive interactions direct early regionalization of the mouse forebrain. Dev. Camb. Engl. *124*, 2709–2718.

Shuai, K., and Liu, B. (2003). Regulation of JAK-STAT signalling in the immune system. Nat. Rev. Immunol. *3*, 900–911.

Siegenthaler, J.A., Tremper-Wells, B.A., and Miller, M.W. (2008). Foxg1 haploinsufficiency reduces the population of cortical intermediate progenitor cells: effect of increased p21 expression. Cereb. Cortex N. Y. N 1991 *18*, 1865–1875.

Smart, I.H. (1973). Proliferative characteristics of the ependymal layer during the early development of the mouse neocortex: a pilot study based on recording the number, location and plane of cleavage of mitotic figures. J. Anat. *116*, 67–91.

Smart, I.H. (1976). A pilot study of cell production by the ganglionic eminences of the developing mouse brain. J. Anat. *121*, 71–84.

Smart, I.H. (1982). Radial unit analysis of hippocampal histogenesis in the mouse. J. Anat. *135*, 763–793.

Smart, I.H.M., Dehay, C., Giroud, P., Berland, M., and Kennedy, H. (2002). Unique morphological features of the proliferative zones and postmitotic compartments of the neural epithelium giving rise to striate and extrastriate cortex in the monkey. Cereb. Cortex N. Y. N 1991 *12*, 37–53.

Sofroniew, M.V., and Vinters, H.V. (2010). Astrocytes: biology and pathology. Acta Neuropathol. (Berl.) *119*, 7–35.

Sousa, V.H., Miyoshi, G., Hjerling-Leffler, J., Karayannis, T., and Fishell, G. (2009). Characterization of Nkx6-2-derived neocortical interneuron lineages. Cereb. Cortex N. Y. N 1991 *19 Suppl 1*, i1–i10.

Spigoni, G., Gedressi, C., and Mallamaci, A. (2010). Regulation of Emx2 expression by antisense transcripts in murine cortico-cerebral precursors. PloS One *5*, e8658.

Srinivasan, K., Leone, D.P., Bateson, R.K., Dobreva, G., Kohwi, Y., Kohwi-Shigematsu, T., Grosschedl, R., and McConnell, S.K. (2012). A network of genetic repression and derepression specifies projection fates in the developing neocortex. Proc. Natl. Acad. Sci. U. S. A. *109*, 19071–19078.

Storm, E.E., Garel, S., Borello, U., Hebert, J.M., Martinez, S., McConnell, S.K., Martin, G.R., and Rubenstein, J.L.R. (2006). Dose-dependent functions of Fgf8 in regulating telencephalic patterning centers. Dev. Camb. Engl. *133*, 1831–1844.

Stumm, R.K., Zhou, C., Ara, T., Lazarini, F., Dubois-Dalcq, M., Nagasawa, T., Höllt, V., and Schulz, S. (2003). CXCR4 regulates interneuron migration in the developing neocortex. J. Neurosci. Off. J. Soc. Neurosci. *23*, 5123–5130.

Sun, Y., Nadal-Vicens, M., Misono, S., Lin, M.Z., Zubiaga, A., Hua, X., Fan, G., and Greenberg, M.E. (2001). Neurogenin promotes neurogenesis and inhibits glial differentiation by independent mechanisms. Cell *104*, 365–376.

Sur, M., and Rubenstein, J.L.R. (2005). Patterning and plasticity of the cerebral cortex. Science *310*, 805–810.

Sussel, L., Marin, O., Kimura, S., and Rubenstein, J.L. (1999). Loss of Nkx2.1 homeobox gene function results in a ventral to dorsal molecular respecification within the basal telencephalon: evidence for a transformation of the pallidum into the striatum. Dev. Camb. Engl. *126*, 3359–3370.

Tabata, H., and Nakajima, K. (2003). Multipolar migration: the third mode of radial neuronal migration in the developing cerebral cortex. J. Neurosci. Off. J. Soc. Neurosci. *23*, 9996–10001.

Taghdiri, M.M., and Nemati, H. (2014). Infantile spasm: a review article. Iran. J. Child Neurol. *8*, 1–5.

Takahashi, T., Nowakowski, R.S., and Caviness, V.S. (1995). The cell cycle of the pseudostratified ventricular epithelium of the embryonic murine cerebral wall. J. Neurosci. Off. J. Soc. Neurosci. *15*, 6046–6057.

Tanaka, K., Watase, K., Manabe, T., Yamada, K., Watanabe, M., Takahashi, K., Iwama, H., Nishikawa, T., Ichihara, N., Kikuchi, T., et al. (1997). Epilepsy and exacerbation of brain injury in mice lacking the glutamate transporter GLT-1. Science *276*, 1699–1702.

Tao, W., and Lai, E. (1992). Telencephalon-restricted expression of BF-1, a new member of the HNF-3/fork head gene family, in the developing rat brain. Neuron *8*, 957–966.

Theil, T., Alvarez-Bolado, G., Walter, A., and Rüther, U. (1999). Gli3 is required for Emx gene expression during dorsal telencephalon development. Dev. Camb. Engl. *126*, 3561–3571.

Thomas, P., and Beddington, R. (1996). Anterior primitive endoderm may be responsible for patterning the anterior neural plate in the mouse embryo. Curr. Biol. CB *6*, 1487–1496.

Tissir, F., and Goffinet, A.M. (2003). Reelin and brain development. Nat. Rev. Neurosci. *4*, 496–505.

Tiveron, M.-C., Rossel, M., Moepps, B., Zhang, Y.L., Seidenfaden, R., Favor, J., König, N., and Cremer, H. (2006). Molecular interaction between projection neuron precursors and invading interneurons via stromal-derived factor 1 (CXCL12)/CXCR4 signaling in the cortical subventricular zone/intermediate zone. J. Neurosci. Off. J. Soc. Neurosci. *26*, 13273–13278.

Tohyama, J., Yamamoto, T., Hosoki, K., Nagasaki, K., Akasaka, N., Ohashi, T., Kobayashi, Y., and Saitoh, S. (2011). West syndrome associated with mosaic duplication of FOXG1 in a patient with maternal uniparental disomy of chromosome 14. Am. J. Med. Genet. A. *155A*, 2584–2588.

Toma, K., Kumamoto, T., and Hanashima, C. (2014). The timing of upper-layer neurogenesis is conferred by sequential derepression and negative feedback from deep-layer neurons. J. Neurosci. Off. J. Soc. Neurosci. *34*, 13259–13276.

de la Torre-Ubieta, L., and Bonni, A. (2011). Transcriptional regulation of neuronal polarity and morphogenesis in the mammalian brain. Neuron *72*, 22–40.

Tyler, W.A., and Haydar, T.F. (2010). A new contribution to brain convolution: progenitor cell logistics during cortex development. Nat. Neurosci. *13*, 656–657.

Vallejo, M. (2009). PACAP signaling to DREAM: a cAMP-dependent pathway that regulates cortical astrogliogenesis. Mol. Neurobiol. *39*, 90–100.

Van Antwerp, D.J., Martin, S.J., Kafri, T., Green, D.R., and Verma, I.M. (1996). Suppression of TNF-alpha-induced apoptosis by NF-kappaB. Science *274*, 787–789.

Vigevano, F., Fusco, L., Cusmai, R., Claps, D., Ricci, S., and Milani, L. (1993). The idiopathic form of West syndrome. Epilepsia *34*, 743–746.

Vucurovic, K., Gallopin, T., Ferezou, I., Rancillac, A., Chameau, P., van Hooft, J.A., Geoffroy, H., Monyer, H., Rossier, J., and Vitalis, T. (2010). Serotonin 3A receptor subtype as an early and protracted marker of cortical interneuron subpopulations. Cereb. Cortex N. Y. N 1991 *20*, 2333–2347.

Walz, W., and Hertz, L. (1982). Ouabain-sensitive and ouabain-resistant net uptake of potassium into astrocytes and neurons in primary cultures. J. Neurochem. *39*, 70–77.

Wilson, D.A., and Rennaker, R.L. (2010). Cortical Activity Evoked by Odors. In The Neurobiology of Olfaction, A. Menini, ed. (Boca Raton (FL): CRC Press/Taylor & Francis),.

Wonders, C.P., and Anderson, S.A. (2006). The origin and specification of cortical interneurons. Nat. Rev. Neurosci. *7*, 687–696.

Xuan, S., Baptista, C.A., Balas, G., Tao, W., Soares, V.C., and Lai, E. (1995). Winged helix transcription factor BF-1 is essential for the development of the cerebral hemispheres. Neuron *14*, 1141–1152.

Yeung, A., Bruno, D., Scheffer, I.E., Carranza, D., Burgess, T., Slater, H.R., and Amor, D.J. (2009). 4.45 Mb microduplication in chromosome band 14q12 including FOXG1 in a girl with refractory epilepsy and intellectual impairment. Eur. J. Med. Genet. *52*, 440–442.

Yoshida, M., Assimacopoulos, S., Jones, K.R., and Grove, E.A. (2006). Massive loss of Cajal-Retzius cells does not disrupt neocortical layer order. Dev. Camb. Engl. *133*, 537–545.

Zupanc, M.L. (2003). Infantile spasms. Expert Opin. Pharmacother. *4*, 2039–2048.